CHARACTERIZING THE ROLE OF ACTIN BINDING, BUNDLING, AND TYROSINE PHOSPHORYLATION IN MODULATING VINCULIN FUNCTION

Caitlin Elizabeth Tolbert

A dissertation submitted to the faculty at the University of North Carolina at Chapel Hill in partial fulfillment of the requirements for the degree Doctorate of Philosophy in the Department of Developmental and Cell Biology

Chapel Hill
2013

Approved by:

Keith Burridge

Sharon L. Campbell

James Bear

Richard Cheney

Ben Major

ABSTRACT

CAITLIN E. TOLBERT: Characterizing the Role of Actin Binding, Bundling, and Tyrosine Phosphorylation in Modulating Vinculin Function
(Under the direction of Dr. Keith Burridge and Dr. Sharon Campbell)

Vinculin is an essential adhesion protein involved in controlling motility and force transduction, in part by coupling the actin cytoskeleton to the extracellular matrix. Vinculin is regulated by intramolecular interactions between the N-terminal head domain (Vh) and the C-terminal tail domain (Vt) which are linked by a proline-rich region. Upon binding to F-actin, Vtundergoes a conformational change that exposes a cryptic dimerization site that enables it to self-associate and bundleF-actin.Previous publications have investigated vinculin variants that are deficient in F-actin binding and have found a number of cellular defects; however, these constructs either lack Vt or contain large deletions that significantly destabilize Vt, and it is likely that the observed phenotypes are due to a number of disrupted interactions.

In an effort to improvethe vinculin/F-actin model using select mutations with little structural consequences, we have identified residues that selectively bind and/or bundle F-actin. Deletion of the C-terminal hairpin (VtΔC5) maintains a normal structure and binding to other interaction partnersin comparison to wildtype (WT) Vt. However, VtΔC5 is unable to bundle F-actin and forms a non-functional dimeric species. To disrupt the vinculin/F-actin interaction, we characterized two variants: I997A and V1001A. When these variants are expressed in cells, cells are smaller and have fewer with larger adhesions when allowed to spread on FN. Cells expressing these variants are unable to reinforce when pulses of force are applied via integrins.

These data suggest that vinculin-mediated F-actin binding and bundling plays a role in cell spreading and cellular reinforcement.

The C-terminal hairpin contains the only tyrosine phosphorylation site in Vt (Y1065). However, the role of tyrosine phosphorylation in Vt and its full impact on regulating vinculin have not been elucidated. I provide evidence that Src-mediated phosphorylation of Vt modulates F-actin bundling. I have structurally characterized both phosphorylatedVt and Vt variants that either mimic or prevent phosphorylation to understand its impact on vinculin function. Furthermore, I utilize the variants to study the cellular role of Y1065 phosphorylation on cell spreading and cellular reinforcement. With the results of these studies, we propose an interface the enables actin-induced vinculin dimerization.

ACKNOWLEDGMENTS

To my family, my parents, Clarence and Diana, as well as my sister, Jessica, and my close friends, I would not have completed this work without your love and support. To my advisors, Keith Burridge and Sharon Campbell, thank you for the opportunity to work in your laboratories; both of you have given me so much.

TABLE OF CONTENTS

LIST OF TABLES

Table

LIST OF FIGURES

LIST OF ABBREIVATIONS

3DFM	Three-dimensional force microscopy
ΔC	Vinculin C-terminal deletion (lacks residues 1052-1066)
ΔC1	Vinculin C-terminal deletion (lacks residue 1066)
ΔC2	Vinculin C-terminal hairpin deletion (lacks residues 1065-1066)
ΔC5	Vinculin C-terminal hairpin deletion (lacks residues 1061-1066)
ΔN5	Vinculin N-terminal strap deletion (lacks residues 879-883)
Δstrap	Vinculin N-terminal strap deletion (lacks residues 879-892)
A/V	Actin/Vinculin Tail Ratio
BME	β-mercaptoethanol
BS3	Bis[sulfosuccinimidyl] suberate
CAP	Cbl-associated protein
CD	Circular dichroism
CI	Cell index
CT	C-terminus (residues 1051-1066)
DMD	Discrete molecular dynamics
DMEM	Dulbecco's modified Eagle's medium
DSS	Disuccinimidyl suberate
DTT	Dithiothreitol
ECM	Extracellular matrix
EM	Electron microscopy
EPR	Electron paramagnetic resonance

ERK	Extracellular signal-regulated kinase
F-actin	Filamentous actin
FA	Focal adhesion
FAK	Focal adhesion kinase
FBS	Fetal bovine serum
FCX	Focal Complex
FN	Fibronectin
FRAP	Fluorescence recovery after photobleaching
FRET	Fluorescence resonance energy transfer
G-actin	Monomeric actin
HIC	4-methyl histidine
HIS	Canonical histidine
HSQC	Heteronuclear Single Quantum Coherence
KO	Knockout
LD	Lipid-deficient
NMR	Nuclear magnetic resonance
NT	N-terminus (residues 879-892)
PC	Phosphatidylcholine
PE	Phosphatidylethanolamine
PIP_2	Phosphatidylinositol (4,5)-bisphosphate
PKCα	Protein Kinase C alpha
PS	Phosphatidylserine
RTCA	Real-time cell analyzer

SUVs	Small unilamellar vesicles
TIRF	Total internal reflection fluorescence
VASP	Vasodilator-stimulated phosphoprotein
VBS	Vinculin-binding sites
Vin -/- MEFs	Vinculin knockout murine embryo fibroblasts
VT	Vinculin Tail (residues 879-1066)
VH	Vinculin Head (residues 1-855)
WT	Wildtype

I. Introduction

Vinculin is a widely expressed, 116 kDa protein that is recruited to both adherens junctions and cell-extracellular (ECM) junctions, better known as focal adhesions (FAs). At adhesions, vinculin helps couple the actin cytoskeleton via transmembrane receptors and mediates the recruitment of numerous proteins to these maturating complexes. It is through proteins located in adhesions, such as vinculin, that are necessary to regulate cell adhesion and cytoskeletal changes in order to control cell migration. Efficient control of cell migration is critical during embryonic development or wound healing and under pathological conditions such as cancer progression via invasion(*1-3*). In support of vinculin's role in disease, vinculin knockout (KO) studies reveal defects leading to death during development, cardiovascular dysfunction, and promotion of cancer progression(*2, 4-6*). Furthermore, it is through these adhesion sites that vinculin mediates the transmission of mechanical tension into a global cellular response.[1]

[1]*The text, figures, and figure legends in Chapter I are reprinted and/or modified with permission from the following:*
Tolbert CE, Burridge K, Campbell SL. Vinculin regulation of F-actin bundle formation: what does it mean for the cell? Cell AdhMigr 7: 219-225, 2013
Thompson PM, Tolbert CE, Campbell SL. Vinculin and metavinculin: oligomerization and interactions with F-actin. FEBS Lett 587: 1220-1229, 2013

A. The Role of Vinculin during Development, Cancer, and Cardiovascular Function

During development, areas of adhesion, whether through adherens junctions or FAs, need to be tightly controlled in order for organisms to develop. These adhesions sites mediate signals that transduce messages from between cells and from external stimuli. Vinculin plays a crucial role in regulating a number of processes at both FAs and adherens junctions, and as a result, impacts a number of cellular processes. The importance of vinculin has been previously demonstrated through mice KO studies where embryos die by day E10.5 and have defects in heart and neural tube formation (*2*). Additionally, studies that KO vinculin in *C. elegans* and zebrafish found defects in muscle and cardiac development, with the zebrafish displaying a dilated cardiomyopathy phenotype that includes impairments in blood congestion, pericardial edema, and cardiac contractility (*7, 8*). Upon isolation of fibroblasts from the KO mice embryos, numerous defects were found including difficulties in cell adhesion, spreading, increased motility, higher levels of focal adhesion kinase (FAK) and paxillin signaling that lead to increased extracellular signal-regulated kinase (ERK) signaling, and resistance to apoptosis from a number of stimuli as well as resistance to anoikis(*2-4, 9*). Because of these defects, vinculin is considered to be a tumor suppressor. To further support vinculin's tumor suppressor properties, recent studies have shown that by activating vinculin, melanoma cells become more sensitive to chemotherapeutic treatments (*10*). Moreover, studies show that vinculin protein levels are correlated with very invasive cancers and upon re-expression of vinculin in these cell lines, the cells are less tumorigenic(*11*). Vinculin mislocalization has also been shown to impact the loss of adherens junctions during initial stages of tumor formation (*12-16*).

While vinculin is ubiquitously expressed, it is particularly enriched in muscles along with its larger isoform, metavinculin. Metavinculin's expression is muscle-specific and contains an

additional 68-amino acid insertion within the tail domain. In muscles, both vinculin and metavinculin are enriched in both the I-band and in costameres, structures that link sacromeres to the membrane(*17-19*). While metavinculin serves a very similar purpose as vinculin in muscles, it has some distinct properties that are attributed to the 68-amino acid insertion. For instance, vinculin itself is very conserved between species while metavinculin displays greater sequence variety within the 68-amino acid insertion among different species (*20*). Furthermore, metavinculin displays altered affinities for binding partners to the tail domain in comparison to the vinculin tail domain (Vt). For instance, metavinculin has a higher affinity for raver1 and less affinity for PIP_2(*21, 22*). Interestingly, some of the most striking differences between vinculin and metavinculin come from their differences in their interaction with F-actin. While Vt normally binds and crosslinks F-actin into parallel filaments, metavinculin tail domain is also able to bind F-actin and create an alternative F-actin structure that looks "web-like"(*18*). Due to these differences in F-actin associations, metavinculin displays a specialized role in mechanical tension when external forces are applied to cells(*23*). For instance, metavinculin varies in expression levels when forces are applied to cells that appear to be muscle-type dependent(*17, 19, 22,24-26*). When examining common mutations in metavinculin that occur within the 68-amino acid insert region (A934V, ΔL954, and R975W), these mutations are believed to be involved in metavinculin's mechanosensitive properties due to altered interactions with F-actin and with the metavinculin head domain, and are found in cardiomyopathies(*27-29*). These diseases occur due to the improper generation of force and lead to stress-induction on the heart.

While most mutations that lead to cardiomyopathies are found in metavinculin within the specific 68-amino acid insert region, there are select mutations that occur in vinculin. For instance, a mutation within Vh (L277M) is believed to predispose individuals to hypertrophic

cardiomyopathy (*30*). A recent report highlighted a pedigree containing a missense mutation in vinculin (K815R) was associated with familial dilated cardiomyopathies and congenital heart abnormalities (*31*).

B. The Role of Vinculin during Cell Spreading, Migration, and Mechanotransduction

Following activation, vinculin is recruited to two main sites of adhesion: adherens junctions and FAs. In both sites, vinculin mediates a similar function: to recruit additional interaction partners to these sites as the adhesion matures and to help link the transmembrane receptors to the actin cytoskeleton(*32*). While less is known about vinculin in adherens junctions since the most focus in the field has examined vinculin is FAs, recent reports have highlighted the importance of vinculin in adherens junctions and have suggested vinculin serves three functions: vinculin acts downstream of myosin VI, a minus end-directed motor that is necessary for E-cadherin dependent border-cell migration; regulates the expression of E-cadherin on the surface of cells; vinculin plays a mechanosensitive role in response to force applied to E-cadherin (*33*).

As implicated by fibroblasts isolated vinculin KO mice, cells have a number of defects that are directly mediated through their FAs. These defects include deficiencies in cell adhesion, spreading, migration, responses to force as well as resistance to anoikis(*2-4, 9*). Once activated at FAs, vinculin facilitates recruitment of additional proteins and links to F-actin, thereby enabling vinculin-mediated regulation of FA dynamics, efficient cell spreading, migration, or respond to external forces.

During migration and early stages of cell spreading, the leading edges of cells are defined by the balance between dynamics in actin polymerization and formation and turnover of

adhesions. Only through the interplay of these two components can effective migration and spreading be achieved. Following integrin engagement and recruitment of key cytoskeletal proteins, including talin and vinculin that establishes the link between active integrins and F-actin, actin flow slows and transmits force on the ECM to enable cells to move(*34*) and allow adhesions to mature(*35*). In studies examining motility and spreading in the absence of vinculin, spreading is severely impaired but the cells are able to migrate at a higher rate (*36*). These data suggest that vinculin is needed to stabilize adhesions in order to spread instead of impacting rapid actin polymerization and depolymerization that is necessary for effective migration. Recent studies have suggested that, in addition to bundling F-actin, vinculin can promote actin polymerization and cap filaments (*37-39*). However, it has been hard to observe the result of these different functions in cells due to the use of large and destabilizing vinculin C-terminal deletion variants. Humphries *et al*. showed that expression of vinculin tail domain alone was sufficient for vinculin to be recruited to areas of high contractility that were under mechanical tension, such as FAs, but not to the lamellipodia(*40*). An actin deficient deletion mutant lacking helix 2 and 3 within Vt displayed not only larger and denser FAs, but also prevented an invasive phenotype (*41*), indicating that the F-actin/vinculin interaction may regulate cellular functions that organize the actin network during migration. However, given the size of this deletion and likelihood that Vt is destabilized, this variant likely possesses multiple defects. A recent report that utilizes a more specific actin-binding deficient variant, vinculin^{I997A}, implicates the role of the F-actin/vinculin interaction in cell migration by regulating the flow velocity of F-actin at the leading edge of cells and this in turn modulates FA maturation (*42*).

Many cellular processes are dependent on locally generated forces in their environment, including migration as evidenced by durotaxis, cell survival, or death (*33, 43,44*). The ability of

cells to sense changes in stiffness is believed to be primarily mediated through proteins at FAs, including vinculin. In addition its ability to sense external forces, vinculin has been reported to regulate how applied mechanical stress alters adhesion composition in order to induce cell morphological changes (*45-47*). Recent data indicates that vinculin is crucial for transmission of mechanical forces resulting from either actomyosin or cell-generated forces, since the recruitment of vinculin to FAs corresponds to the amount of force applied to the extracellular matrix (ECM) (*48, 49*). Furthermore, the F-actin/vinculin interaction may be required for these forces since, without Vt, vinculin does not follow the retrograde flow of actin (*50*). The need for vinculin to bind F-actin and transduce force is further supported through measurements of force fluctuations, and correlating them to the degree of coupling displayed by the speckle motions of F-actin and vinculin during protrusion and retraction events at the leading edge of cells (*51*). Further, recent studies have shown that vinculin mutants deficient in actin binding are unable to generate traction on the ECM within the leading edge of cells(*42*). However, vinculin-mediated F-actin bundling appears to be a key factor in regulating how cells respond to an external force since expression of a vinculin variant deficient in actin bundling, ΔC5 vinculin, prevented cells from responding to pulses of force when a magnetic bead coated in fibronectin (FN) was applied (*39*). These data suggest that it is not only the connections between vinculin and F-actin that are necessary to respond to extracellular stimuli, but also the vinculin-mediated F-actin bundles that are needed to properly transduce external forces.

C. Vinculin's Binding Partners and its Auto-Inhibited Structure

Vinculin consists of three main domains: a large multi-helical head domain (Vh), a flexible proline-rich linker, and a smaller helical tail domain (Vt). Each of these regions has their own distinct set of binding partners. Vh associates with talin, α-actinin, α/β-catenin, MAPK, and IpaA from *Shigellaflexneri*(*52-57*). The proline-rich linker region binds to vasodilator-stimulated phosphoprotein (VASP), Cbl-associated protein (CAP)/Ponsin, nArgBP2, vinexin-α/β, p130CAS and the Arp2/3 complex(*58-63*). Finally, Vt interacts with protein kinase C-α (PKCα), F-actin, paxillin, Hic-5, PIP2, raver1 and α-synemin(*21, 64-70*).

Through x-ray crystallography, many structures of vinculin examining the full-length molecule, isolated domains, and domains bound to ligands have been solved. Bakolista *et al*., showed the full-length structure in the inactive, or auto-inhibited, conformation of vinculin, revealing the multi-helical regions of the protein (*71*). As shown in Figure 1.1, Vh (D1-D4) consists of multiple tandem pairs with multiple helices. From D4, there is a flexible, proline-rich region that connects to Vt, a five-helix bundle. It has been shown that isolated Vt shares a number of structural similarities to Vt within the full-length protein(*71, 72*). In the inactive state, there are a number of intramolecular interactions that are responsible for the auto-inhibited conformation. A number of these interactions occur between Vt-D1 while a few additional contacts occur between Vt-D3 and Vt-D4 (Figure 1.1). Through these multiple intramolecular interactions, the proposed K_d for inactive vinculin is ~ 1 nM.

Using the information gained from the x-ray crystal structure of inactive vinculin, the sites responsible for auto-inhibition were identified through biochemical assays (*73*). Cohen *et al*., found that the affinity for Vt for D1-D4 (10^{-7} M) was much higher than for Vt to D1 alone

(10^{-5} M) which supports the idea that other regions within Vh have additional contacts to Vt in order to mediate the inactive conformation(*73*). It was determined that contacts within D4 also interact with Vt and upon mutation of residues within D4 (N773/E775A), head-tail interactions were reduced about 100-fold and talin binding was still permitted. In order to create a constitutively active vinculin mutant, the T12 mutant (D974/K975/R976/R978A) was utilized to disrupt head-tail interactions. Upon expression of the activating-vinculin mutant in cells, size and residency of vinculin in FAs were both increased (*73*). While a third site was identified in the x-ray crystal structure of auto-inhibited vinculin between Vt and D3, this interaction has not been verified (*33*).

D. Vinculin Activation

When it is in the auto-inhibitory conformation, vinculin has tight intramolecular interactions between Vh and Vt at multiple distinct sites. Once these intramolecular interactions are released, vinculin transitions into its 'active' state, or rather the exposure of additional binding sites for its interaction partners. How these intramolecular interactions are relaxed that enables for vinculin activation have not been fully elucidated. Vinculin activation can occur through two main mechanisms: application of external mechanical forces or through interaction of multiple binding partners to both the Vh and Vt. It has been found that when external forces are applied to cells, there is a fast and robust recruitment of vinculin to sites of integrin engagement(*74*). However, the exact mechanism that enables vinculin's activation in response to this external stimuli has yet to be fully understood; furthermore, it yet remains to be elucidated if this method

of vinculin activation is solely integrin-dependent or if external forces to cadherins can elucidate a similar response.

In the better characterized model for vinculin activation, the combinatorial model, suggests that multiple binding partners relax the interactions between Vh and Vt in order to activate the molecule. The specific binding partners that aid in vinculin activation are presumably dependent on their location; for vinculin activation at FAs, these binding partners are typically talin and F-actin. It has been shown that talin alone is sufficient to disrupt interactions between isolated Vt and D1 domains. However, talin is not able to break all the intramolecular interactions to enable for vinculin activation in the context of the full-length protein. Only in the presence of both talin and F-actin does vinculin activate in a dose-dependent manner (*75*).

Currently, there is no single protein that is endogenous to the cell that can activate vinculin. The only protein that can activate vinculin by itself is the virulent protein, IpaA, from *Shigellaflexneri(76)*. Within IpaA, there are two vinculin-binding sites (VBS) and the binding site between IpaA and Vh seem to mimic VBS from both talin and α-actinin(*77*). Interestingly, the VBS from IpaA has reported having a much higher affinity (10-fold) for D1 of Vh when compared to other VBS from talin(*77*). This accounts for why IpaA can solely activate vinculin. However, when F-actin was added to the vinculin fluorescence resonance energy transfer (FRET)-activation biosensor in the presence of IpaA, vinculin's activation was increased, suggesting that F-actin also plays a role in activation although it is not necessarily required in the presence of IpaA (*75*). While the only interaction between IpaA and Vh appears to be through the D1 domain of Vh, it cannot be excluded that IpaA coulddisrupt interactions between D3-Vt or D4-Vt.

While the majority of these studies have been performed with purified proteins and have significantly improved our understanding of how vinculin can become activated, studies from cells have implicated that vinculin activation is much more complicated than anticipated. Using a FRET-based vinculin activation biosensor, the conformation of vinculin can be monitored in live cells. While it was no surprise that vinculin is found to be active and in an open conformation when located at FAs and cytoplasmic vinculin was inactive, there are distinct pools of vinculin within FAs that are inactive when vinculin is initially recruited to FAs and as adhesions turnover (*74*). These results suggest that there are additional signaling events controlling the activation state of vinculin, and it is tightly regulated by unknown ligands prior to FA turnover. Additionally, these data suggest that vinculin recruitment is decoupled from its activation, which is likely due to the lack of additional binding partners available to activate vinculin upon immediate localization to FAs. For instance, while talin can recruit vinculin, an additional binding partner such as F-actin is not necessarily in the same vicinity in order to bind and activate vinculin. This hypothesis is supported by the distances between talin and F-actin according to recent high-resolution microscopy studies (*78*). These data could account for the multiple pools of vinculin in different conformations at FAs.

E. The Vinculin Tail Domain and its Binding Partners

1. The Structure of the Vinculin Tail Domain

Vt (residues 879-1066) comprises a five-helix bundle, as shown by its crystal structure (*72*). Within the designated residues, there is a flexible N-terminal strap and a C-terminal hairpin (Figure 1.2A). As mentioned previously, the structure of isolated Vt is nearly identical to Vt in

the context of the full-length molecule. However, the isolated domain was solved as a dimer; a non-physiological dimer that has been previously observed by rotary-shadowing electron microscopy (EM) that occurs when Vt is in abundance beyond ~360 μM, a requirement for forming crystals. The interface where this non-physiological occurs is the same interface where Vt interacts with D1 in the auto-inhibited conformation and where F-actin interacts with Vt.

The N-terminal strap (residues 879-893) is a flexible area of the protein as suggested by the multiple conformations that are observed for this region. When the N-terminal strap is more ordered, it packsnext to helix 1 and 2 where it forms multiple contacts. Specifically, residues D882 interacts with S914 and K924 that are located in the loop between helix 1 and 2 and along helix 2, respectively. Additionally, residues K1061 and Y1065, which are located in the C-terminal hairpin, are the major residues that enable the N- and C-terminal interactions. Moreover, residue F885 within the strap packs into a hydrophobic patch between helix 1 and 2 in order to make contacts with H906 (Figure 1.2A) (*71*, *72*).

There are two distinct basic regions on Vt that have been proposed to play a role in lipid interactions and are termed the basic ladder and the basic collar (Figure 1.2B). The basic ladder consists of basic, exposed residues along helix 3 and within the loop that serves as the base for the helical bundle (residues K944, R945, K956, R963, K966, K970, R978, R1008, and R1049). The basic collar consists of exposed, basic residues from helix 1, 5, and the C-terminus (residues R910, K911, R1039, R1060, and K1061).

The final region of Vt that is of note is the C-terminus (residues 1047-1066). The C-terminus is positioned of the bottom of the helix core and interacts with the core, helix 1, the loop between helix 1 and 2, and helix 5. Additionally, residues W1058 and W912 pack against each other in order to maintain the structure of the C-terminus (*72*, *79*) (Figure 1.2A). The C-

terminal hairpin, also referred to as the hydrophobic hairpin, consists of the last five amino acids (TPWYQ) and has contacts with the N-terminal strap.

2.Interactions with PIP_2

Multiple groups have shown Vt's propensity for binding to acidic phospholipids, specifically phosphatidylinositol 4,5-bisphosphate (PIP_2)(*67, 71, 72, 80-83*). PIP_2 itself has been noted as a potent molecule that helps mediates a number of signaling events such as regulating cell morphology and actin dynamics(*84, 85*). Due to the role of PIP_2 in these cell signaling events, it could help explain vinculin's role in these processes, moreover the specific role of Vt. The interaction between PIP_2 and Vt has been shown to impact the binding between Vt's other interaction partners such as F-actin and PKCα (*65, 71, 72,86*). The PIP_2/Vt interaction has also been proposed to help disrupt head-tail interactions leading to vinculin'sactivation(*65, 71, 80, 83,86*). However, these studies were performed with purified components and excess lipids. Additionally, recent reports have shown that the affinity for PIP_2 is significantly reduced in the context of the full-length protein and is unable to activate vinculin(*80*). Furthermore, it has beenproposed that the purpose of the PIP_2/vinculin interaction is to control adhesion formation,FA turnover and force transduction (*81, 87*).

From the multiple reports studying the role of the PIP_2/vinculin interaction has come multiple binding sites with many mutations and deletions. The C-terminus has been implicated in modulating PIP_2 binding due to the "hydrophobic" hairpin and that it can possibly insert itself into membranes(*72*). Deletion of the C-terminus that lacks residues 1052-1066 showed a significant disruption in binding to lipids; however, recent nuclear magnetic resonance (NMR) studies have shown a number of perturbations with this deletion variant indicating a drastic and destabilizing structural change occurs when a major section of the C-terminus is deleted (*88*).

Palmer *et al*. showed that deletion of R1060 and K1061 cause the significant structural changes as these residues play a crucialrole in maintaining the tertiary structure of Vt (*88*). Furthermore, the authors also showed that deletion of the C-terminal hairpin (Vt ΔC5) did not disrupt binding to PIP_2. This is in contrast with other recent reports that implicate the C-terminal hairpin in membrane insertion as shown by a 23-mer peptide of the C-terminus in the excess of lipids(*89*). However, using a peptide in place of Vt or the full-length protein is not a true representation of the interaction and additional studies would be needed to verify if the C-terminal hairpin inserts itself into the membrane, an unlikely result given previous reports.

Another group identified a lipid-deficient (LD) variant that introduced a number of mutations within the basic collar, ladder and C-terminus (residues K952/K956/R963/K966/R1060/K1061Q)(*81*). While these mutants showed a significant disruption in binding to PIP_2, no structural studies were performed. Given recent evidence that showed deletion of R1060 and K1061 significantly destabilized Vt, it is likely that the LD mutant is also destabilizing (*88*). Palmer *et al*. were able to show that removal of the N-terminal strap greatly enhanced binding to $PIP_{2,}$ which points to residues in the basic collar as the most likely candidates for mediating PIP_2 binding (*88*). This is further supported by other studies that have highlighted residues K911 and K924,residues within the basic collar, as sites that mediate PIP_2 interactions (*72, 79*).

3. Interactions with F-actin

One of vinculin's main functions is to bind F-actin in order to help link transmembrane receptors to the actin cytoskeleton(*40*). Vt contains an F-actin binding site that is partially masked due to autoinhibitory interactions with Vh in the inactive, full-length protein (*72*).This is supported by data that shows F-actin only binds to full length vinculin when in the presence of

additional binding partners, such as IpaA or talin(*76, 90*). When Vt is further broken down into two fragments, both fragments can bind to F-actin indicating that there are two binding sites on Vt, although these sites do not look like typical actin-binding sites(*66*). Studies that examined variations intryptophan fluorescence and protease sensitivity when bound to F-actin indicate that there are additional conformational changes in Vt when it binds to F-actin (*72*). In addition to binding F-actin, Vthas been shown to self-associate through a cryptic dimerization site that enables actin filaments to be crosslinked (Figure 1.3) (*90*).

Janssen *et al*. combined negative stain EM, computational docking and mutagenesis approaches and proposed a structural model for the Vt/F-actin complex (Janssen model) (*91*). In the Janssen model, F-actin interacts with Vt at two sites; the top of helix 2 and 3 (upper site) as well as the bottom of helix 3 and helix 5 (lower site) leading into the C-terminal hairpin (Fig. 1.3) (*91*). They also proposed that deletion of the amino (N)-terminal strap impaired actin bundling while deletion of the C-terminus enhanced the bundling efficiency of Vt(*91*).However, taking into consideration a number of factors including the resolution used to dock Vt (50 Å), computational modeling revealing a number of conformational clashes occur on both Vt and actin, and a lack in supporting mutagenesis data, suggest that the current model needs additional refinement.

Another recent report used molecular dynamics simulations to identify the actin binding sites on Vt. While the lower site is consistent with the model proposed by Janssen *et al*., the upper site contains an entirely different surface and points to residues in the hydrophobic surface of helix 4(*92*). Despite the proposed models, there has not been a single point mutant identified that specifically disrupts the F-actin interaction. Rather, large deletions have been used to study the role of the F-actin/vinculin interaction. Deletion mutants lacking helix 2 and 3 within Vt

impacted cell morphology and promoted an invasive phenotype, indicating that the F-actin/vinculin interaction may mediate a number of cellular processes (*41*). However, given the size of this deletion, Vt is likely to be destabilized, and this could attribute the number of defects observed.

4. Vinculin Tail Oligomerization

i. Vinculin's Non-Physiological Dimer

One of the most intriguing properties of Vt is its propensity to oligomerize under varying conditions and with different binding partners. Vt dimerizes at high concentrations in the absence of any other ligands (*23, 72,93*). Atphysiological protein concentrations, it can also homodimerizein the presence of actin (*66, 72, 91*), and oligomerize (dimer and trimer) in the presence of PIP_2 (*72, 88, 94*). Furthermore, vinculin not only homodimerizes via Vt, but can also heterodimerize with the tail domain of metavinculin (*22*).

Vinculin and metavinculin oligomerization was first observed using rotary-shadowed EM (*95*). Tetramers and higher-order oligomers were observed, forming head-head and tail-tail interactions. While Vh-Vh interactions have not been significantly studied, much has been done to elucidate the oligomerization reactions of Vt. At high concentrations in solution, Vt dimerizes in the absence of ligand. The approximate K_d for the formation of the dimer was determined to be 336 μM (*93*). This dimer is often referred to as the "self-association" or "native" dimer (*93*), and was first observed in the Vt crystal structure (*72*). It has since been observed by NMR (*88*) and electron paramagnetic resonance (EPR) (*96*). The structural restraints provided by EPR result in a structure very similar to that observed by crystallography, with some small changes in the positions of helix 1 and helix 5 (*96*). This dimer is mediated through a hydrophobic,

asymmetric interaction between helices 4 and 5 of both Vt molecules (*72, 93,96*), with the two molecules rotated 90° with respect to each other. There are no large-scale conformational changes associated with this dimer. The propensity of Vt to self-associate into this structure often leads to difficulty in experimental design. The percentage of Vt in solution that exists in dimeric form must be accounted for when interpreting results, especially for experiments requiring high protein concentrations greater than 100 μM. Also, in the presence of crosslinking reagents, Vt can form multiple high molecular weight bands indicating a number of different oligomers may be present (*39*).

The self-association dimer is the most-understood Vt oligomer from a structural perspective, but is also the least relevant. In the cell, an abundance of Vt ligands and the presence of Vh mean the concentration of "free" Vt will be very low. When coupled with the weak K_d of the self-association dimer, it is unlikely that this dimer is physiologically relevant. Rather, the hydrophobic interface may be critical for interaction of Vt with its ligands.

ii. Actin-Induced Vinculin Dimer

Vinculin's ability to crosslink F-actin was first observed by Jockusch and Isenberg in 1981, through the "paracrystalline packing" of parallel actin filaments in a tight bundle (*97*).This packing was different than that observed from crosslinking by α-actinin, which bundles actin filaments by forming bridges between the filaments. Proteins that bundle F-actin must do so either through multiple binding sites that permit coordination of two separate filaments or by homodimerization, with each monomer bound to one filament. Vinculin bundles F-actin through the latter mechanism (*90, 91*).As with F-actin binding, the ability of vinculin to bundle F-actin resides in Vt (*98*). No significant changes in bundle morphology were observed between Vt and

larger constructs containing the entire protein (*97*) or residues 154–1066 (*99*), suggesting that either the vinculin head is distant enough or the proline-rich linker is flexible enough to avoid interference of the vinculin head with the actin bundle.

While it is now known that Vt crosslinks F-actin through formation of a Vt dimer, the structure of this dimer is unknown. Complicating the matter is that this dimer is not formed in the absence of F-actin (*90*). It is currently believed that Vt undergoes a conformational change upon binding to F-actin that allows for dimer formation. Previous studies have supported this hypothesis with proteolytic cleavage(*72*), fluorescence (*72*), FRET (*74*), and crosslinking experiments (*39, 90*). The proteolysis studies showed an increase in susceptibility in the strap and the H1-H2 loop to proteases in the presence of F-actin (*72*), while the FRET experiment predicts an increase in the distance between the strap and the C-terminal hairpin (*74*). It was previously hypothesized that the helix bundle "unfurled" upon binding F-actin, resulting in the exposure of the "cryptic" dimerization site (*90*). However, using negative-stain EM, Janssen *et al*. show that there is no significant unfurling of the helix bundle (*91*). Instead, clashes between the N-terminal strap and C-terminus indicate that one or both of these termini change conformation upon association of Vt with actin(*91*). As presented in Chapter II, the C-terminal hairpin has recently been shown to be required for actin bundling (*39*), suggesting that it may form a new interaction with the opposite Vt monomer. Moreover, removal of the N-terminal strap slightly increases the F-actin bundling of Vt, suggesting that it must change conformation to expose a site important for dimer formation (*39*). Together, these studies point to the existence of an actin-dependent conformational change in Vt, likely in the N-terminal strap and C-terminus (which are believed to be conformationally flexible (*72*)), that is important for actin-induced Vt dimer formation and enables F-actin bundling.

While a structure for the actin-induced dimer is lacking, the current data provide a good starting point for model generation. The increase in proteolytic susceptibility (*72*), the FRET studies (*74*), and the differences in the structure of the tail in metavinculin (*29*) suggest that the interactions between the strap and C-terminus are weakened upon binding of the tail to F-actin, resulting in the release of the strap from the helix bundle. This frees the C-terminal hairpin, essential for formation of the dimer (*39*), to interact with the other Vt molecule. The hydrophobicity of the hairpin and the relative orientation of the two tails (*91*) suggests that the hairpin inserts itself into the interior helix bundle of the other tail. This hydrophobic interaction mediated through the C-terminal hairpin is likely the main force behind dimerization, as removal of these residues eliminates actin bundling by Vt(*39*). The specific orientation of the dimerand the resulting F-actin geometry are likely influenced by other interactions, probably involving the helix bundle.

While recent evidence points to the surface where the F-actin/Vt interaction occurs, little is known on how binding to F-actin causes this conformational change to expose the cryptic dimer. A possible scenario is that the conformational change that occurs in Vt upon binding to F-actin is allosteric (*72, 74,90*). Addressing these holes in our understanding of vinculin's ability to bundle F-actin will allow us to better identify the biological consequences associated with vinculin-mediated F-actin bundling and may further clarify the role vinculin in cells and disease.

5. Phosphorylation of Vinculin

Vinculin was one of the first substrates found to be phosphorylated by the tyrosine kinase, Src (*100*), and has also been found to be phosphorylated by PKCα(*65, 101*). While it has been long known which kinases and at what sites they phosphorylate vinculin, how phosphorylation on regulates vinculin is poorly understood.

There have been three tyrosine residues identified in vinculin that can be phosphorylated. Y100, a residue exposed in Vh, Y822 in D4, and Y1065 in Vt that resides within the C-terminal hairpin and is buried by the proline-rich linker in the full-length protein (Figure 1.1). While it has been proposed that all three residues can be phosphorylated by Src, only Y100 and Y1065 have been shown to be directly phosphorylated by Src and the kinase that phosphorylates Y822 has yet to be identified(*102*). Recent studies have started to investigate the purpose of these phosphorylation sites. Y822 has been shown to modulate the interaction between FAK and paxillin which in turn regulates apoptosis; although a non-phosphorylatable variant, Y822F, does not restore the sensitivity to apoptosis in vinculin KO cells (*9*). Cells expressing non-phosphorylatable variants, Y100F and Y1065F, display defects in cell spreading, but only in the presence of the double mutation(*102*). Y1065F has additionally been shown to exert lower cell traction forces and slower exchange rates from FAs. While the phospho-mimetic, Y1065E has a higher exchange rate from FAs(*103*). Phosphorylation at Y1065 has also been implicated in helping to anchoring vinculin to the membrane(*87*), although exactly how this occurs is uncertain. These studies implicate Y1065 in modulating FA dynamics, although the extent of its regulation remains to be elucidated. Additional work with a phospho-specific antibody for Y1065 reveals that higher levels of phosphorylation are detected in focal complexes (FCX) (*104*).However, when lysates from MEFs, Vin -/- MEFs, or cell re-expressing WT- or Y1065F vinculin in Vin -/- MEFs are probed with the phospho-specific Y1065 antibody used by Möhl *et al*., a band is detected in the Vin-/- MEFs despite the lack of vinculin and in the presence of Y1065F, which should not be phosphorylatable (Figure 1.4A). Furthermore, when lysates from rat embryo fibroblasts are probed with the phospho-specific Y1065 antibody, multiple bands are detected, indicating a lack of specificity with this antibody (Figure 1.4B).

In addition to its possible role in FA dynamics, phosphorylation of Vt reduces its affinity for Vh as shown by pulldown assays(*102*). Phosphorylation at Y1065 also implicates its role in regulating the binding of the Arp2/3 complex as prevention of phosphorylation using the Y1065F variant, loses its ability to bind to Arp2/3 complex(*105*). The ability of Y1065 to regulate the binding status of Arp2/3 is supported by the vinculin crystal structure where Y1065 has hydrogen bonds with P878, the specific binding site identified that allows for Arp2/3 binding to vinculin(*62*). The studies that showed Y1065F can disrupt binding to the Arp2/3 complex also showed similar results are observed in the presence of the Y100F mutant; the reason behind this remains to be understood(*105*). However if the phosphorylation state of Y1065 regulates the binding of the Arp2/3 complex, this could explain the phenotypes observed (decreased cell spreading and lower traction forces exerted) when phosphorylation is prevented. Although some observations made *in vitro*, specifically the impact of phosphorylation of Vh/Vt interactions, are a little harder to explain given what has been observed in cells. If phosphorylation at Y1065 was needed for vinculin activation, then a higher proportion of phosphorylated vinculin would be observed in FAs; however, in transformed cells overexpressing v-Src, only 2% of the total vinculin is phosphorylated even though there is a significantly high proportion of active vinculin in the cells(*100, 102*). It could be that Y1065 helps in activation since vinculin has shown to be in multiple activation states in FAs(*74*).

Using molecular dynamic simulations, Golji*et al*. have proposed a mechanism for vinculin activation that utilizes the multiple phosphorylation sites in vinculin(*106*). In this model, it is suggested that phosphorylation at S1033 would prime vinculin for activation, although phosphorylation at this site in cells has yet to be detected. This study also revealed that phosphorylation at Y1065 would make new contacts with K881 and the authors conclude it is

likely that Y1065 does not affect FA formation through its activation status, but rather by impacting binding to PIP_2 or F-actin based on evidence from previous reports. Based on these contrasting reports, the impact of phosphorylation at Y1065 should be more closely examined and is the focus of Chapter IV.

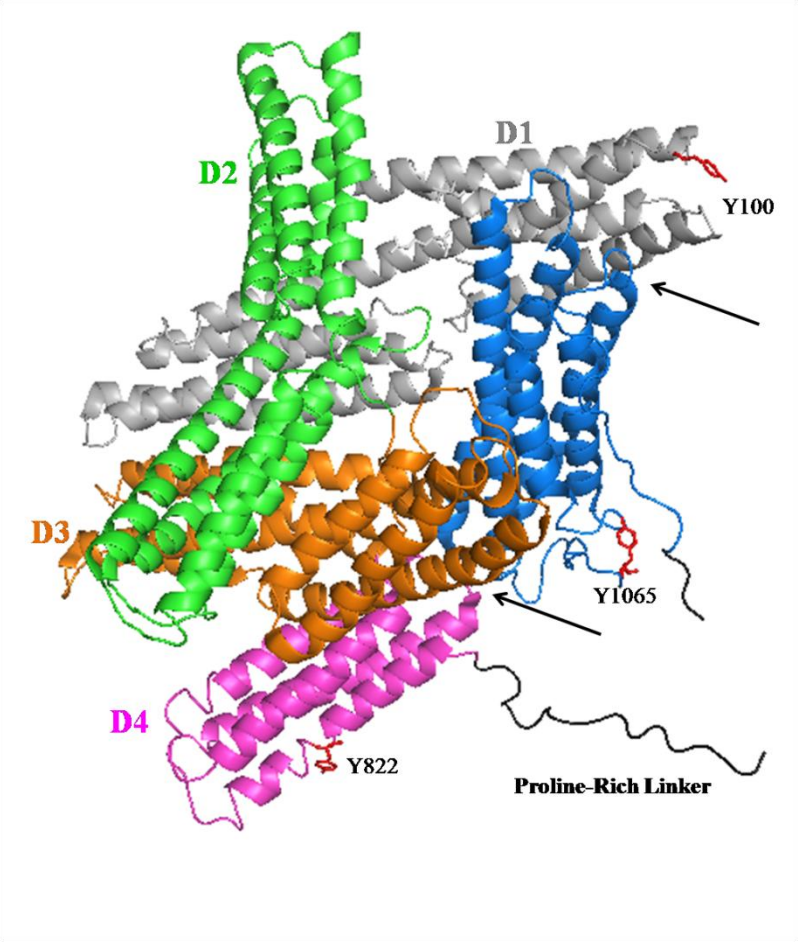

Figure 1.1. Crystal Structure of Full-Length Vinculin. The full-length crystal structure of vinculin (PDB ID 1ST6) is comprised of 8 α-helical bundles that are organized into tandem pairs. The first three tandem pairs in D1 (grey), D2 (green), and D3 (orange) contain two, four helical bundles that are connected by one long helix to D4 (magenta). Domains D1-D4 (residues 1-855) comprises the head domain (Vh). The flexible proline-rich linker (black) connects D4 to the vinculin tail (Vt; blue). In its auto-inhibited state as shown above, Vt makes contacts with D1, D3, and D4. In vinculin, there are three known tyrosine phosphorylation sites (red), Y100 in D1, Y822 in D4, and Y1065 in Vt.

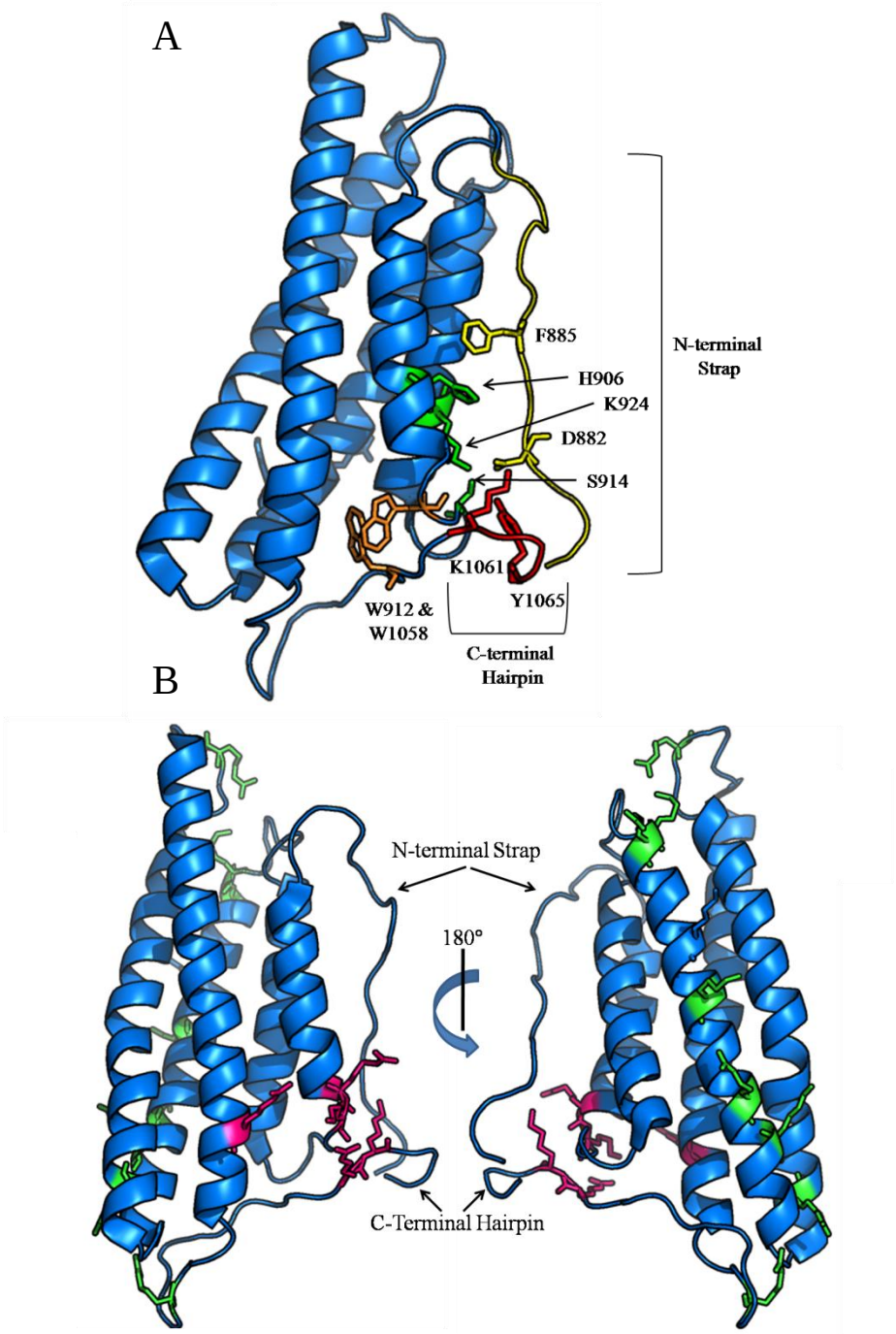

Figure 1.2. The Vinculin Tail Domain.(A) The tail domain (residues 879-1066; PDB ID IST6) is a bundle of five helices, with a flexible N-terminal strap (yellow) and C-terminal hairpin (red).

Interactions between the termini and the helical bundle are labeled, including W1058, K1061, and Y1065 in the C-terminus, and D882 and F885 in the N-terminal strap. (**B**) The basic ladder (green) and basic collar (magenta) are highlighted on structure.

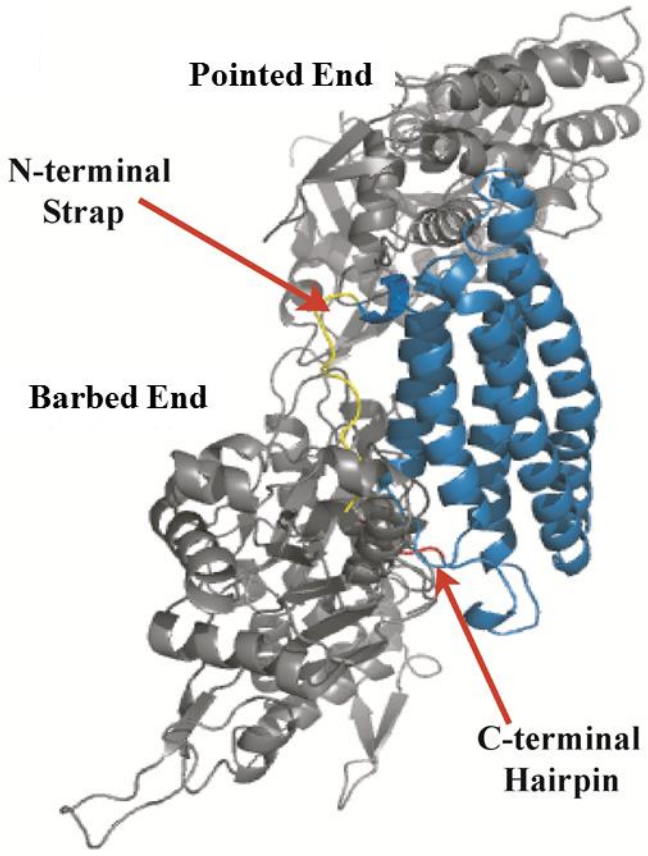

Figure 1.3. Previous F-actin binding model proposed by Janssen *et al*. According to the Janssen model, the C-terminal hairpin (red) and N-terminal strap (yellow) point into the F-actin interface (*91*). However, the Janssen model may require further validation given the resolution of the micrograph, multiple conformational clashes between Vt and F-actin, and contrasting data that has arisen indicating that the C-terminal hairpin is necessary for bundle formation. Hence, given our findings, a refined or alternative model for this critical interaction should lead to more specific tools to study the function of the vinculin/F-actin interaction.

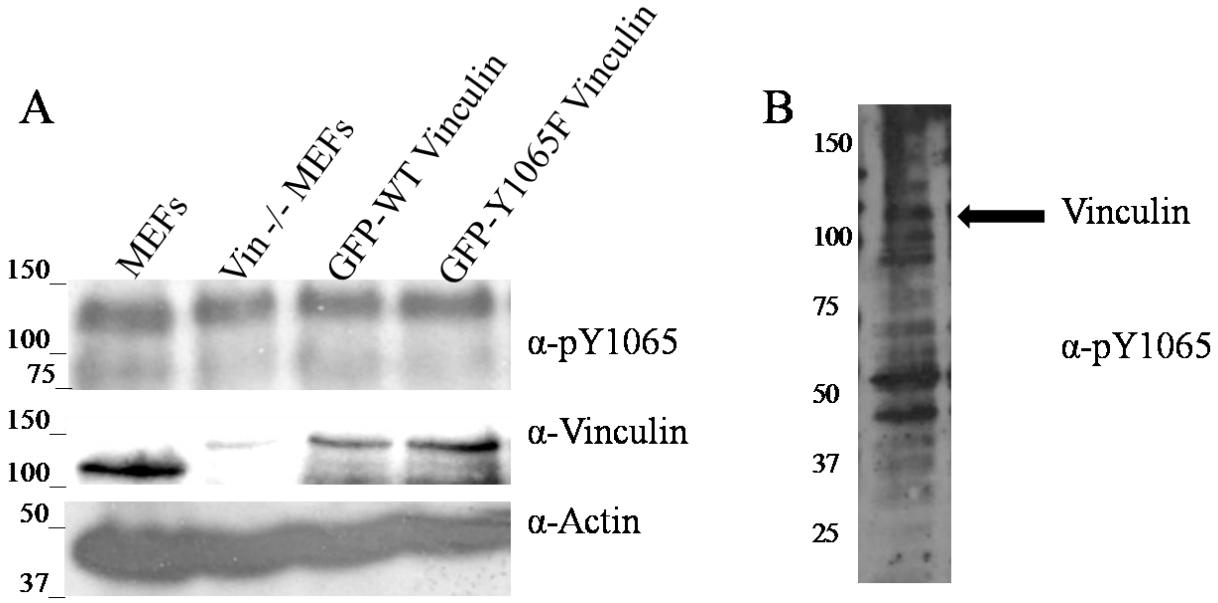

Figure 1.4. Lack of specificity with pY1065 antibody. (A) Probing lysates from either MEFs, Vin-/- MEFs, or Vin-/- MEFs re-expressing either WT- or Y1065F-vinculin shows that the commercially available phospho-specific antibody for Y1065 still recognizes protein bands despite a lack of vinculin or mutation of Y1065. (B) Furthermore, probing lysates from rat embryo fibroblasts with the phospho-specific Y1065 antibody shows that multiple proteins are recognized.

II. The Vinculin C-terminal Hairpin Mediates F-actin Bundle Formation, Focal Adhesion, and Cell Mechanical Properties

A. Overview

Vinculin is an essential and highly conserved cell adhesion protein, found at both focal adhesions and adherens junctions, where it couples integrins or cadherins to the actin cytoskeleton. Vinculin is involved in controlling cell shape, motility and cell survival, and has more recently been shown to play a role in force transduction. The tail domain of vinculin (Vt) contains determinants necessary for binding and bundling of actin filaments. Actin binding to Vt has been proposed to induce formation of a Vt dimer that is necessary for crosslinking actin filaments. Results from this study provide additional support for actin-induced Vt self-association. Moreover, the actin-induced Vt dimer appears distinct from the dimer formed in the absence of actin. To better characterize the role of the Vt strap and carboxyl terminus (CT) in actin binding, Vt self-association and actin bundling, we employed smaller amino terminal (NT) and CT deletions that do not perturb the structural integrity of Vt. While both NT and CT deletions retain actin binding, removal of the CT hairpin (1061-1066) selectively impairs actin bundling *in vitro*. Moreover, expression of vinculin lacking the CT hairpin in vinculin knockout murine embryonic fibroblasts affects the number of focal adhesions formed, cell spreading as well as cellular stiffening in response to mechanical force.

B. Introduction

The ability of cells to sense and respond to environmental cues such as mechanical forces is critical for multiple cellular processes including embryogenesis and wound healing (*107-109*). To transmit forces across the cell membrane in both directions, the actin cytoskeleton couples transmembrane receptors (integrin or cadherin), through points of cell adhesion consisting of multiple protein complexes that form cell - extracellular matrix (focal adhesions) and cell-cell (adherens junctions) contacts (*109, 110*). Vinculin is an abundant protein found in both focal adhesions and adherens junctions, and plays a key role in regulating cell morphology, cell motility and force transduction (*69, 108*). Vinculin is essential during development as vinculin knockout (KO) mouse embryos fail to survive beyond day E10 with extensive defects in myocardial and endocardial structures (*2*). Consistent with a role in muscle structure, vinculin KO mice are predisposed to stress-induced cardiomyopathy (*6*). Moreover, mutations and deletions in the tail domain of metavinculin, a splice isoform of vinculin, are associated with dilated cardiomyopathy (*27, 111,112*). Vinculin also possesses tumor suppressor properties as vinculin KO cells are less adherent, have a rounded morphology, reduced lamellipodial stability, increased motility (*2, 4*), and are resistant to apoptosis and anoikis (*9*).

Vinculin is a highly conserved cytoskeletal protein which has 1066 residues and contains a globular head, a flexible proline-rich linker and a tail domain (*71*). Each discrete vinculin domain recognizes multiple binding partners: the vinculin head (Vh) binds to talin, α-actinin and IpaA (*113-115*); the proline-rich linker interacts with VASP, CAP/ponsin, vinexin and the Arp2/3 complex (*58, 59, 61, 62*); the vinculin tail (Vt) associates with filamentous actin (F-actin), phosphatidylinositol (4,5)-bisphosphate (PIP_2) and paxillin (*64, 66, 67*). In the autoinhibitory form of vinculin, tight intramolecular interactions between Vh and Vt occlude

binding to most of its ligands (*71*). Vinculin becomes activated upon release of autoinhibitory Vh/Vt interactions, leading to recruitment and formation of multiprotein adhesion complexes (*73, 76, 83,116*). When activated at focal adhesions (FAs) (*75*), vinculin serves as a mechanotransducer because it helps establish the link between membrane associated integrins and the cytoskeleton through its association with talin and F-actin. Vinculin interacts with a number of cell adhesion proteins, acidic phospholipids and can be phosphorylated by both tyrosine and serine/threonine kinases. However, it is currently unclear how these interactions and covalent modifications, contribute to its role in regulating cell morphology, motility, and cell survival.

The structure of full length vinculin was solved by X-ray crystallography (pdbs: 1ST6, 1TR2), and found to possess an all helical fold (*71, 117*). Vinculin contains a large 90 kDa Vh domain comprised of helical bundles and is linked to Vt via a proline-rich region. The proline-rich region is likely to be unstructured and/or dynamic as it lacks electron density in the crystal structures of full length vinculin. Vt is comprised of an antiparallel 5 helix bundle that contains an N-terminal strap region (NT, residues 879-892) and a C-terminal arm (CT, residues 1051-1066) that forms interactions with the core helix bundle. The structure of the isolated Vt domain was also solved independently by X-ray crystallography (pdb: 1QKR) (*72*). Although the Vt domain specifically interacts with actin and acidic phospholipids, binding to these ligands is significantly reduced in the context of full length vinculin, as intramolecular interactions between Vh and Vt partially mask their association with Vt. However, as the structure of the isolated tail domain is similar to its structure within the full length protein, a number of studies investigating Vt/ligand interactions have been conducted using the isolated Vt domain, as this is

believed to be a good model of Vt/ligand interactions that occur when Vt is freed from Vh upon activation.

Models for how Vt interacts and bundles F-actin have been proposed. For example, Johnson *et al*. proposed that actin association with Vt promotes a conformational change in Vt that exposes a cryptic dimerization site that promotes actin filament bundling (*90*). In a more recent study combining electron microscopy, computational docking and mutagenesis approaches, Janssen *et al*. proposed a model for the Vt/F-actin complex (*91*) in which F-actin associates through two distinct binding sites on Vt, with site 1 containing residues in helices 2 and 3 of Vt and site 2 comprising a binding interface from helices 3, 4 and the CT. Moreover, results obtained from deletion mutagenesis studies indicate that the NT and CT of Vt have opposing roles in actin bundling. While removal of the NT strap impaired actin bundling, deletion of the CT enhanced the ability of Vt to bundle actin filaments (*91*). However, large deletions within globular proteins can affect their structural integrity. In fact, the CT of vinculin forms contacts with both the strap and the helix bundle, and it has been previously shown that a Vt variant (Vt ΔC, 1052-1066) containing a fifteen amino acid CT deletion alters NMR spectral properties, reduces stability and makes Vt ΔC more susceptible to proteolytic degradation (*79, 88*).

Hence, we made smaller deletions in the NT and CT of Vt that do not significantly alter Vt structure, and have assessed actin binding and bundling properties of these mutants. Contrary to previous results, our studies indicate that the CT hairpin, rather than the NT strap is important for F-actin bundling *in vitro*. We also conducted cross-linking studies on Vt in the presence and absence of actin, and results from these studies provide additional support for formation of an actin-induced Vt dimer that is distinct from a dimer that can be formed in the absence of actin.

Further, we investigated the effect of vinculin CT hairpin deletion on FA morphology and mechanical properties in vinculin KO murine embryonic fibroblasts (Vin -/- MEFs). Our results demonstrate that deletion of the CT hairpin affects the number of focal adhesions and alters its response to mechanical forces (*118*).

C. Materials and Methods

1. Vinculin tail protein expression and purification

The tail domain of chicken vinculin (Vt) containing residues 879-1066 was cloned into a pET15b vector (Novagen, Madison, WI) (*88*). Several deletion variants were generated from this Vt construct, including two Vt NT strap deletions (a five amino acid strap deletion (884-1066 (ΔN5)) and a full strap deletion (893-1066 (Δstrap)), and three CT deletion variants (879-1061 (ΔC5), 879-1064 (ΔC2) and 879-1065 (ΔC1)). All Vt variants were generated using QuikChange site-directed mutagenesis (Stratagene, La Jolla, CA), with sequences verified by DNA sequencing. Vinculin protein expression and purification have been reported previously (*88*). Briefly, Vt plasmids were transformed into *E. Coli* strain BL21(DE3)RIPL. Cells were grown either in Lysogeny Broth rich media or M9 minimal media with $^{15}NH_4Cl$ as the sole nitrogen source at 37 °C to an OD_{600} of 0.6. The cell cultures were cooled to 18 °C before adding isopropyl β-D-1-thiogalactopyranoside to a final concentration of 0.5 mM to induce Vt expression overnight. Cells were then pelleted by centrifugation at 5,800 X g for 30 min and re-suspended in the lysis buffer (20 mM Tris, 150 mM NaCl, 5 mM imidazole, 2 mM β-mercaptoethanol (BME), pH 7.4) before sonication. The cell lysate was then clarified at 25,000 X g for 1 h, and the supernatant was loaded onto a nickel (Ni) affinity column (Qiagen,

Germantown, MD) and washed twice with an Ni wash buffer (20 mM Tris, 150 mM NaCl, 60 mM Imidazole, 5 mM BME, pH 7.5). Histidine (his)-tagged Vt protein was then eluted with a Ni elution buffer (20 mM Tris, 150 mM NaCl, 500 mM imidazole, 5 mM BME, pH 7.5). The his-tag was removed by addition of thrombin (Sigma, St. Louis, MO), and further purified by cation-exchange (Hiprep SP XL 16/10) fast protein liquid chromatography (GE Healthcare, Piscataway, NJ). All Vt variants were examined by SDS-PAGE gel to assess purity and protein integrity before being employed for biochemical assays.

2. Actin co-sedimentation assay

The actin binding and bundling properties of the Vt variants were assessed using an adapted actin co-sedimentation assay (*119*). Briefly, 4.6 mg/ml monomeric actin (G-actin) purified from rabbit muscle acetone powder (Pel-Freez Biologicals, Rogers, AR) was polymerized with an equal volume of 2X actin polymerization buffer (20 mM Tris, 200 mM KCl, 5 mM $MgCl_2$, 4 mM dithiothreitol (DTT), pH 7.5) at room temperature for 30 min. To assess binding of the Vt variants with F-actin, a 100 µl sample in 1X actin polymerization buffer containing actin at concentrations ranging from 0-30 µM and 10 µM Vt protein was incubated at room temperature for 1 h. It should be noted that the A/V ratio was determined based on the G-actin concentration, given difficulties associated with quantifying F-actin concentration due to the heterogeneity of F-actin polymers. The samples were centrifuged at high speed (184,200 X g) on a Beckman-Coulter TLA 100 rotor for 30 min at 25 °C. For bundling assays, a 100 µl sample in 1X actin polymerization buffer containing 20 µM actin and 10 µM Vt protein was incubated at room temperature for 1 h. Samples containing F-actin bundles were obtained by careful extraction of the supernatant upon low speed centrifugation (5,000 X g). The pellet was then re-suspended in 100 µl 0.1% SDS buffer (0.1% SDS, 25 mM glycine and 25 mM Tris, pH 8.3).

Actin and Vt protein contained in both the supernatant and solubilized pellet were separated using 15% SDS-PAGE gels. Actin and Vt proteins in both samples were quantified using the densitometry software package Alpha EaseFC (Alpha Innotech, San Leandro, CA). Actin binding properties of Vt variants are reported in percentage

$$\%Vt\ binding = \frac{Vt_{denso\ ,pellet}}{Vt_{denso\ ,pellet} + Vt_{denso\ ,supernatant}}$$

Where $Vt_{denso\ ,pellet}$ is the densitometry reading of Vt pelleted at 184,200 X g while$Vt_{denso\ ,supernatant}$ is the densitometry reading of Vt retained in the supernatant. Actin bundling properties of Vt variants are calculated as follows:

$\%F\ actin\ bundled = \frac{Actin_{\ denso\ ,pellet}}{Actin_{\ denso\ ,pellet} + Actin_{\ denso\ ,supernatant}}$Where $Actin_{denso\ ,pellet}$ is the densitometry reading of actin pelleted at 5,000 X g while $Actin_{denso\ ,supernatant}$ is the densitometry reading of actin retained in the supernatant.

3. Fluorescence microscopy of F-actin bundles

F-actin bundles induced by the addition of WT or VtΔC5, were visualized using fluorescence microscopy, as previously described (*119*). Samples were prepared following conditions described for the actin bundling assay. Briefly, 20 µM pre-polymerized actin was incubated alone or with 10 µM Vt proteins (WT Vt or Vt ΔC5) at room temperature for 1 h. The mixture was then diluted 20 X with 1X actin polymerization buffer (10 mM Tris, 100 mM KCl, 2.5 mM $MgCl_2$, 2 mM DTT), pH 7.5. Alexa Fluoro-488 phalloidin (Invitrogen, Carlsbad, CA) was added to the mixture to a final concentration of 1.5 µM and then incubated for 5 minutes at room temperature. The sample was diluted to an actin concentration of 50 nM. Five microliter sample aliquots were placed on a glass slide and covered with a glass coverslip. Fluorescence

images were acquired on a Zeiss axiovert 200M microscope equipped with a 60 X objective lens and a Hamamatsu ORCA-ERAG digital camera.

4. NMR spectroscopy

^{15}N-enriched Vt samples were exchanged into NMR buffer (10 mM potassium phosphate, 50 mM NaCl, 0.1 % NaN_3, 2 mM DTT, pH 5.5) and concentrated to 0.3 mM with 10 % D_2O added. 2D ^{1}H-^{15}N Heteronuclear Single Quantum Coherence (HSQC) NMR spectra were acquired on a Varian INOVA 700 MHz spectrometer at 37 °C (*120*). NMR data were processed with NMRPipe (*121*) and analyzed using NMRViewJ (*122*).

5. Chemical cross-linking of Vt proteins

Chemical cross-linking of Vt in the presence and absence of actin was carried out using a procedure similar to that described by Johnson *et al*(*90*). However, instead of using Disuccinimidyl suberate (DSS), Bis[sulfosuccinimidyl] suberate (BS3, Thermo Scientific, Rockford, IL), a water soluble DSS analog, was employed. In the cross-linking reactions, freshly purified Vt proteins were buffer exchanged into a cross-linking sample buffer (10 mM sodium phosphate, 100 mM NaCl, 0.02% NaN_3, pH 7.5). Actin was polymerized as described in the actin co-sedimentation assay. Vt proteins (2.5 µM) were mixed with 0-10 µM actin in the cross-linking reaction buffer (2 mM $NaHCO_3$, 100 mM NaCl, 2 mM $MgCl_2$, 0.2 mM $CaCl_2$, 0.2 mM ATP, 0.02 % NaN_3, pH 7.6). Cross-linking reactions were carried out by adding BS3 to a final concentration of 25 µM. After incubation at room temperature for 40 min, the cross-linking reaction was quenched with 1M Tris (pH 7.5) to a final concentration of 50 mM Tris. The cross-linked products were separated by either 7% tris-acetate gradient gels (Invitrogen) or 15% SDS-PAGE gel followed by western blot analysis. Vt protein bands were detected using a rabbit anti-

chicken Vt antibody (*90*), a gift from Dr. Susan Craig (John Hopkins University), and HRP-conjugated anti-rabbit IgG (Promega, Madison, WI). Actin containing bands were detected using a rabbit anti-actin polyclonal antibody (Sigma Life Science, St. Louis, MO).

6. Cell culture

Vinculin-null murine embryo fibroblasts (Vin -/-) (6) were obtained from Dr. Eileen Adamson (Burnham Institute, La Jolla, CA) and were grown in Dulbecco's modified Eagle's medium (DMEM; Invitrogen) supplemented with 10 % fetal bovine serum (Sigma) and antibiotic-antimycotic solution (Sigma).

7. DNA constructs and transfection

GFP-tagged full length chicken vinculin (1-1066) plasmid in pGZ21XdZ vector was obtained from Dr. Kenneth Yamada (NIH). The ΔC5 variant of GFP vinculin was generated using a QuikChange site-directed mutagenesis kit (Stratagene) and verified by DNA sequencing. Cells were transfected with vinculin expression constructs using Lipofectamine (Invitrogen) and Plus Reagent (Invitrogen) according to manufacturer's protocol and examined 48 hours following transfection.

8. Adhesion site analysis

Cells were seeded onto glass coverslips coated with fibronectin (FN) (50 µg/ml). After 120 min, cells were washed with phosphate buffered saline (PBS), fixed in phosphate-buffered 4 % paraformaldehyde for 15 min, permeabilized in 0.3% Triton X-100 for 10 min, blocked for 10 min in 5 % bovine serum albumin and incubated with Alexa Fluoro 594-conjugated phalloidin (Molecular Probes) for 30 minutes. Immunofluorescence images were taken with a Zeiss axiovert 200M microscope equipped with a Hamamatsu ORCA-ERAG digital camera and

Metamorph workstation (Universal Imaging Corp.). A previously described method was adapted to identify and quantify the properties of the vinculin stained adhesions (*123*). This method applies a high pass filter to the images and applies a user-specified threshold to identify adhesions. We found that the watershed-based segmentation method proposed in (*123*) was unnecessary for our application, instead objects connected in a four-pixel neighborhood were assigned unique adhesion labels. Adhesions touching the edge of the field of view were removed and any holes in individual adhesions were filled. Finally, adhesion sizes and the number of adhesions per image were counted.

9. Force microscopy

Three dimensional force microscopy (3DFM) (*118*)was used for applying controlled and precise 60-100 pN local force to the magnetic beads. Tosyl-activated magnetic dynabeads (2.8 μm, Invitrogen) were washed with phosphate buffer and incubated for 24 h with FN at 37 °C. After three washes with PBS, the beads were sonicated and incubated with cells for 40 min. Upon force application, bead displacements were recorded with high speed video camera (Jai Pulnix, San Jose, CA) and tracked using Video Spot Tracker software developed by the Center for Computer Integrated Systems for Microscopy and Manipulation at the University of North Carolina – Chapel Hill (http://cismm.cs.unc.edu). The 3DFM system was calibrated prior to experiments using a fluid of known viscosity. Beads that showed displacements less than 10 nm (detection resolution of the 3DFM) were not selected for analysis. Custom Matlab scripts were used to calculate the creep compliance J_{max}, also referred to as deformability, which is defined as the average time dependent deformation normalized by the constant stress applied:

$$J_{\max} = r_{\max} \Big/ F \times 6\pi a$$

wherer_{max} is the displacement of the bead due to an applied force, F and *a* is the radius of the bead. Each compliance curve was then fit to a Jeffrey's (modified Kelvin-Vogit) model for viscoelastic materials (*124, 125*). Stiffness was reported as the value of k in Pa. Subsequent pulses were fit in the same manner and the average k for each cell type and pulse number was obtained and reported as mean ± standard error of the mean (SEM). All statistical analyses, including two-tailed Student's t-test for p values, were performed in Microsoft Excel.

D. Results

The structure of the chicken Vt domain has been solved by X-ray crystallography (*72*), and is comprised of a 5 helix bundle fold containing both NT and CT extensions that form contacts with the helix bundle. The NT extension (residues 879-892), termed 'strap', packs against an interface formed between Vt helices 1, 2 and the CT hairpin. Johnson *et al*. (*90*)performed chemical cross-linking studies on Vt in the absence and presence of F-actin using a Vt construct with a partial deletion in the strap (884-1066), and proposed a model in which actin binding to Vt induces a conformational change in Vt that promotes Vt dimerization and F-actin bundling. Moreover, results obtained by Janssen *et al*. indicated that the strap region of Vt was important for F-actin induced Vt dimerization, as removal of the strap (893-1066) significantly reduced actin bundling efficiency by ~60 % (*91*). On the other hand, removal of 15 CT amino acids (VtΔC), was found to increase bundling by 23 %. Based on these results, the authors suggested that the Vt CT may act to obstruct actin-mediated Vt dimer formation and actin bundling. However, the CT of vinculin forms contacts with the strap and the helix bundle, and it has been previously shown that VtΔC alters NMR spectral properties, reduces stability and is more susceptible to proteolytic degradation (*79, 88*). As the study from Janssen and co-

workers focused on large deletions (13-15 amino acid) of the NT and CT of Vt that could potentially alter the structural integrity of the protein, we conducted actin binding and bundling analyses with smaller deletion variants of Vt.

1. Deletion of the Vt strap does not affect actin binding and bundling.

We first compared actin bundling properties of WT Vt (879-1066) with the Vt variant that lacks the strap (Vt Δstrap, 893-1066) as well as a smaller five amino acid NT deletion mutant (Vt ΔN5, 884-1066). While actin binding and bundling assays on vinculin have been reported with different actin/vinculin (A/V) molar ratios (*90, 91, 119, 126*), this ratio is an important consideration, since a low A/V ratio will limit the amount of the Vt dimer induced in the presence of F-actin and consequently the amount of actin bundling. Therefore, we have employed an A/V ratio in our actin bundling experiments which results in saturation or close to saturation binding of Vt to actin. According to the structure based model of the Vt/actin complex, one Vt molecule binds to two adjacent actin molecules located on the same actin filament (*91*). Given this model, we expect that an A/V ratio of 2 will saturate the F-actin binding sites on Vt, assuming all of the G-actin polymerizes into functional F-actin polymers. We therefore screened A/V ratios from 0.5 up to 4 while keeping WT Vt concentration constant (10 μM), with quantification of the A/V ratio described in the Experimental Procedure section. The amount of Vt associated with F-actin at various A/V ratios is illustrated in Figure 2.1A. Consistent with the model of Janssen *et al.*(*91*), we find that most of the Vt associates with F-actin at an A/V ratio of 2 (actin concentration: 20 μM), with a small increase from 60 to 66% observed at A/V ratios of 4.

To assess the role of the Vt NT strap in actin binding, we conducted actin co-sedimentation experiments at actin concentrations of 0-30 μM and a Vt concentration of 10 μM, and compared actin binding properties of WT Vt with two NT deletion mutants, Vt ΔN5 and Vt Δstrap, with the results shown in Figure 2.1. Results from these studies (Figure 2.1B) indicate that both the partial (ΔN5) and full (Δstrap) strap deletion variants show slightly enhanced association with actin compared with WT Vt. We also examined actin bundling properties of the two NT deletion variants, at an A/V ratio of 2. As shown in Figure 2.1C, we observe similar actin bundling efficiency for both VtΔN5 and Vt Δstrapcompared to WT Vt. Importantly, previous work by our lab suggested that deletion of five NT amino acids (Vt ΔN5) from Vt does not affect the structural integrity of the Vt helix bundle (*88*). Taken together, these results suggest that neither a small deletion of the N-terminus or removal of the entire strap impairs actin binding or bundling, in contrast to previous findings (*91*).

2. Vt CT deletion mutants are impaired in actin bundling but not actin binding.

Studies by Janssen *et al*. (*91*)found that removal of 15 amino acids from the Vt CT arm (Vt ΔC), enhanced the ability of vinculin to bundle F-actin, and proposed that the Vt CT arm may require a conformational rearrangement so that it doesn't obstruct formation of the F-actin induced Vt dimer. However, the Vt CT arm forms multiple interactions with the helix bundle and strap, and removal of the Vt CT arm has been shown to alter both the structural integrity and stability of the tail domain (*88*). In particular, our previous NMR studies indicate that deletion of seven or more amino acids from the CT may alter the structural integrity of Vt, consistent with previous findings that Vt ΔC is highly sensitive to protease degradation (*79*). Therefore, we

examined the effect of smaller deletions within the CT hairpin (1061-1066) on the ability of Vt to bind and bundle F-actin.

As shown in Figure 2.2A, the CT deletion variants, Vt ΔC5 (879-1061), Vt ΔC2 (879-1064) and Vt ΔC1 (879-1065), showed similar actin binding relative to WT Vt, over an A/V ratio range of 0.5 to 3. These results indicate that smaller (five amino acids or less) amino acid deletions of the Vt C-terminus do not alter the actin binding to Vt. We then compared the ability of these deletion variants to bundle actin filaments. These analyses were conducted at an A/V ratio of 2 where WT Vt and the deletion variants show close to maximum actin binding. Our findings indicate that all three C-terminal deletion variants impair the ability of Vt to form actin bundles. As shown in Figure 2.2B, removal of one residue (Q1066) from the Vt C-terminus significantly reduces the percentage of bundled F-actin from 75% down to 55%. Removal of a second amino acid, Y1065, from Vt results in an even more dramatic reduction in actin bundling to 17%, which corresponds to a 77% drop in bundling relative to WT Vt. Further deletion of the entire hairpin (VtΔC5) leads to an additional decrease in bundling F-actin to 14%. In the absence of Vt, we observe approximately 10% of actin is bundled in our control samples (Figure 2.2B). Quantification of Vt variants associated with F-actin bundles reveals that the amount of Vt variants (Figure 2.2C) correlates with the amount of actin bundles observed in Figure 2.2B. For example, deletion of CT hairpin (VtΔC5) leads to ~78% reduction in Vt associated with F-actin bundles whereas the amount of F-actin bundles decreases by 81%. As removal of the CT hairpin severely attenuates actin bundling properties of Vt but does not affect actin binding, the Vt CT hairpin appears to play a critical role in bundling actin.

We further examined the role of the Vt CT hairpin in bundling F-actin by fluorescence microscopy. As shown in Figure 2.3A, few actin bundles are observed for pre-polymerized actin

in the absence of WT Vt. However, in the presence of WTVt (Figure 2.3B), most actin filaments are incorporated into thick actin bundles at the A/V ratio of 2. These observations agree well with our actin bundling assay results, indicating that approximately 80% of the actin filaments form bundles. However, removal of the CT hairpin precludes the ability of the mutant to bundle actin filaments in comparison to WTVt (Figure 2.3C). Only randomly oriented thin F-actin fragments are observed, corresponding to a small percentage of actin bundles (~ 14%) (Figure 2.2B). Both actin co-sedimentation assay results and the fluorescence micrograph analyses suggest that the Vt CT hairpin plays an indispensable role in bundling F-actin.

3. Vt CT deletion within the hairpin does not alter Vt conformation.

We previously conducted NMR and CD analyses on a CT deletion variant (VtΔC5) of Vt that lacks the hairpin (*88*). Results from these studies indicated that loss of five amino acids from the Vt CT, does not alter the structural integrity of the helix bundle. However, results shown in Figure 2.2B indicate that amino acids in CT hairpin play an important role in the ability of Vt to bundle F-actin filaments, as Vt ΔC1, Vt ΔC2 and Vt ΔC5 have significantly impaired actin bundling abilities compared to WT Vt, with Vt ΔC2 possessing similar bundling efficiency to Vt ΔC5. Although our previous NMR studies suggested that VtΔC5 doesn't alter the structural integrity of Vt (*88*), given the dramatic drop in actin bundling properties associated with both the Vt ΔC2 and Vt ΔC5 variants, we wanted to further compare NMR spectra of Vt ΔC2 and Vt ΔC5 with that of WT Vt. Two-dimensional ^{1}H-^{15}N HSQC NMR spectra are often employed to examine whether mutations or deletions within proteins produce localized or global perturbations by comparison of NH chemical shifts between the WT and mutant protein, as each amino acid

with the exception of proline contains a backbone amide that can be used as a site specific probe. Perturbation of a backbone amide's chemical environment will alter its chemical shift as reflected by a change in resonance position within the HSQC spectrum. Moreover, changes in peak intensity and/or line width, often reflect alterations in protein dynamic properties. If large scale perturbations in the chemical shifts and/or intensities of the NH peaks are observed, this can indicate that a mutation alters the structural or dynamic properties of the protein, but quantification and verification require additional experiments. We have previously obtained backbone NMR resonance assignments of Vt (*120*), and demonstrated that the ^{1}H-^{15}N HSQC 2D NMR spectrum of the Vt ΔC5 variant overlays well with WT Vt (*88*), indicating that deletion of the C-terminus does not alter the structural integrity of the helix bundle fold. It is therefore not surprising that the 2D ^{1}H-^{15}N HSQC spectrum of the Vt ΔC2 mutant also overlays quite well with WT Vt (Figure 2.4A), further supporting our earlier observations that deletions within the hairpin do not alter the helix bundle fold of Vt. Y1065 in the CT hairpin has a number of contacts with helix 2 (e.g.: K924) and with the loop between helices 1 and 2 (e.g. S914) (pdb: 1ST6). Additionally, residues on helix 5 form salt bridges with their counterparts on helix 2 (e.g., R1039 on helix 5 and E908 on helix 1) (*4*). Thus, removal of Y1065 may alter the chemical environment of residues on helices 1 and 2, especially those close to the CT, and subsequently, helix 5. Furthermore, it is intriguing that the amide peaks associated with K915 in the loop between helix 1 and 2, M930 in helix 2 and K1035 in helix 5, display small chemical shift changes in Vt ΔC2 compared to WT Vt, but not in Vt ΔC5, indicating that residues proximal to the CT deletion site (T1062 through W1064) may be needed for propagation of chemical shift changes to these residue (Figure 2.4A).The P1063 NH resonance is unobservable in the HSQC spectrum as it lacks a backbone amide.

To corroborate our NMR data, we also acquired CD spectra on both WTVt and Vt ΔC2 (Figure 2.4B). Both far- and near- UV spectra of WTVt and Vt ΔC2 overlay very well, suggesting that neither the secondary structure nor the tertiary structure of Vt ΔC2 is altered. Among the three tryptophan residues (W912, W1058, and W1065) in Vt, W912 located in the loop between helix 1 and 2, packs against W1058 in the C-terminus, forming a tertiary interaction (pdb:1ST6). The near- UV CD spectrum is likely dominated by Vt tryptophan residues and does not change upon deletion of the last two residues within the CT hairpin, suggesting that this tertiary interaction is unaffected. Therefore, both the NMR and CD data indicate CT deletion within the hairpin does not alter the Vt helix bundle fold.

4. Vt association with F-actin promotes Vt dimerization.

Vt has a weak propensity to dimerize at sub-millimolar concentrations (*37*). However, Johnson *et al*. detected formation of a Vt dimer in the presence of F-actin, at concentrations where the native dimer was not observed. They proposed that actin binding to Vt induces a conformational change that exposes a cryptic dimerization site, with dimer formation important for bundling of F-actin filaments (*90*). These earlier chemical cross-linking studies were performed using DSS to detect formation of the F-actin induced Vt dimer. Given our results that removal of the CT hairpin impairs actin bundling but not binding, we postulated that the CT hairpin plays an important role in the formation of the actin-induced Vt dimer. To test this hypothesis, we performed chemical cross-linking studies on WTVt in the presence and absence of F-actin. Instead of using DSS, which is hydrophobic and requires organic solvents for dissolution in aqueous solution, we employed BS3, the water soluble analogue of DSS. Similar

to DSS, BS3 forms chemical crosslinks with lysine side chains. We first added BS3 to purified WTVt and incubated the mixture at room temperature for 40 min in the absence of actin. The reaction products were monitored by western blot analysis using a Vt antibody. In the presence of BS3 (Figure 2.5A), Vt bands were observed at positions on the gel that correspond to both monomeric and dimeric forms of Vt. Densitometry quantification indicated that the dimer band accounts for ~ 22 % of total Vt in the sample. This result was not too surprising, as Vt can dimerize in solution (*37, 72*), however, with a weak affinity (K_d ~ 360 μM)(*93*). In fact, a similar dimer contact, which is located at the helix 4/5 interface, was reported (*71*). Our previous NMR studies revealed that the dimer observed by X-ray crystallography was similar to that observed by us in solution (*93*), suggesting that the Vt dimer observed in the presence of BS3 corresponds to the dimer observed by both X-ray crystallography and NMR (*71, 93, 120*). To evaluate whether actin bundling is altered by the presence of BS3, we conducted actin co-sedimentation experiments on WT Vt, Vt ΔC2, and Vt ΔC5, in the absence or presence of a water soluble crosslinker BS3. As shown in supplemental Figure 2.S1, the amount of bundled actin is essentially the same in the absence or presence of BS3, indicating that actin bundling is not artificially enhanced by the use of the cross-linking agent.

We also performed chemical cross-linking experiments in the presence of actin to assess whether the actin-induced dimer was distinct from the native dimer. For these experiments, A/V ratios over the range of 0:1 to 6:1. As shown in supplemental Figure 2.S3C, multiple higher order Vt species form in the absence of actin and the ability for vinculin to form these higher order oligomers has been previously observed(*95, 127*). Because these higher order Vt oligomers disappear with increasing actin concentrations and since Vt ΔC5 is a F-actin bundling deficient mutant, we have chosen to focus on changes in the dimer and trimer bands with increasing

concentrations of actin to see if differences are observed between WT Vt and Vt ΔC5. As shown in Figure 2.5A, WTVt forms two distinct dimer bands that are observed in the presence of actin whereas only one (upper dimer band; native dimer) exists in the absence of actin. These results suggest that the actin-induced Vt dimer is distinct from the native dimer. Intriguingly, as the A/V ratio is increased, the upper band shows a reduction in intensity whereas the lower band displays almost disappears, suggesting that in the presence of actin, the actin-induced dimer is favored. One possible explanation for these results is that the native dimer competes with the ability of actin to bind Vt and/or promote formation of the actin-induced Vt dimer. As Vt is completely saturated in the presence of excess actin, few Vt molecules are available to form the native dimer.

Interestingly, we observe a band at ~ 65 kDa in the absence and presence of actin indicating a trimeric Vt species. However, this band is not observed by western blot analysis using an anti-actin antibody (Supplemental Figure 2.S3D), suggesting that this band corresponds to a higher order Vt oligomer. Since this band forms in both the absence and presence of actin, we cannot conclude if a Vt trimer contributes towards bundling F-actin or if this is an artifact of using a crosslinker. We do observe that the intensity of the trimer band weakens with increasing actin concentrations. This could be attributed to the possibility that in the presence of excess actin, Vt is saturated and the incidence for 'native' dimer and trimer formation decreases. This coincides with our observations that with excess actin beyond an A/V ratio of 2:1, bundling efficiency decreases (Supplemental Figure 2.2).

The most notable difference between WTVt and Vt ΔC5 occurs at the corresponding dimer band. Since Vt ΔC5 shows significantly lower actin bundling ability relative to WT Vt, we expected that Vt ΔC5 would show a reduction in the Vt dimer observed upon actin binding. The

chemical cross-linking results on VtΔC5, however, are inconsistent with this prediction. Figure 2.5A shows that in the presence of actin, a distinct Vt ΔC5 dimer band emerges that is a lower molecular weight than the "native" dimer that WT Vt has been shown to form. While this could initially be attributed to a difference in length of the protein, Vt ΔC5 typically is the same molecular weight as WT Vt as shown by the monomer (Figure 2.5B) and trimer bands (Figure 2.5A). Intriguingly, the intensity of the lower actin induced Vt ΔC5 dimer band is comparable to that of the "native" dimer band, similar to that in the WT Vt (Figure 2.5A). Additionally, the lower induced Vt ΔC5 dimer band decreases in intensity at higher A/V ratios. These results suggests that not only does the lower actin induced Vt ΔC5 dimer band hold a more compact conformation than the WT Vt actin-induced dimer, but that the dimer formed by Vt ΔC5 in the presence of actin is distinct from the WT Vt actin-induced dimer and is likely the reason why Vt ΔC5 does not bundle F-actin efficiently.

5. Vinculin CT deletion affects cell adhesion.

To explore the role of the vinculin CT hairpin during cell adhesion, vinculin knockout murine embryo fibroblasts (Vin -/- MEFs) were transfected with GFP tagged WT vinculin or a CT hairpin deletion mutant (ΔC5). In Vin -/- MEFs, the transfection efficiencies and expression levels of WT and ΔC5 vinculin as determined by immunoblots were identical (data not shown). When plated onto fibronectin (FN), Vin -/- MEFs expressing the ΔC5 mutant were less spread than cells expressing full length WT vinculin (Figure 2.6 A,C). The average cell area was 1,270 ± 134 μm^2 (mean ± SEM) for the ΔC5-expressing cells and 1,968 ± 200 μm^2 for the WT (Figure 2.6C). We also observed that the Vin -/- MEFs transfected with the ΔC5 mutant formed fewer

than half of the focal adhesions (FA) (79 FAs *per* cell as median value) than cells transfected with WT vinculin (191 FAs *per* cell as median value) (Figure 2.6B). In cells expressing ΔC5 vinculin, the decrease in FAs number was associated with a slight increase in adhesion size (39 %) compared to cells expressing WT vinculin (Figure 2.6C). However, the difference in adhesion size was not statistically significant ($p = 0.22$).

6. The vinculin CT hairpin is necessary for the mechanical response to force on integrins.

Applying force on FAs either by cell-generated tension or by external forces has been shown to trigger local stiffening in cells, also called reinforcement, which has been shown to be central to many aspects of cell biology. Vinculin has been demonstrated to play an important role in force transduction (*51, 128*). To determine whether the vinculin's CT hairpin contributes to the stiffening response to force on integrins, we used magnetic tweezers to apply a controlled force on magnetic beads coated with FN. The local viscoelastic properties of the cells were determined by measuring bead displacements due to a known force induced by a magnetic field (*129*). We observed that the basal stiffness of Vin -/- MEFs transfected with ΔC5 vinculin was not significantly different from Vin -/- MEFs transfected with WT vinculin (2.6 Pa *versus* 2.2 Pa) (Figure 2.7A). When pulses of constant force were applied, we measured a local increase in spring constant of the Vin -/- MEFs transfected with WT vinculin (48 % after the second pulse) (Figure 2.7B). However, cells expressing the ΔC5 vinculin lost this stiffening response following force application (Figure 2.7B).

E. Discussion and Conclusions

Vinculin has been implicated in cell morphology and adhesion turnover as Vin -/- MEFs possess a less adherent, round morphology and increased motility (*2, 4*). Vinculin is also believed to play a critical role in sensing and transducing force. Interactions between actin and vinculin are believed to be critical for vinculin's functional properties, but the role of this interaction in regulation of cell morphology, motility and force transduction is poorly understood. Models for how vinculin binds and bundles actin have been proposed. One common feature of these models is that the tail domain of vinculin binds to F-actin through two distinct binding sites, with F-actin binding promoting a cryptic dimerization site on Vt that facilitates crosslinking of actin filaments (*90, 91*). In this study, we examined the role of the Vt NT strap and CT hairpin in actin binding and bundling. Removal of the Vt NT strap slightly increases its actin binding. However, in contrast to earlier observations (*91*), we report here that the Vt CT hairpin, rather than the NT strap region, is indispensable for F-actin bundling. In particular, removal of the CT hairpin results in significant loss of actin bundling, not actin binding, which may result from the formation of an actin-induced Vt dimer that is unable to crosslink actin filaments or possibly functional differences associated with higher order oligomers. We also observe that loss of the CT hairpin leads to reduced adhesion number, decreased cell spreading, and impaired cell stiffness responses upon applied force, suggesting that the CT hairpin plays an important role in adhesion formation and cell mechanical responses.

1. Regulatory role of the Vt CT hairpin in F-actin bundling.

Results from our studies indicate that removal of the Vt CT hairpin maintains actin binding but shows significantly impaired actin bundling, whereas removal of the Vt NT strap is

dispensable for both actin binding and bundling. We characterized three small CT hairpin deletion variants of Vt, namely Vt ΔC1, Vt ΔC2 and Vt ΔC5. All three Vt variants showed impaired bundling and reduced association of Vt with F-actin bundles, indicating that the Vt CT hairpin structure affects formation and/or function of the actin-induced Vt dimer. As F-actin binding to Vt has been proposed to expose a dimerization site in Vt important for cross-linking of F-actin filaments, we performed chemical crosslinking studies to monitor formation of the Vt dimer in the presence and absence of actin. Results from these studies indicate that the Vt dimer formed in the presence of F-actin, is distinct from native Vt dimer observed previously by X-ray crystallography and NMR (*72, 93*). Moreover, the F-actin induced Vt dimer appears to compete with the native Vt dimer, suggesting that F-actin binding or bundling interferes with formation of the native Vt dimer (Figure 2.5A, Supplemental Figure 2.3). While it is somewhat surprising that the actin induced Vt dimer bands are present for the Vt ΔC5 variant (Figure 2.5A, lower dimer band) at comparable levels to that of WT Vt, the dimer that is formed is at a lower molecular weight possibly indicating a more tightly packed conformation. Given that there is a 78% reduction in Vt ΔC5 associated with F-actin bundles, the actin-induced Vt dimer or trimer may not be competent to induce bundling of actin filaments, possibly due to geometric constraints. We carefully optimized the cross-linker concentration to detect the actin-induced Vt oligomers while reducing nonspecific cross-linking reactions. Under these conditions, we expect to see an excess of monomeric Vt, as previously reported (*90*). We also observe a decrease in the intensity of dimer and trimer bands for both WT Vt and Vt ΔC5 at higher A/V ratios. We speculate (as illustrated in Figure 2.8) that this is due to a reduction in the total number of Vt oligomer species that is able to properly form, resulting in a reduction in the number of bundled actin filaments. Although we also see a significant population of the Vt monomer remaining, it has been

previously observed that not all the Vt monomer will be incorporated into a dimer even when high amounts of a cross-linking agent are used (*90*). However, at lower concentrations similar to the amount used in this study, both monomer and dimer bands will be observed. Additionally, because actin can also be cross-linked and we use high A/V ratios in this study, it is possible that excess actin reacts with the cross-linker and contributes to the decrease in the dimer and trimer intensity we observe (Supplemental Figure 2.3D). By using a lower concentration of the cross-linking agent, we are able to differentiate between dimer and/or higher order oligomers that form specifically in the presence of actin. Previous results have indicated that Vt optimally binds to F-actin through two binding sites at an A/V ratio of 2:1 (*90*, *91*). Consistent with this model, our data shows optimal actin bundling occurs at an A/V ratio of ~2:1 with bundling efficiency decreasing at high A/V ratios (Supplemental Figure2.S2). Based on these observations, we postulate that when actin is in excess, Vt is not uniformly distributed along each filament to efficiently bundle F-actin, or rather, there is a lack in reinforcement by Vt to stably bundle actin filaments. Although we cannot distinguish whether the Vt oligomer responsible for bundling is a dimer or a trimer, we only observe differences between WT Vt and the bundling-deficient Vt ΔC5 variant, with the dimer and not the trimer bands. We are currently pursuing studies to characterize the actin-induced Vt dimer and trimer structures derived from WT Vt and CT deletion variants.

2. Vinculin CT hairpin affects focal adhesion properties.

We also demonstrate that when ΔC5 vinculin is expressed in $Vin^{-/-}$ cells, the cells have fewer, slightly larger adhesions in comparison to WT vinculin (Figure2.6B and D). In addition, cells expressing ΔC5 are smaller than cells expressing WT vinculin (Figure2.6C). Considering

the bundling deficiencies of Vt ΔC5 observed *in vitro*, cells expressing this mutant might be expected to have smaller and less stable adhesions related to possibly enhanced release of bound ΔC5 vinculin from F-actin. However, because this is the first vinculin mutant reported where actin binding is decoupled from its actin bundling capabilities, it is yet to be determined whether the phenotype observed results from the inability of vinculin to cross-link actin filaments and/or other factors. The phenotype observed could be due to overcompensation from other actin-bundling proteins. Alternatively, deletion of the CT hairpin may either alter binding of an interacting molecule that modulates focal adhesion properties or result in formation of weaker adhesions, as supported by our mechanical force data. We plan to explore whether deletion of the CT hairpin alters binding of interaction partner(s) in future studies to discern between these possibilities.

3. Vinculin CT hairpin contributes to mechanical response to force.

Due to its particular localization within the FA (*78*), vinculin plays a central role in the regulation of cell mechanics and its depletion has been shown to dramatically alter cellular rigidity (*130*). Force, either internally generated or externally applied, has been shown to trigger the recruitment of vinculin to FA (*131*, *132*), which in turn increases the linkage between actin cytoskeleton and extracellular matrix (*133*). The force sensing abilities of vinculin have also been shown to contribute to cell migration and FA stabilization (*128*). Here, we demonstrate that vinculin CT hairpin deletion does not change the basal stiffness of the cells but prevents cellular stiffening in response to force (Figure2.7). Previous work using a vinculin mutant lacking 15 CT residues similarly found that there was a reduced stiffening response to mechanical force applied to fibronectin-coated beads (*87*). In that study, it was suggested that differences in the ability of

this vinculin mutant to respond to cell mechanical forces were due to loss of its anchorage to lipids. However, our previous studies have demonstrated that deletions beyond the CT hairpin significantly disrupt the structural integrity of Vt and that deletion of the CT hairpin does not alter the ability of the vinculin tail domain to interact with phosphatidylinositol (4,5)-bisphosphate (*88*). Because the vinculin CT hairpin is critical for actin bundling *in vitro* but not for lipid association, our results suggest that vinculin-dependent actin bundling may strengthen the link between integrin-based adhesion and the actin cytoskeleton in response to force. Other bundling proteins, such as α-actinin (*134*), have also been suggested to contribute to adhesion reinforcement. However, the fact that vinculin-mediated actin bundling only alters the dynamic stiffening in response to tension and does not impact basal stiffness is surprising. Another possibility is that altered actin bundling may not be the only cause for the absence of the strengthening response observed in cells transfected with the ΔC5 mutant. Adhesion reinforcement requires a complex signaling cascade from mechanosensor stimulation to actin machinery activation and assembly. Vinculin is known to interact with many other FA components (*70*) and actin cytoskeleton regulators, such as Arp2/3 (*62*). The CT hairpin could potentially act as a scaffold and contribute to the proper subcellular localization of molecular actors involved in the dynamic cytoskeleton remodeling observed in response to force. Potentially, phosphorylation of Tyr-1065 within the CT hairpin could either affect actin bundling or regulate binding of vinculin toward unknown ligands because Src, the only kinase shown to phosphorylate this residue, has been shown to be activated in response to force. Further work is necessary to elucidate the precise molecular mechanism by which vinculin CT hairpin regulates reinforcement.

We also demonstrate that when ΔC5 vinculin is expressed in Vin -/- cells, the cells have fewer, slightly larger adhesions in comparison to WT vinculin (Figure 2.6B, D). In addition, cells expressing ΔC5 are smaller than cells expressing WT vinculin (Figure 2.6C). Considering the bundling deficiencies of Vt ΔC5 observed *in vitro*, cells expressing this mutant might be expected to have smaller and less stable adhesions related to possibly enhanced release of bound vinculin ΔC5 from F-actin. However, since this is the first vinculin mutant reported where actin binding is decoupled from its actin bundling capabilities, it is yet to be determined whether the phenotype observed results from the inability of vinculin to cross-link actin filaments and/or other factors. The phenotype observed could be due to overcompensation from other actin bundling proteins. Alternatively, deletion of the CT hairpin may either alter binding of an interacting molecule that modulates focal adhesion properties or result in formation of weaker adhesions, as supported by our mechanical force data. We plan to explore whether deletion of the CT hairpin alters binding of interaction partner(s) in future studies to discern between these possibilities.

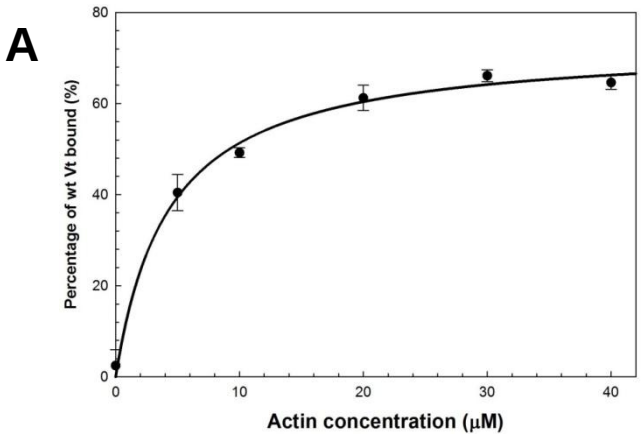
A
Percentage of wt Vt bound (%)
Actin concentration (μM)
0
20
40
60
80
0
10
20
30
40

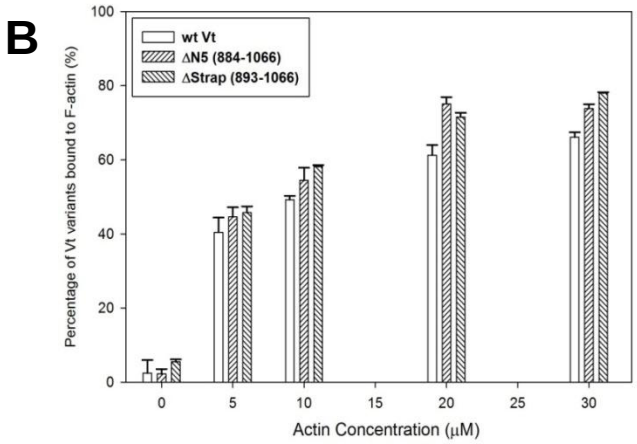
B
wt Vt
ΔN5 (884-1066)
ΔStrap (893-1066)
Percentage of Vt variants bound to F-actin (%)
Actin Concentration (μM)
0
20
40
60
80
100
0
5
10
15
20
25
30

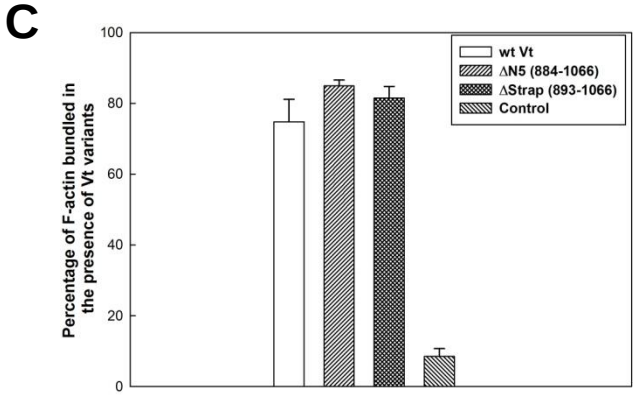
C
wt Vt
ΔN5 (884-1066)
ΔStrap (893-1066)
Control
Percentage of F-actin bundled in the presence of Vt variants
0
20
40
60
80
100

Figure 2.1.Vt NT deletions within the strap do not affect actin binding and bundling. A, binding of WT Vt to F-actin at actin concentrations ranging from 0 to 40 μM. The solid line provides visual guidance; binding to F-actin reaches a plateau at actin concentrations of ~20 μM or higher; WT Vt concentration: 10 μM; B, compared with WT Vt, both the ΔN5 and Δstrap Vt variants show slightly enhanced actin binding. Vt variant concentration: 10 μM; actin concentration: 0-30 μM. C, Vt variants with partial (ΔN5) and complete deletion of the strap (Δstrap) show comparable actin bundling to that of WT Vt. Vt variant concentration: 10 μM, actin concentration: 20 μM.

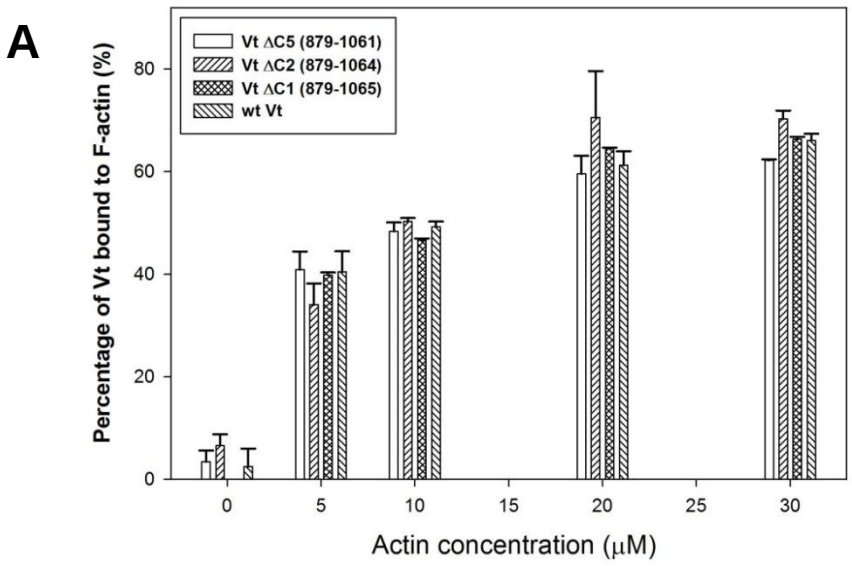
A
Vt ΔC5 (879-1061)
Vt ΔC2 (879-1064)
Vt ΔC1 (879-1065)
wt Vt
Percentage of Vt bound to F-actin (%)
0
20
40
60
80
0
5
10
15
20
25
30
Actin concentration (μM)

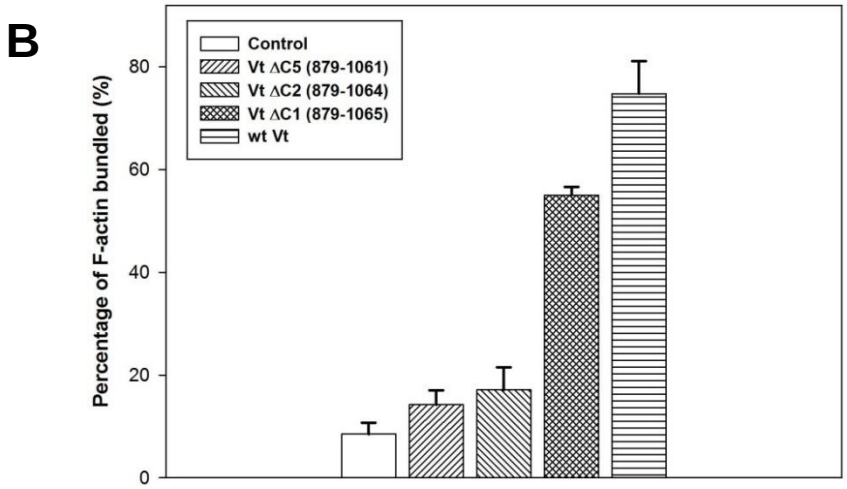
B
Control
Vt ΔC5 (879-1061)
Vt ΔC2 (879-1064)
Vt ΔC1 (879-1065)
wt Vt
Percentage of F-actin bundled (%)
0
20
40
60
80

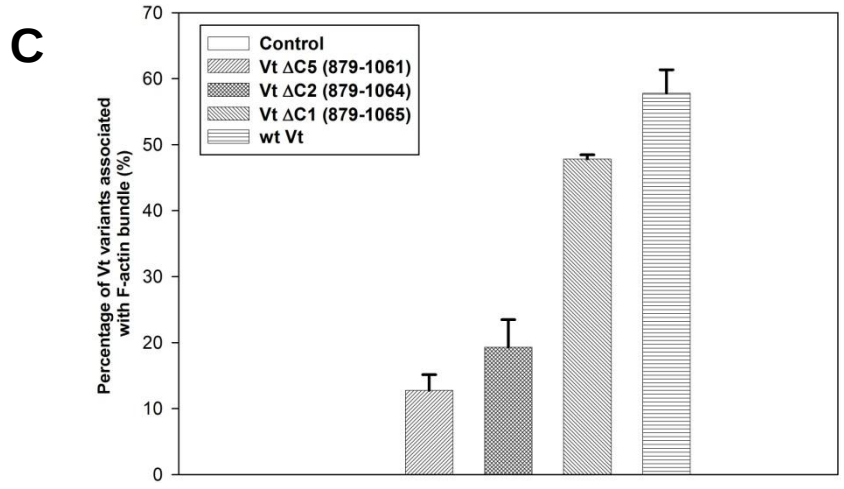
C
Control
Vt ΔC5 (879-1061)
Vt ΔC2 (879-1064)
Vt ΔC1 (879-1065)
wt Vt
Percentage of Vt variants associated with F-actin bundle (%)
0
10
20
30
40
50
60
70

Figure 2.2.Vinculin CT hairpin is critical for bundling F-actin, but not for binding F-actin. A, compared with WT Vt, Vt variants containing deletions of residues within the CT hairpin does not alter binding to F-actin. Vt variant concentration used: 10 µM; actin concentrations ranged from 0 to 30 µM; B, deletion of C-terminal residues 1062 to 1066 (Vt ΔC5) impairs Vt induced F-actin bundling. Vt concentration used: 10 µM, actin concentration used: 20 µM. Vt protein was not present in the control runs; C, deletion within the Vt C-terminal hairpin reduces the amount of Vt associated with F-actin bundles. Vt concentration used: 10 µM, actin concentration used: 20 µM. In the absence of Vt, a protein band at ~ 23 kDa was not observed in the control run.

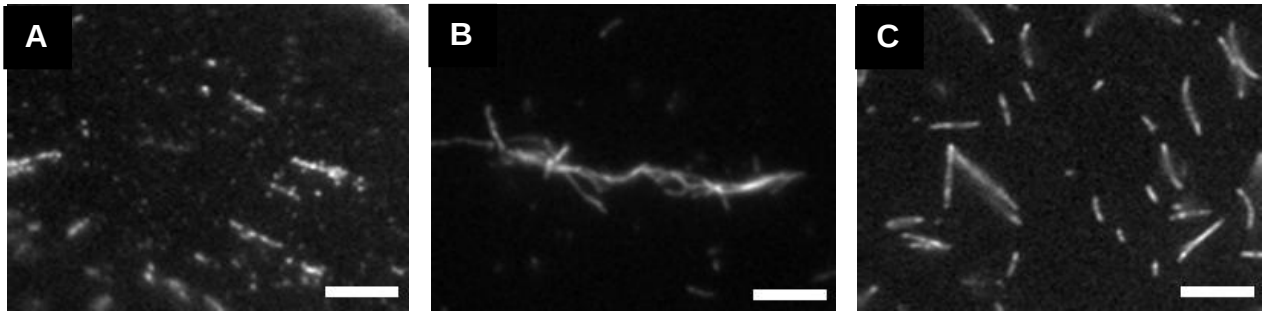

Figure 2.3.Visualization of actin bundles in the presence and absence of WT Vt and VtΔC5 using fluorescence microscopy. Removal of the CT hairpin significantly impairs F-actin bundling. A, In the absence of Vt , only F-actin fragments are observed; B, when incubated with WT Vt, F-actin forms thick and stable actin bundles; C, upon incubation with Vt ΔC5, F-actin forms randomly oriented thin fragments, similar to those observed in A). Samples were prepared using the procedure described for the actin bundling assay. The nominal actin and Vt concentrations during image acquisition are 50 nM and 25 nM, respectively. Scale bar: 25 µm.

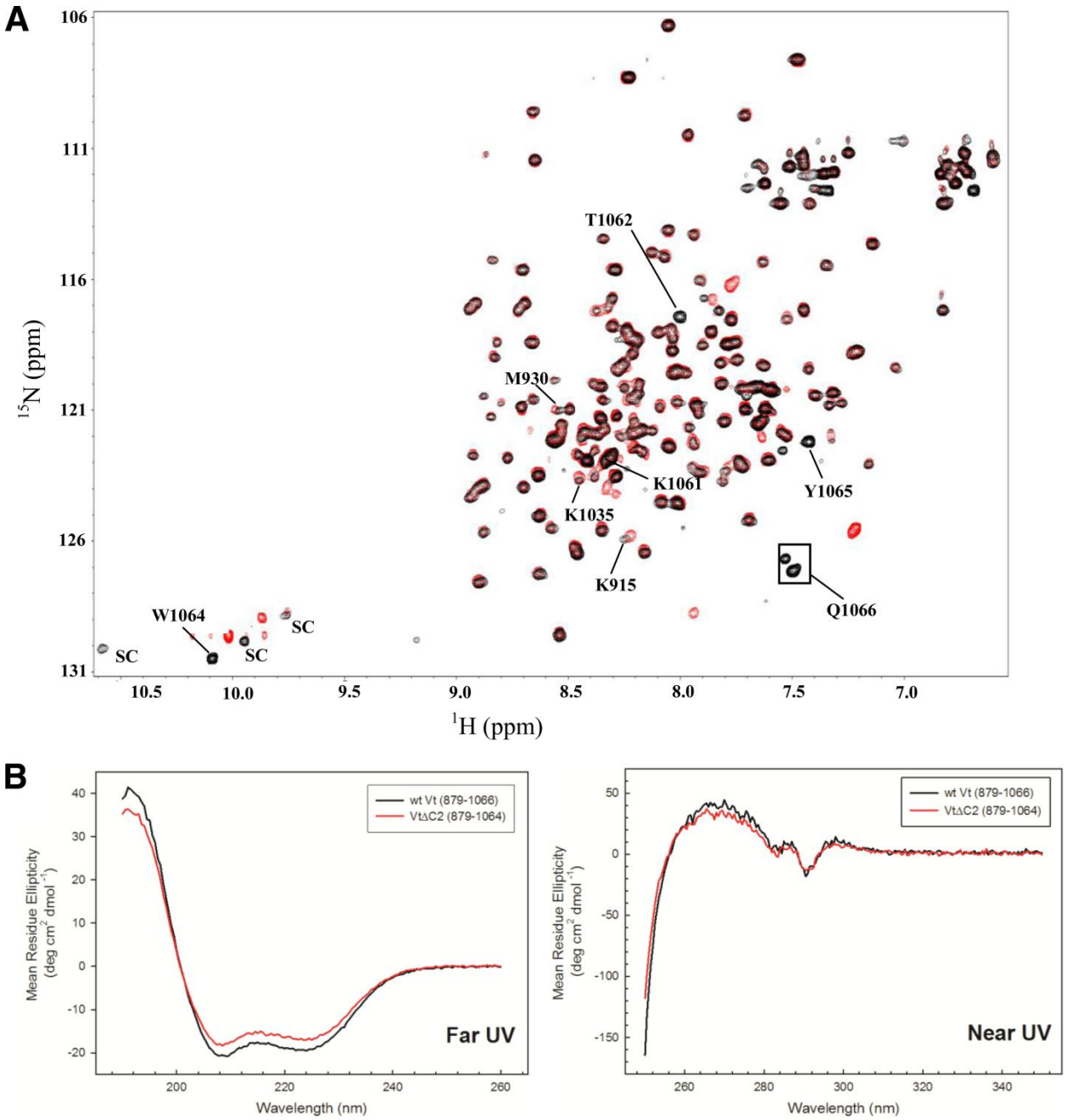

Figure 2.4.Removal of residues within the Vt C-terminal hairpin does not alter Vt conformation. A, 2D ^{1}H-^{15}N HSQC spectral overlay of WT Vt (black) and Vt ΔC2 (red). Note that T1062 and W1064 resonances shown significant changes in chemical shift while K915,

M930, and K1035 show slight chemical perturbations (within a linewidth). SC: side chain. The weak resonance associated with Q1066 represents its minor conformation. B, CD spectra overlay of WT Vt (black) and Vt ΔC2 (red). Left panel: far UV; right panel: near UV.

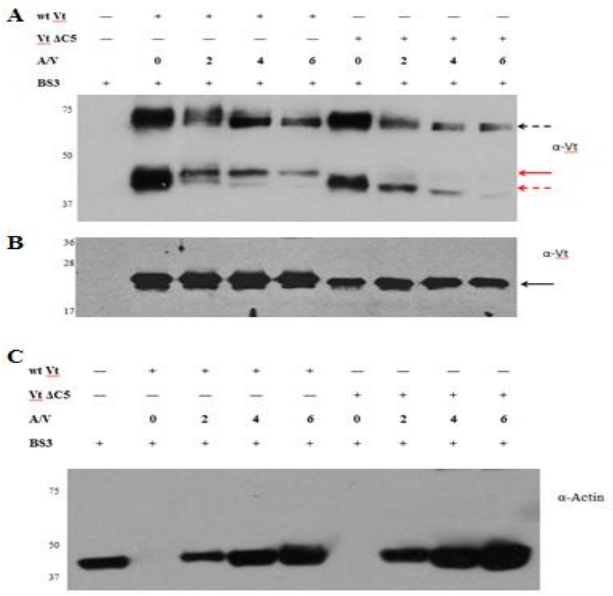

Figure 2.5.Vt forms a distinct dimer (~45 kDa) in the presence of F-actin. Cross-linking experiments were conducted at room temperature for 40 min. Final Vt concentration: 2.5 µM; BS3 concentration: 25 µM; Western blots of WT Vt and Vt ΔC5 in the presence of increasing concentrations of actin probed against Vt (A & B) or actin (C). The relative intensity ratio of the lower 'native' dimer band to the upper (actin-induced) dimer band, gradually increases when actin/Vt ratio (A/V) ratio is raised from 0 to 6. Crosslinking samples were run on SDS-PAGE gels (B) to observe the Vt , monomer band (black arrow) or tris-acetate 7% gradient gels (A&C) to observe dimer and trimer species. Although Vt ΔC5 is impaired in actin bundling, a distinct dimer is formed in the presence of actin (lower band, ~40 kDa), the smaller dimer band that is observed is distinct in molecular weight and likely differs from the actin-induced dimer that is formed by WT Vt (C). Red arrows in both panels indicate the positions of Vt dimer bands (Red solid arrow for the actin-induced dimer and the red dashed arrow for the native dimer or a different dimer species in the case of Vt ΔC5). The black dashed arrow indicates a Vt trimer species.

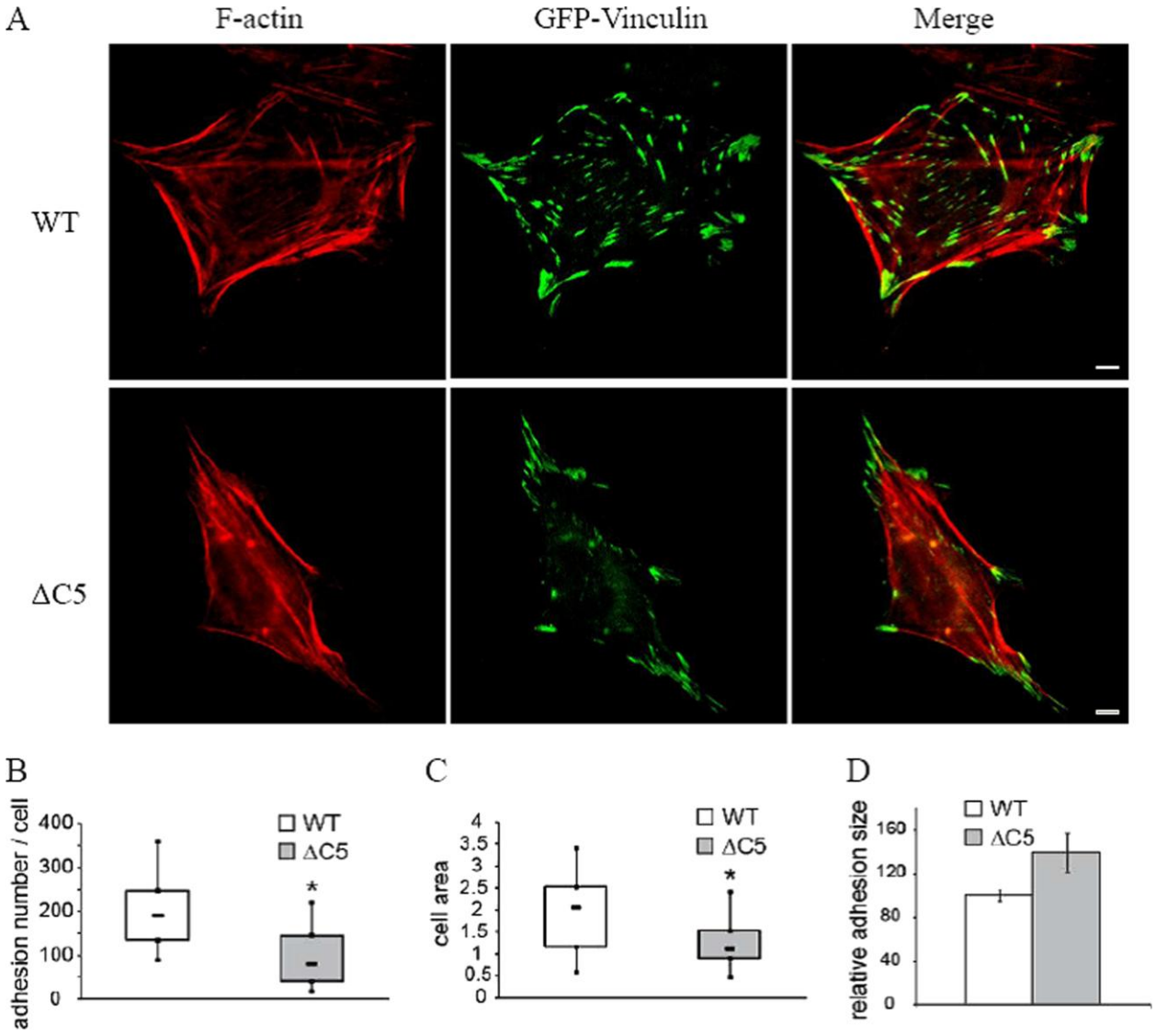

Figure 2.6.Vt CT hairpin deletion affects cell adhesion. A, Vin -/- MEFs were transfected with WT or ΔC5 vinculin and plated on FN. After fixation, F-actin and FAs were stained using phalloidin and GFP tagged vinculin variants, respectively. Scale bar is 25 μm. B-D, adhesion number per cell (B), cell area (C), and adhesion size (D) were analyzed (n=19; * $p<0.01$). Box plots indicate median values and capture 50 % of data in boxes and 80 % in whiskers.

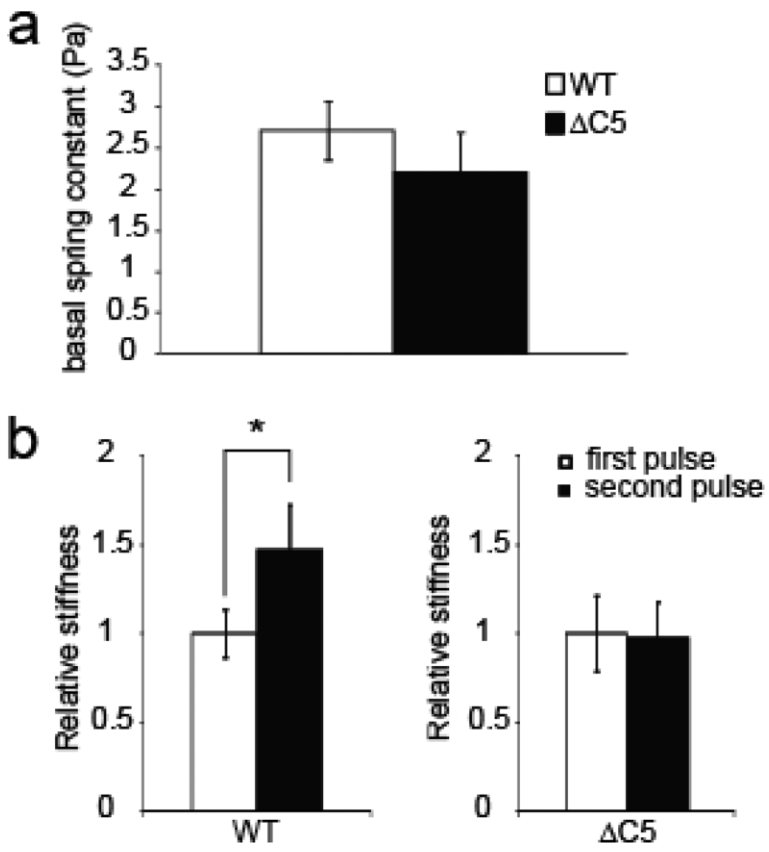

Figure 2.7.The Vt CT hairpin is necessary for the mechanical response to force on integrins. A, within measurement errors, WT vinculin and ΔC5 vinculin have comparable basal stiffness. Spring constant was calculated for the first pulse of force applied to FN-coated beads bound to Vin -/- MEFs transfected with WT or ΔC5 vinculin (*n* = 15). B, upon applying pulses of a constant force, relative stiffness of Vin -/- MEFs transfected with WT vinculin increases, whereas the stiffness of Vin -/- MEFs transfected with ΔC5 vinculin does not change within errors. For the relative stiffness measurements, two force pulses were applied to FN-coated beads bound to Vin -/- MEFs transfected with either WT or ΔC5 vinculin (*n* = 15).

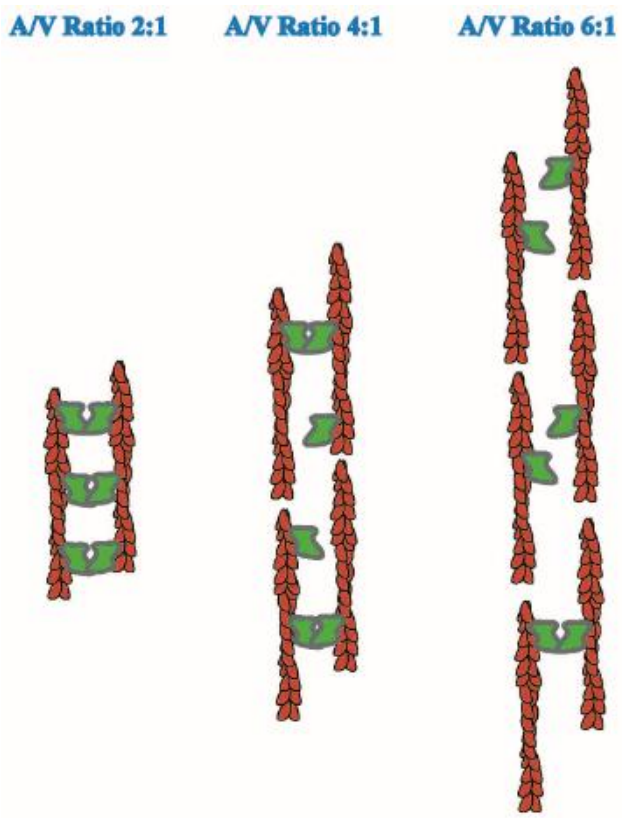

Figure 2.8.Model for Actin-Induced Vinculin Tail Oligomerization and Bundling of F-Actin. According to the dimer model and as supported by supplemental Figure S2, we would expect optimal bundling of actin by Vt to occur at an A/V ratio of 2:1, assuming Vt binds to two sites on an F-actin unit and upon binding to actin, Vt dimerizes which in turn promotes bundling of actin. As demonstrated in the model, when actin (red) is in excess and Vt (green) is saturated, the bundling efficiency decreases as seen by our crosslinking data and F-actin bundling saturation curves. We hypothesize that a result of a lack of reinforcement by Vt to bundle F-actin when actin is in excess, the bundling efficiency decreases as well as formation of actin-induced dimer species.

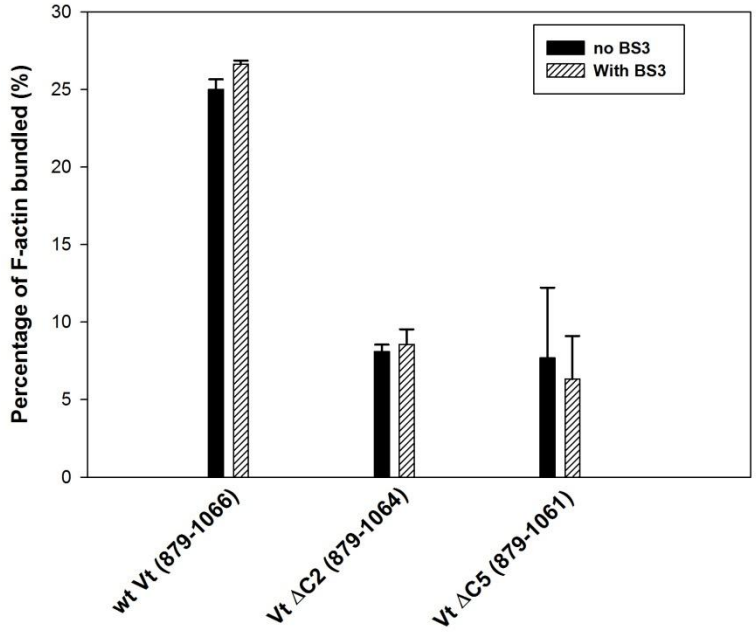

Supplemental Figure2.1.The crosslinking agent, BS3, does not enhance F-actin bundling.

The actin bundling assay was performed using experimental conditions employed for the crosslinking reactions.

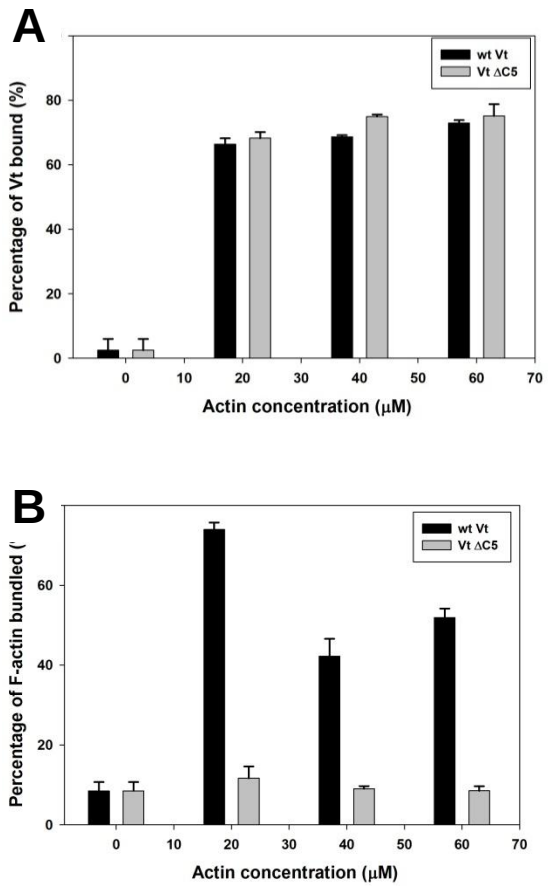

Supplemental Figure 2.2Effects of increased actin concentration on the ability of Vt to bind and bundle F-actin.A, BothWT Vt and Vt ΔC5 show similar F-actin binding properties at actin concentration ranging from 0 to 60 μM. WT Vt and Vt ΔC5 concentration: 10 μM; B, F-actin bundling induced by Vt variants reaches a maximum at A/V =2. Vt variants concentration: 10 μM; actin concentration: 0 - 60 μM.

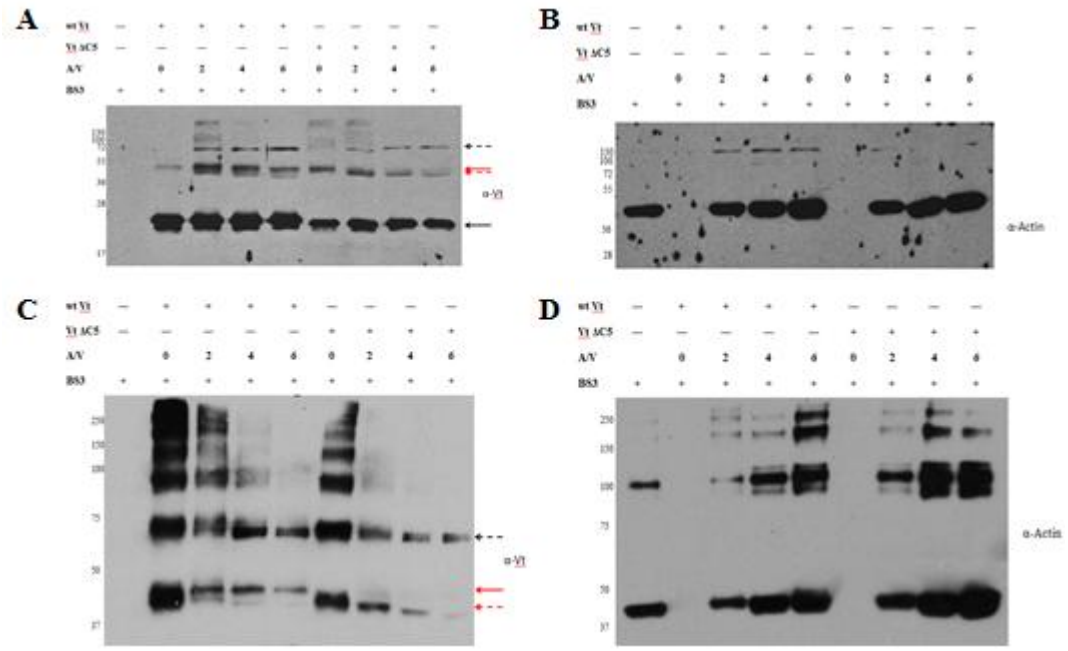

Supplemental Figure 2.3.Vt forms a distinct dimer (~45 kDa) in the presence of F-actin. Cross-linking experiments were conducted at room temperature for 40 min. Final Vt concentration: 2.5 µM; BS3 concentration: 25 µM; Western blots of WT Vt and Vt ΔC5 in the presence of increasing concentrations of actin probed against Vt (A & C) or actin (B & D). The relative intensity ratio of the lower 'native' dimer band to the upper (actin-induced) dimer band gradually increases when actin/Vt ratio (A/V) ratio is raised from 0 to 6. Crosslinking samples were run on SDS-PAGE gels (A & B) or tris-acetate 7% gradient gels (C & D). Although Vt ΔC5 is impaired in actin bundling, an actin induced dimer is observed (lower band) when the sample is run on a gradient gel (C). However, the dimer species differs from the actin-induced dimer that is formed by WT Vt (C). Red arrows in both panels indicate the positions of Vt dimer bands (Red solid arrow for the actin-induced dimer and the red dashed arrow for the native dimer or a different dimer species in the case of Vt ΔC5). The black arrow indicates the Vt monomer species which is only observed on the SDS-PAGE gel. The black dashed arrow indicates a

Vttrimer species. Bands observed at 80 kDa and higher in A & C represent higher order Vt oligomer species that likely occur through the native dimerization site as these higher order species disappear with increasing concentrations of actin.

III: Identification of a New Actin Binding Surface on Vinculin that Mediates Cellular Mechanical and Focal Adhesion Properties

A. Overview

Vinculin is a large, highly conserved cytoskeletal protein that is a prominent component of focal adhesions and adherens junctions, and is critical for cell migration, cell survival, and embryogenesis. The tail domain of vinculin binds multiple ligands, including filamentous actin (F-actin). While association with F-actin is believed to be critical for vinculin function, the interaction and its cellular consequences are poorly understood. Here we report a novel F-actin binding surface on vinculin and the identification and characterization of vinculin variants impaired in actin binding. Expression of a vinculin variant deficient in actin binding in vinculin knockout fibroblasts fails to fully rescue cell-spreading defects and results in a reduced response to external force. These findings mirror results obtained with an actin-bundling deficient variant and reveal the importance of this new actin-binding surface.

B. Introduction

Vinculin is a large, (1066-residue) highly conserved, and abundant protein that localizes to focal adhesions (FAs), focal complexes, and adherens junctions(*109, 135*).Vinculin plays an essential role in embryogenesis, as knockout mice show defects in heart and nerve formation and

do not survive past embryonic day 10(*2*). Cells deficient in vinculin exhibit rounded morphology, increased motility(*2*), and resistance to apoptosis and anoikis(*9*). Consistent with these observations, vinculin has been implicated in the regulation of FA turnover(*79*), adhesion dynamics at the leading edge of cells(*42*), and force transduction(*128*). However, the mechanisms by which vinculin regulates these functions are still poorly understood.

Vinculin is comprised of three domains: a large (91 kDa) helical head domain (Vh), a proline-rich linker, and a 22 kDa tail domain (Vt). It functions as a molecular scaffold capable of associating with multiple binding partners at each domain(*69*). Cytosolic vinculin exists in an inactive, autoinhibited conformation mediated by a strong interaction between Vh and Vt that obscures binding to many ligands(*98, 113*). Disruption of this autoinhibitory interaction by binding of ligands at Vh and Vt is believed to be required for vinculin activation and its localization to FAs(*33*).

Vinculin binds to F-actin through Vt and subsequently crosslinks F-actin filaments into fibers(*66, 98*). This interaction links the actin cytoskeleton to integrins and the extracellular matrix, and is believed to be critical for FA maturation(*40, 42*), cell movement(*42*), and force transduction(*39, 128, 136*). In addition to binding F-actin, Vt also binds raver1(*137*), paxillin(*64*), and phosphatidylinositol 4,5-bisphosphate (PIP_2)(*88*). Structurally, Vt exists as a five-helix bundle with an N-terminal strap (residues 879-892) and C-terminal arm (residues 1046-1066)(*71, 72*). Interactions between the N-terminal strap and C-terminal hairpin (residues 1051-1066) bring the termini in close proximity to each other(*71, 72*).

The current structural model from Janssen *et al*. (J-model) for the interaction between the Vt and F-actin, derived from low resolution EM data, places helices 2 and 3 (H2 and H3) of Vt in a hydrophobic cleft at the junction between two of the actin subunits(*91*). However, this model

lacks supporting mutagenesis data. Although vinculin variants deficient in F-actin binding have previously been employed to probe the functional consequences of this interaction, results from these studies are difficult to interpret, as the variants possess multiple mutations or large deletions in Vt that could potentially disrupt vinculin structure and/or interactions with other tail ligands as implicated in recent NMR studies(*88*). A more recent computational model has been published, but lacks experimental evidence to support it(*92*).

Herein, we employ mutagenesis, negative-stain electron microscopy (EM), and molecular modeling to identify a novel actin binding surface as well as a single conservative point mutation within vinculin that retains Vt structure and PIP_2 binding, yet disrupts binding to F-actin. Interestingly, the mutation site (V1001) is outside the reported actin-binding interface(*91*). While this hydrophobic site is distinct from the surface identified in the J-model, it is consistent with current mutagenesis data, known ligand interactions, and occlusion of the site in the full length protein(*39, 98, 137*). To examine the consequences of disrupting the F-actin:vinculin interaction, we transfected the F-actin deficient variant into vinculin knockout murine embryonic fibroblasts (Vin-/- MEFs) and monitored cellular behavior. Our results confirm that loss of actin binding by vinculin alters cell and FA size and limits the ability of cells to respond to pulses of force.

C. Materials and Methods

1. Vinculin expression and purification

Expression of the tail domain of chicken vinculin (Vt, residues 879-1066) was performed as previously described(*88*). Briefly, *E. coli* BL21-DE3 RIPL cells were transfected with a pET15b (Novagen) vector containing the gene for chicken vinculin residues 879-1066. Cells

were grown at 37°C until an OD of 0.6 was reached. Cells were then induced with isopropyl β-D-1-thiogalactopyranoside (0.25 mM) and the temperature was dropped to 18°C. Cells were grown for an additional 18 hours, centrifuged, and resuspended in lysis buffer. Cells were lysed by sonication and the lysate cleared by centrifugation. No protein was purified from the insoluble fraction. Vt was purified using Ni-NTA-agarose beads (Qiagen; Germantown, MD) and cation-exchange chromatography. Vt variants were generated by QuikChange site-directed mutagenesis (Stratagene; La Jolla, CA) and sequences verified by DNA sequencing (Genewiz; Research Triangle Park, NC).

Full-length chicken vinculin and its variants were expressed and purified in a similar manner to Vt. Full length vinculin cDNA was cloned into the vector pET15b, and then transformed into *E. coli* strain BL21-DE3 RIPL cells. Cells were grown in LB at 37°C to an A_{600} of 0.6. Isopropyl β-d-1-thiogalactopyranoside (0.5 mM) was added to induce protein expression. Cells were harvested after three hours by centrifugation at 5,800× *g* for 15 min and resuspended in lysis buffer (20 mM Tris, 150 mM NaCl, 5 mM imidazole, 2 mM β-mercaptoethanol, pH 7.4). Cells were lysed by sonication, and the lysate cleared by centrifugation at 25,000× *g* for 50 minutes. The supernatant was loaded onto a Ni-NTA column. The column was washed (20 mM Tris, 150 mM NaCl, 40 mM imidazole, 5 mM β-mercaptoethanol, pH 7.5) and vinculin was eluted (20 mM Tris, 150 mM NaCl, 500 mM imidazole, 5 mM β-mercaptoethanol, pH 7.5). Thrombin (Sigma) was used to remove the His tag, and vinculin was further purified by anion exchange (Hiprep Q XL 16/10) column chromatography using Tris pH 8.0 and a gradient of 0.05 to 1 M NaCl. The final product was evaluated by SDS-PAGE for purity and determined to be >95% pure. PMSF, benzamidine, antipain, and leupeptin were used to limit protease activity during purification.

2. Actin co-sedimentation assays

Actin binding and bundling by Vt were measured with a co-sedimentation assay as previously described(*39*). Actin binding by vinculin was measured in the same way, using 10 µM vinculin in the place of Vt. IpaA peptide was used at a concentration of 100 µM, in ten-fold excess to vinculin. The percent vinculin pelleted was determined in the same way as before. Briefly, the supernatant and pellet fractions were run on a gel, and the band intensity was calculated using ImageJ (*138*). Percent binding was determined by dividing the intensity of the pellet by the sum of the intensities of the pellet and supernatant and multiplying by 100%.

3.Lipid co-sedimentation assays

Vinculin tail binding to phosphatidylinositol 4,5-bisphosphate (PIP_2) was evaluated by lipid co-sedimentation assays using small, unilamellar vesicles (SUVs) as reported(*88*). SUVs were generated using 250 µg lipid per reaction, with the reported PIP_2% and a 3:1 ratio of phosphatidylethanolamine (PE) to phosphatidylcholine (PC). The lipids were resuspended (40 mM MES pH 6.0, 150 mM NaCl, and 2 mM DTT) and subsequently extruded in a mini-extruder (Avanti Polar Lipids; Alabaster, Alabama). Relative protein amounts were quantified using ImageJ(*138*).

4. EM sample preparation and analysis

G-actin was prepared from rabbit skeletal muscle(*139*) and clarified by chromatography over a Superdex-200 column. G-actin in complex with calcium was polymerized (20 mM imidazole-HCl, pH 7.2, 50 mM KCl, 2 mM $MgCl_2$, and 1 mM EGTA) for 2-3 hours at 23°C. Decoration of actin filaments was performed on carbon-covered EM-grids. One drop of 1.5-2 µM F-actin was applied to the glow-discharged grid, blotted and then washed with 1-3 drops of 2.5 µM Vt^{WT} or Vt variants. The last drop was incubated up to 1 min, the grid was blotted and negatively stained with a 2% (w/v) solution of uranyl acetate.

A Tecnai-12 electron microscope at an accelerating voltage of 80 keV and a nominal magnification of 30X was employed. BSOFT package(*140*) was used to determine defocus values in order to correct for the contrast transfer function in the images. Images were digitized at a raster of 4.28Å/pixel, and 6416 segments (100 pixels long) were processed using the SPIDER(*141*) and IHRSR(*142*) packages. Cross-correlation approach was used to extract segments of filaments fully decorated with Vt. Two models were initially created. The first was a model of actin filament (pdb 3MFP)(*143*), while the second contained the actin filament model with Vt (pdb 1QKR)(*72*) attached to each of the actin protomers as suggested by Janssen *et al*.(*91*). Segments that yielded the best correlation with the second model (n=1716) converged to a helical solution of -167° rotation and 27.8 Å translation. The resolution of the resultant 3D-reconstruction was judged to be ~ 20 Å using the Fourier shell correlation equal to 0.5 criterion. UCSF Chimera software(*144*) was used to fit the model of the actin filament (pdb 3MFP) and the crystal structure of Vt (pdb 1QKR) into the experimental map. Atomic coordinates from crystal

structures were converted to density maps, filtered to the resolution of the experimental map, and docked manually.

5. DMD model generation

The 6.6 Å electron cryo-microscopy map for F-actin was used to reconstruct the long-pitch helix F-actin dimer(*143*). Parameters for accurate rotation and rise per subunit were obtained from the header of the corresponding protein databank deposition (PDB: 3MFP). The actin dimer generated was used in the EM-fitting, done with Situs 2.5(*145*). Prior to the fitting process, the 4-methyl histidine (HIC) at position 73 (pdb 3MFP) was replaced with a canonical histidine (HIS) for compatibility. Coordinates for Vt (residues 879-1065) were obtained from the crystal structure of vinculin (PDB: 1ST6)(*71*). Density for Vt alone was obtained upon subtraction of the density corresponding to actin using Chimera(*144*). The crystal structure of Vt was fit into the isolated density using Situs 2.5(*145*).

Steric clashes resulting from 3D reconstruction using EM constraints were resolved using Chiron(*146*). Various orientations of Vt with respect to the actin dimer were sampled using discrete molecular dynamics (DMD) simulations(*147, 148*). The backbone of the actin dimer was maintained static during the simulations, while the side chains were allowed to freely sample different rotameric states. Rigid body movement of Vt was allowed to sample different orientations of Vt with respect to the actin dimer. In order to maintain Vt in the vicinity of the actin dimer for enhanced sampling, appropriate constraints were imposed between the center of mass of the actin dimer and that of Vt. One thousand snapshots from the simulations were retrieved at regular time intervals and were clustered based on total energy. One representative

structure from the largest cluster was chosen for prediction of binding free energy change upon mutation.

6.Cell culture

Vin-/- MEFs were obtained from Dr. Eileen Adamson (Burnham Institute; La Jolla, CA) and grown in Dulbecco's modified Eagle's medium (DMEM; Invitrogen) supplemented with 5% fetal bovine serum and antibiotic-antimycotic solution.

7.DNA constructs and transfection

DNA constructs were generated for cell culture as previously reported(*39*). Cells were transfected with vinculin expression constructs using Lipofectamine (Invitrogen) and Plus Reagent (Invitrogen) according to the manufacturer's protocol and examined 48-72 hours following transfection.

8.Cell Resuspension and Spreading Assay

Prior to plating, cells were serum-starved in DMEM media supplemented with 0.5% delipidated BSA and antibiotic-antimycotic solution. Cells were then resuspended in the serum-free de-lipidated BSA media for approximately two hour. For the real-time cell analyzer (RTCA) xCELLigence System (Acea Biosciences), 2500 cells per well were seeded into the E-plate 16that were coated with 50 µg/mL FN. Attachment and spreading, monitored by impedance and given out as cell index (CI), was recorded with the RTCA apparatus every 15 seconds over a 13

hour time period. For the adhesion site analysis, cells were prepared as described above prior to seeding onto glass coverslips containing FN (50 µg/mL).

9. Adhesion site analysis

Adhesion sites were analyzed as previously reported(*39*), except that cells were permeabilized in 0.5% Triton X-100 instead of 0.3%.

10. 3D force microscopy

Three-dimensional force microscopy (3DFM) was used to apply controlled and precise 60–100 pN local force to focal adhesions. Tosyl-activated magnetic dynabeads (2.8 µm, Invitrogen) were washed with PBS and incubated for 24 hours with FN at 37°C. After three washes with PBS and incubation with 5% de-lipidated BSA (Sigma) for 1 hour at 37°C, the beads were sonicated and incubated with cells for 30 min. Force application and bead displacement were performed as previously described(*39*). The tracked displacements are reported as mean ± S.E.M. Statistical analyses, including two-tailed Student's *t* test for *p* values were performed.

D. Supplementary Methods

1. IpaA peptide

The IpaA peptide (NNIYKAAKDVTTSLSKVLKNIN) with N-terminal acetylation and C-terminal amidation was synthesized by the UNC High-Throughput Peptide Synthesis and

Array Facility (Chapel Hill, NC) and LifeTein (South Plainfield, NJ). Peptide concentration was determined by absorbance at 280 nm using the extinction coefficient for tyrosine (1200 M-1 cm-1).

2. Circular dichroism (CD) spectroscopy

Circular dichroism (CD) spectra were collected as reported (*88*). Briefly, spectra were collected from 350-250 nm (near-UV) and 260-190 nm (far-UV) at protein concentrations of 450 and 5 μM, respectively. Data were collected on a Jasco J-815 CD Spectrometer (Jasco; Easton, MD) at 25°C in 10 mM potassium phosphate, pH 5.5 or 7.5, 50 mM Na2SO4, and 1 mM dithiothreitol.

3. NMR spectroscopy

Vt samples for NMR were prepared from cells grown in M9 media with $^{15}NH_4Cl$ as the sole nitrogen source. The ^{15}N-Vt samples were exchanged into NMR buffer (10 mM potassium phosphate, pH 5.5, 50 mM NaCl, 0.1% NaN3, 2 mM DTT, and 10% D2O) and concentrated to 30 μM. Two-dimensional heteronuclear single quantum coherence (HSQC) spectra were collected on a Varian INOVA 700 MHz spectrometer at 37 °C (*120*). Processing was done with NMRPipe (*121*) and spectral analysis with NMRViewJ (*149*).

CLEANEX(*150*)experiments were performed on a Varian INOVA 600 MHz spectrometer at 37 °C with mixing times of 0.2, 15.3, 30.4, 55.5, 85.6, 125.7, 180.8, and 300 msec. fast-HSQC (*151*) experiments were performed on a Varian INOVA 700 MHz spectrometer at 37 °C . Samples for the fast-HSQC experiments were exchanged into 95% D2O, 10 mM potassium

phosphate, pD 5.9, 50 mM NaCl, 0.1% NaN3, and 2 mM DTT using a pre-equilibrated PD-10 column (GE Healthcare Life Sciences; Pittsburgh, PA). Ninety two data sets were collected at increasing intervals over 18 days. Protein samples were collected and added to NMR tubes at a concentration of 200 μM for CLEANEX and 700 μM for fast-HSQC. Experiments were processed with NMRPipe and rates were analyzed with NMRViewJ.

Heteronuclear NOE experiments(*152*) were performed on a Varian INOVA 600 MHz spectrometer at 37°C. Proton saturation was achieved over 4.5 seconds.

4. Calculation of $\Delta\Delta G_{bind}$

Prior to estimation of change in binding free energy ($\Delta\Delta G_{bind}$), the structure of the Vt:F-actin complex was relaxed while maintaining a fixed backbone. $\Delta\Delta G_{bind}$ for all Vt variants was computed using Eris (*153*). One thousand independent runs were performed for computing $\Delta\Delta G_{bind}$ for each of the Vt variants using the following relation:

$$\Delta\Delta G_{bind} = (\Delta G_{C-MUT} - \Delta G_{C-WT}) - (\Delta G_{V-MUT} - \Delta G_{V-WT})$$

where the subscripts MUT and WT refer to the mutant and wild-type forms of the complex (C) and Vt (V).

E. Results

1. Identification of Vt variants deficient in actin binding

Although vinculin variants impaired in actin binding have been identified, they contain multiple point mutations(*73*) or deletions(*41, 66, 154*) and have not been fully characterized to determine

whether Vt structure and other ligand binding interactions are altered. While performing alanine scanning to disrupt the Vt dimer that forms at high concentrations in solution(*72, 120*), we generated two Vt variants, Vt^{I997A} and Vt^{V1001A}, that exhibit a significantly decreased affinity for F-actin (Figure. 3.1A,B). This finding was unexpected, as the surfaces associated with the J-model for the Vt:F-actin interface did not include residues I997 or V1001(*91*), and actin-deficient variants at these sites have not been previously reported.

To compare and quantify actin binding of these Vt variants, we performed F-actin co-sedimentation experiments (Figure3.1A,B). Vt^{1997A} exhibited the greatest deficiency in actin binding. Approximately 40% Vt^{WT} pellets with F-actin at 5 µM F-actin (the concentration required for approximately half-saturation), while only ~14% Vt^{I997A} associates with the actin-containing pellets. Vt^{V1001A} also exhibits decreased binding to F-actin, with ~26% Vt^{V1001A} pelleting at 5 µM F-actin. As both I997 and V1001 lie outside the actin binding site defined in the J-model, we generated another variant, Vt^{I948A}, which lies within the reported F-actin:Vt interface(*91*). However, Vt^{I948A} did not significantly decrease the affinity of Vt for F-actin (Figure3.1B). Additionally, we performed actin co-sedimentation experiments on several additional variants (summarized in Table 1). We also assessed actin binding properties of a subset of these mutations in the context of the full-length protein. While the actin-binding site of vinculin resides in Vt, it is partially masked in the full-length protein due to autoinhibitory contacts between Vh and Vt(*73*). Consistent with these observations, we find that binding of F-actin by $vinculin^{WT}$ is significantly reduced compared to the isolated Vt domain (Supplemental Figure3.1). The interaction between Vh and Vt can be disrupted by an IpaA peptide from *Shigella*(*77, 155*). Addition of this peptide at a 10-fold excess activates $vinculin^{WT}$ and enhances binding to F-actin (Supplemental Figure3.1). In comparison, full length $vinculin^{I997A}$ and

vinculin^{V1001A} bind F-actin poorly, in both the absence and presence of the IpaA peptide (Supplemental Figure3.1). In contrast, actin binding profiles observed for vinculin^{I948A} are similar to those observed for vinculin^{WT}, with enhanced F-actin binding observed in the presence of the IpaA peptide (Supplemental Figure3.1). These results suggest Vt variants impaired in actin binding show similar impairment in full-length vinculin. Interestingly, vinculin^{I997A} binds a significant amount of F-actin in the absence of the IpaA peptide, while vinculin^{V1001A} does not, suggesting that the I997A mutation may partially disrupt vinculin head:tail interactions.

Binding of F-actin to vinculin facilitates bundling of F-actin filaments. This is currently believed to occur through a conformational change that promotes Vt dimerization, allowing it to crosslink F-actin filaments(*90, 91*). We recently showed that the vinculin C-terminal hairpin is required for generation of this actin-induced dimer as well as for F-actin bundling(*39*). Consistent with these findings, Vt variants deficient in F-actin binding are also significantly impaired in their ability to bundle F-actin (Figure3.1C), with deficiencies in F-actin binding and bundling correlated. For example, the Vt variant most impaired in F-actin binding, Vt^{I997A}, is most impaired in F-actin bundling. The bundling defect is similar to our previously characterized CT hairpin deletion variant (Vt$^{\Delta C5}$)(*39*). Moreover, Vt^{V1001A} is able to partially bind and bundle F-actin, whereas Vt^{I948A} retains F-actin binding (Vt^{I948A}) and is fully capable of bundling F-actin. To test if the structural integrity of Vt is disrupted by the actin-deficient mutations, we employed circular dichroism (CD) and NMR spectroscopy. Far-UV CD spectra for all variants are similar, with characteristic minima at 208 and 222 nm (Supplemental Figure3.2A, B), indicating that the α-helical secondary structure of Vt is unaltered by these mutations. For Vt, near-UV CD primarily reflects tertiary packing of tryptophan residues 912 in the H1/H2 loop with 1058 in the C-terminus. This packing interaction generates a distinct CD signal between 270 and 300

nm(*88*), and is not perturbed for Vt^{I997A}, Vt^{V1001A}, or Vt^{I948A} (Supplemental Figure3.2C, D). To further confirm the structural integrity of Vt^{I997A} and Vt^{V1001A}, we acquired Heteronuclear Single Quantum Coherence (HSQC) 2D NMR spectra on ^{15}N-enriched Vt^{WT} and the actin deficient Vt variants. The peaks in the ^{1}H-^{15}N HSQC spectra for both Vt^{I997A} and Vt^{V1001A} variants remain dispersed, indicative of well-folded protein, and overlap well with the peaks of Vt^{WT}(Supplemental Figure 3.3A, B). The peaks that shift correspond to residues very near to the site of mutation (Supplemental Figure3.3C, D). The amide (NH) line widths and intensity are also unchanged from those of Vt^{WT}, suggesting that the mutations do not significantly alter dynamics properties of Vt. The CD and NMR data, taken together, suggest that the actin-binding deficiencies of Vt^{I997A} and Vt^{V1001A} are not the result of structural impairment (Supplemental Figure3.3).

To determine if mutations that disrupt actin binding alter Vt interactions with other ligands, we performed lipid co-sedimentation experiments to assess Vt association with PIP_2. We find that the F-actin deficient variants Vt^{I997A} and Vt^{V1001A} retain specificity for PIP_2 over PS, but that Vt^{I997A} exhibits approximately a 50% decrease in binding to PIP_2 (Figure3.1D). While both variants share an F-actin binding defect, the change in affinity for PIP_2 in Vt^{I997A} necessitated evaluation of the cellular effects of both variants to discriminate the consequences of the common defect in actin binding.

2. Deficiencies in Actin Binding by Vinculin Alter Cellular Properties

Vinculin variants containing multiple mutations(*73*) or large deletions that remove helix 2 and 3(*41*) or the entire tail domain(*40*) have been previously created to prevent the interaction of vinculin with F-actin. However, these variants likely display cellular defects resulting from disruption of multiple ligand interactions in addition to the actin defect. While the vinculin:F-

actin interaction has been proposed to play a critical role in adhesion turnover, cell motility and force transduction, it remains to be determined if the phenotypes associated with these deletion variants are directly attributed to the interaction between vinculin and F-actin. By creating vinculin variants that are defective in actin binding but retain similar structure and PIP_2 association, we are able to conduct studies in cells and obtain more targeted results. With this new tool, we explored the role of actin-binding by expressing either vinculin^{I997A} or vinculin^{V1001A} in Vin-/- MEFs.

We previously reported a vinculin variant that retains actin binding but is deficient in F-actin bundling(*39*). Expression of this variant (vinculin$^{\Delta C5}$) in Vin-/- MEFs resulted in larger FAs and smaller cell area when cells were allowed to adhere and spread on fibronectin (FN). We anticipated similar results for a loss of actin-binding by vinculin, as a deficiency in binding necessitates a deficiency in bundling. First, we examined the ability of the cells to attach and spread over time on FN using the real-time cell analyzer (RTCA) xCELLigence system, an impedance-based system (given in arbitrary units as cell index, CI) that monitors changes in electrical resistance as cells adhere to the microelectrode in the dish (Figure3.2A,B)(*156*). Cells expressing vinculin^{WT} readily spread as indicated by the higher CI, while and Vin-/- MEFs have lower cell impedance suggesting a defect in cell spreading. This supports previous findings that these cells have difficulties in adhering and spreading on substrates(*4*). MEFs expressing vinculin^{I997A} and vinculin^{V1001A} did spread, but not as well as cells expressing vinculin^{WT}, suggesting that vinculin binding to F-actin plays an important role in cell spreading. Vinculin^{V1001A} impairs spreading less than vinculin^{I997A}, in agreement with its increased relative affinity for F-actin. We also performed immunofluorescence studies on vinculin^{WT}, vinculin^{I997A}, and vinculin^{V1001A} to verify that vinculin^{I997A} and vinculin^{V1001A}retain localization to FAs upon

expression in Vin-/- MEFs and to look for the spreading defect indicated by the RTCA experiment (Figure3.2C). Our finding that the vinculin variants localize properly is not surprising, since the head domain of vinculin is sufficient to localize vinculin to FAs(*40*). We also find that cells expressing vinculin^{I997A} have significantly larger and fewer adhesions in comparison to cells expressing vinculin^{WT}, as did cells expressing vinculin^{V1001A} (Figure3.2D, E). However, cells expressing vinculin^{V1001A} did not show a significant change in cell area, while cells expressing vinculin^{I997A} were significantly smaller than those expressing vinculin^{WT} (Figure3.2F). While there is slightly higher CI with vinculin^{V1001A} over vinculin^{I997A}, and cells expressing vinculin^{V1001A} do not exhibit a change in cell area, the observed CI could be attributed to the number and size of FAs found in these cells, as the system is sensitive enough to detect cytoskeletal changes and an increase in adhesion to the substrate(*156*). These results suggest that the number and average size of FAs during spreading events are directly influenced by vinculin's interactions with F-actin.

Vinculin plays a critical role in regulation of the cellular response to force(*128, 136*). We recently reported that the ability of vinculin to bundle F-actin is essential for reinforcement, the process by which cells locally stiffen when force is applied to FAs(*39*). Given these observations, we predicted that disruption of vinculin binding to F-actin (which is necessary for bundling) will also prevent reinforcement in cells. To test this, we exposed Vin-/- MEFs expressing vinculin^{WT}, vinculin^{I997A}, or vinculin^{V1001A} with FN-coated magnetic beads. Using the three dimensional force microscope (3DFM), we applied pulses of constant force to cells transfected with the various GFP-vinculin mutants(*129*). The relative displacement of the bead was determined for the first and second pulses. Cells transfected with vinculin^{WT} showed a significant decrease in the displacement of the bead upon application of the second pulse (p-

value 0.05×10^{-7};Figure3.3), suggesting that these cells are stiffening in response to pulses of force. Cells transfected with vinculin^{V1001A} exhibited a slight stiffening response, though it was not significant (p-value 0.07). Vin-/- MEFs transfected with vinculin^{I997A} showed an increase in the relative displacement of the bead upon application of a second pulse (p-value 0.08; Figure3.3). The failure of vinculin^{I997A}- and vinculin^{V1001A}-transfected cells to exhibit reinforcement further supports the role of the vinculin/actin interaction in force transmission.

3.Identification of an alternative actin binding surface

We have identified conservative vinculin variants that retain Vt structure and PIP_2 binding but disrupt F-actin binding. The mutations most impaired in actin binding are located on H4, outside of actin binding surfaces identified in the J-model(*91*) (Figure3.5A). Given the discrepancy between the actin binding surface suggested by our Vt mutants and that identified previously, we collected electron micrographs of F-actin filaments decorated with Vt and were able to generate a reconstruction with a resolution of ~20 Å (Figure3.4A,B). An atomic model of the actin filament (PDB 3MFP) and the Vt crystal structure (PDB 1QKR) were docked manually into the 3D-reconstruction of F-actin-Vt complex using Chimera software(*144*). As we find multiple plausible orientations of the Vt domain in agreement with the EM map, we conclude that the orientation of Vt cannot be uniquely defined by the EM reconstruction at this resolution. However, an orientation that fits our experimental data but is distinct from the J-model is plausible, and is shown in Figure 3.4B. Cryo-EM attempts were unsuccessful, as Vt decoration on F-actin was lost upon blotting and freezing, and bundling activity created sample heterogeneity. In addition to manual docking of Vt into the EM reconstruction, we applied computational refinement approaches using discrete molecular dynamics (DMD) to fit the EM map and generated an alternative model of the Vt:F-actin complex (Figure3.4C). While manual

docking and DMD yielded different orientations of Vt with respect to the actin filament, in both models the surface identified by mutagenesis faces the actin filament to mediate binding (Figure3.4D).

The DMD model was further evaluated by comparing the F-actin binding properties of Vt^{WT} and several Vt mutants (Table 1) with the predicted change in binding energy (ΔΔG) for the mutants (Supplemental Figure3.4A). The mutations evaluated are listed in Table 1, with the mutation sites mapped onto the Vt structure in Supplemental Figure 3.4B. These ΔΔG values show good agreement with our experimental data, with a high correlation coefficient of 0.68. This model is also very similar to that proposed by Golji*et al.*, though their model was generated entirely *in silico*(*92*).

In both the manual fit and DMD models, the orientation of Vt within the EM reconstruction places the N- and C-termini of Vt outside of the reconstructed volume(Figure 4B,C). These regions are either not present or have larger B-factors relative to the helix bundle(*72*) in the Vt crystal structure suggesting conformational heterogeneity. To further evaluate whether regions presenting low density in the averaged reconstruction are conformationally mobile, we used heteronuclear NOE(*152*) experiments to evaluate the fast dynamics of Vt^{Q1018K}, a Vt variant with a decreased propensity to form the non-physiological Vt dimer at NMR concentrations(*72*) (Supplemental Figure3.4D). Low heteronuclear NOE values at the C-terminal hairpin suggest that these residues are mobile and would be less likely to contribute a signal by EM. We also used fast-HSQC(*151*) and CLEANEX(*150*) NMR experiments to look at solvent exchange. These results show that NMR-based hydrogen exchange results reveal that backbone amides associated with the N-terminal strap and C-terminus for both Vt^{WT} and Vt^{Q1018K}possess high rates of solvent exchange, further suggesting

that these regions are intrinsically disordered and likely more conformationally variable (Supplemental Figure3.4C). Taken together, the NMR data suggest that the N-terminal strap and C-terminal arm are unlikely to be observed by EM as they do not have a single defined orientation, consistent with our inability to fit these regions in the micrograph.

While both pseudo-atomic models obtained using manual and computational approaches yielded a reasonable match with the EM density, the resolution limits interpretation of the Vt:F-actin complex on a per-residue basis. Despite the ambiguity in positioning the Vt domain onto the actin filament, the actin surface that interacts with Vt is similar to the J-model(*91*). However, the orientation of Vt in our manual and DMD models is significantly different from the J-model. The manual fit places the bottom of the helix bundle at the pointed end of the actin filament instead of the barbed end. In both of our models, H3 and H4 are oriented towards the F-actin filament, as opposed to the strap, H2, and H3(*91*) (Figure3.5A,B). Again, due to resolution limitations, we cannot strongly advocate one our models over the other (e.g. manual versus DMD); however, both of our models are supported by mutagenesis data and contain a similar actin-binding surface that contains residues (I997, V1001) critical for actin binding, Notably, this novel actin binding surface is distinct from that previously proposed by Janssen *et al* (Figure3.5C) and is the first report of hydrophobic residues driving the interaction between F-actin and vinculin.

F. Discussion and Conclusions

Vinculin is an essential scaffolding protein that binds multiple ligands and plays key roles in regulating FA assembly and disassembly. While recent studies have begun to unravel multi-component functions of vinculin(*42, 157*), the challenge of generating vinculin variants deficient

in a specific interaction has limited the ability to correlate a specific interaction with a specific role at the FA. Here, we report the characterization of two vinculin variants, I997A and V1001A, which retain vinculin structure but are deficient in actin binding.

Previously, studies with vinculin variants deficient in actin binding utilized deletion(s) that removed part of the helix bundle, thereby disrupting the domain structure(*66*, *90, 154*). Although a vinculin variant (T10) that contained three point mutations was identified as deficient in actin binding, only a modest 20% drop in actin binding was observed (2 μM Vt, 5 μM F-actin)(*73*). In contrast, our I997A and V1001A point mutations result in 50% and 30% reductions, respectively, in actin binding (5 μM Vt, 10 μM F-actin, Figure3.1B). Importantly, both variants maintain Vt structure and PS binding. While Vt^{I997A} shows reduced affinity for PIP_2, Vt^{V1001A} retains PIP_2 binding, making these variants useful tools for studying the F-actin:Vt interaction.

The significant decrease in actin binding by both Vt^{I997A} and Vt^{V1001A} was especially intriguing, considering that both mutations reside on H4 and are outside of the binding sites reported by Janssen *et al*.(*91*) (Figure3.5). This data, along with other findings(*92*), suggest that the J-model is incomplete in its description of the actin-binding interface. The J-model places the F-actin binding interface on H2 and H3 of Vt, split between two sites(*91*), relying on the mutagenesis of Cohen *et al.* (*73, 91*). The variants most deficient in F-actin binding, identified in this earlier study (T9, T10, and T19, though defects in binding are small, <20%), all support the involvement of the lower site in the J-model, which resides primarily on H3 and at the N-terminus of H4. However, less evidence exists for the upper site. MD simulations by Golji*et al.* also support the lower site identified in the J-model, but their upper site contains the surface we identify here(*92*). Our identification of vinculin variants impaired in actin binding support the

importance of the hydrophobic surface on Vt H4 in mediating interactions between vinculin and actin.

While Vt^{I997A} retains PS binding, a reduction in PIP_2 association is observed, suggesting that the actin and lipid binding interfaces on Vt overlap. This observation is further supported by data that vinculin binding to F-actin and PIP_2 are mutually exclusive events(*86*). To better understand the implications of these binding events and their interplay, an improved understanding of how Vt binds PIP_2 is required. We are currently pursuing a structural model for this interaction that will help explain the decreased affinity for PIP_2 in Vt^{I997A} and provide ways to probe the function of the vinculin:PIP_2interaction in cells.

As demonstrated in Figures 3.2 and 3.3, cells expressing these variants display defects in cell spreading and have abrogated responses to pulses of force, a phenotype similar to that observed for an actin-bundling deficient mutant(*39*). These results are not surprising given that actin binding is required for filament bundling. While cells transfected with $vinculin^{I997A}$ or $vinculin^{V1001A}$ show a loss of reinforcement, the effect is more dramatic for $vinculin^{I997A}$, likely due to its weaker affinity for F-actin. However, the variant with the greatest impairment in binding, $vinculin^{I997A}$, resulted in a more extreme phenotype, as would be expected.

The cellular phenotypes associated with these actin-deficient vinculin variants closely match and support findings published by Thievessen*et al*(*42*). We observed a decrease in cell spreading, in FA number, and an increase in FA size in cells expressing vinculin variants defective in F-actin binding. Similarly, Thievessen*et al.* found that average FA size did increase in cells expressing $vinculin^{I997A}$, likely due to an increase in FA growth rate. Additionally, they reported an increase in F-actin flow rates in the lamellipodium and at FAs and a decrease in FA formation density. Similar phenotypes were observed when activating mutations in the vinculin

head were introduced in the context of the vinculin^{I997A} mutation, indicating that alterations in cellular phenotype are due to the actin binding defect(*42*). The increase in F-actin flow resulting from decreased vinculin:F-actin affinity is likely a significant contributor to the observed cell spreading defect. Moreover, the decrease in FA density likely plays a role in the cell spreading defect, and is congruent with our observation of fewer total FAs present in cells expressing these vinculin variants.

Our findings that actin-binding deficient vinculin variants increase the average FA size agree with those published earlier(*42*) and help to shed light on the factors influencing FA growth and maturation. The size of FAs is influenced by multiple factors such as rate of assembly and disassembly, density of the matrix to which the cells are adhering, mechanical tension and other factors that have not been fully determined. Further, the role of mechanical tension in the assembly and growth of FAs has become controversial(*158*). Initial studies implicated tension as a critical factor(*159, 160*). However, work from Gardel's group has questioned the role of tension in adhesion maturation(*161*). Interestingly, we find that cells expressing actin-binding deficient vinculin variants have larger and fewer FAs than cells expressing vinculin^{WT}. These cells also exhibit a deficit in their mechanotransduction response and fail to stiffen when external tension is applied to FN-coated beads that are attached to the cells. The observation that these cells have larger FAs argues that mechanical tension at FAs mediated by the vinculin:F-actin interaction is not required for FA maturation and stabilization(*42*).

In addition to changes in FAs, transfecting cells with actin-binding deficient vinculin variants resulted in changes on the cellular level. We observed that Vin-/- MEFs expressing vinculin^{I997A} were significantly smaller than those expressing vinculin^{WT} or vincuiln^{V1001A}. These

observations are similar to those described earlier by Shen *et al.*, where Vin-/- MEFs expressing vinculin variants deficient in F-actin bundling are significantly smaller than those expressing vinculin^{WT}(*39*). We suspect that vinculin^{I997A} has a more drastic effect than vinculin^{V1001A} due to its reduced affinity for F-actin. It cannot be ruled out, however, that decreased affinity for PIP_2 could also play a role in regulating cell area. While these observations seem at odds with the finding that MEFs expressing just the vinculin head (and losing all Vt functions) are larger(*162*), our data indicate that the vinculin:F-actin interaction plays a role in maintaining cell size, though other vinculin functions are also important in regulating this attribute.

Additionally, there is evidence that both Vt and F-actin undergo a conformational change upon binding(*37, 90*). Lower resolution of negative-stain EM coupled with likely conformational changes associated with complex formation place limitations on fitting isolated structures of Vt and actin into the complex. In this case, model selection or elimination requires additional data, such as the mutagenesis data described above. Moreover, as Vt is able to simultaneously bind F-actin and the RNA binding protein raver1(*137*), it is unlikely that these interfaces overlap. The binding site for raver1 was identified through x-ray crystallography and is supported by mutagenesis. This interface overlaps the upper site in the J-model (Figure3.5C), suggesting that, at best, the upper site of the J-model is incomplete.

Based upon these concerns and the new data presented herein, we propose a new F-actin binding surface on Vt. This new surface on H4 is located at the Vt:F-actin interface in both of the models generated in this work (Figure3.5A,B). It is obscured in full length vinculin due to autoinhibitory interactions with Vh, consistent with previous work showing that the Vh:Vt interaction impairs binding to F-actin(*98*). Additionally, this actin binding surface is not involved in interactions with raver1, allowing for simultaneous binding to both ligands. The hydrophobic

nature of the new surface, as shown by the importance of the isoleucine and valinesidechains, is congruent with reports that many actin-binding proteins recognize a hydrophobic cleft in actin(*163, 164*). Our surface is also supported by the differences in how vinculin and metavinculin interact with F-actin. Structurally, metavinculin tail is nearly identical to Vt at our binding surface, and shows structural differences near the C-terminus and strap(*29*), regions thought to be important for crosslinking of F-actin(*39*). These observations are in agreement with metavinculin tail's ability to bind F-actin and inability to crosslink F-actin into tight bundles(*99, 165*). Thus, while we are unable to uniquely determine the orientation of Vt with respect to F-actin or identify specific residue-residue contacts given the resolution of our EM data (~20 Å), we have identified a novel surface of vinculin important for actin binding. This surface is supported not only by our mutagenesis and cellular data, but also by the current literature.

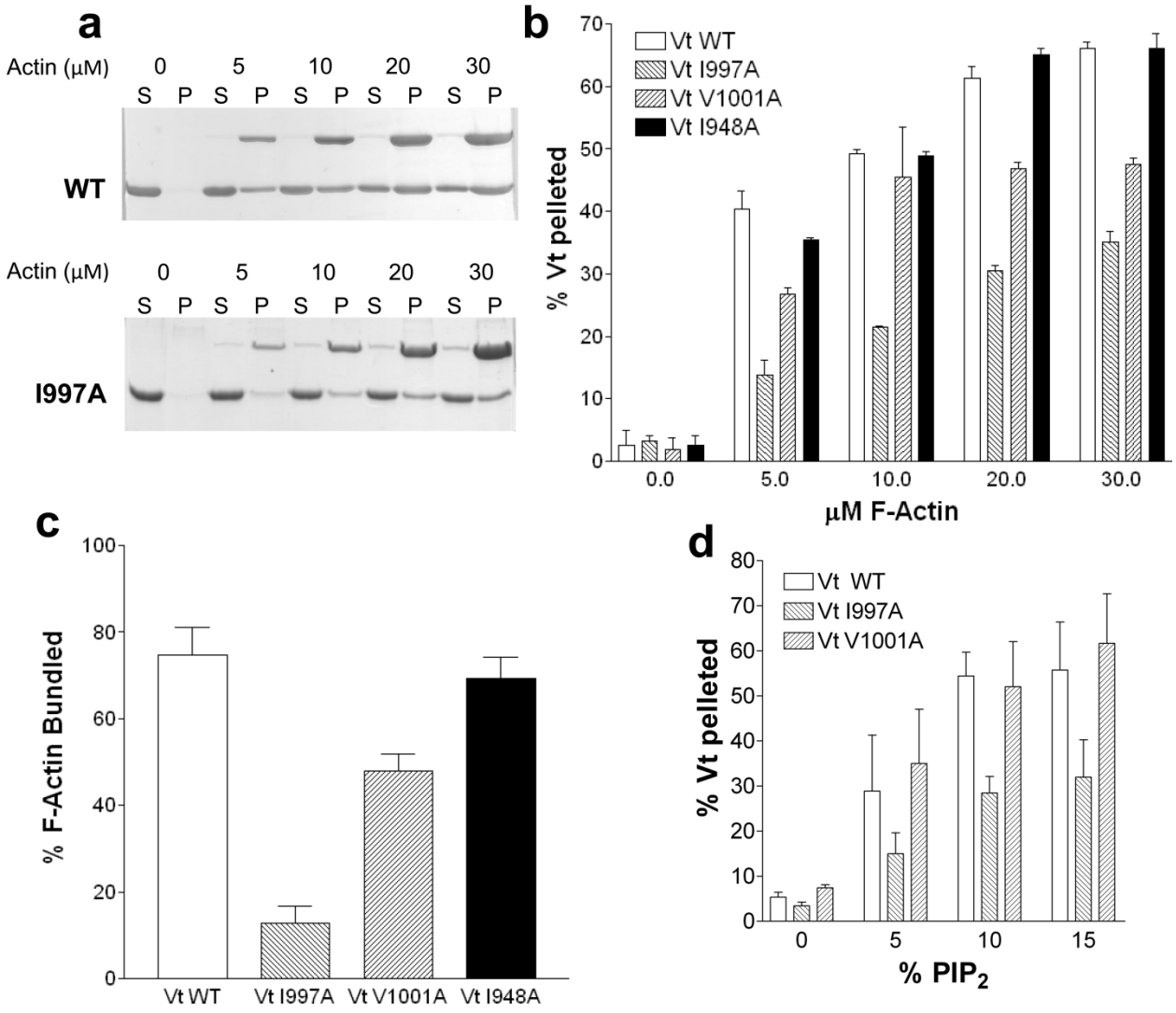

Figure 3.1.Vt^{I997A} and Vt^{V1001A} are deficient in F-actin binding and bundling yet retain specificity and association with PIP_2. (A) SDS-polyacrylamide gel electrophoresis of supernatant (S) and pellet (P) fractions after co-sedimentation of Vt with F-actin. Actin concentrations and Vt variants are noted. (B) Quantification of F-actin co-sedimentation assays identifies Vt variants in H4 deficient in F-actin binding. (C) Vt variants deficient in binding to F-actin are also defective in F-actin bundling. (D) Vt^{V1001A}, while deficient in actin binding, retain PIP_2 binding comparable to Vt^{WT}. Vt^{I997A}, however, is impaired in PIP_2 binding. Error bars are standard deviation, n= 3.

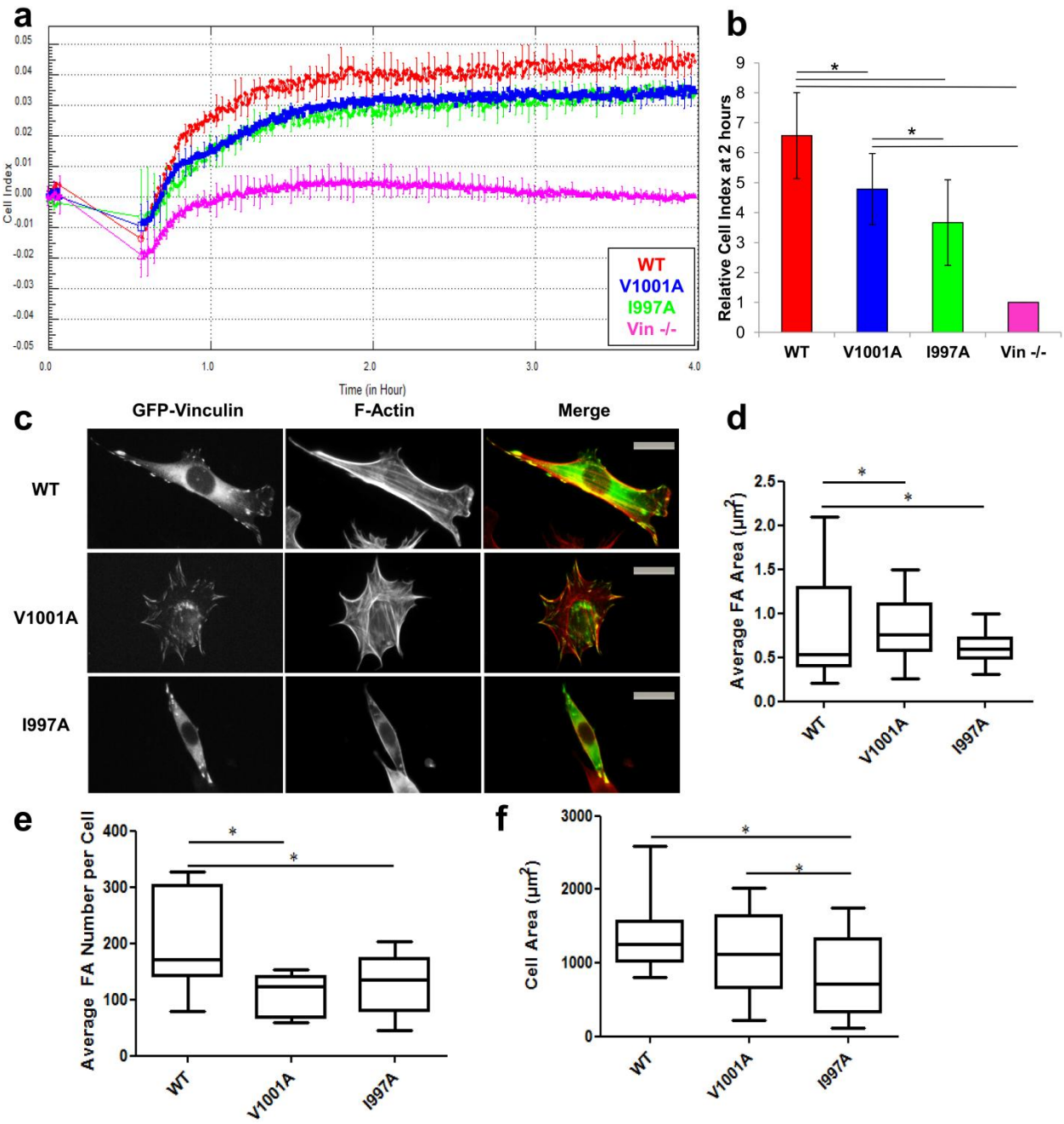

Figure 3.2.Vinculin variants deficient in actin binding affects spreading and cell adhesion in MEFs. (A) RTCA using the xCELLigence system shows that Vin-/- cells expressing vinculin^{WT} have higher cell impedance, hence more spread, than cells expressing vinculin^{V1001A}, vinculin^{I997A} or Vin -/-.MEFs. A representative trace of cell impedance (graphed as cell index (CI)) taken every 15 seconds for 13 hours; lower impedance indicates less contact with the

sensor. Each data point represents an average CI of at least triplicate wells for each condition. (B) A graph showing the relative CI of cells spread on FN two hours following plating, which corresponds to the same time as the pictures shown in (c). Data is the average ± SEM combined from four independent experiments. *p≤ 0.05, in comparison to vinculin^{WT}.(C) Vin-/- MEFs transfected with GFP-tagged vinculin^{WT}, vinculin^{I997A}, or vinculin^{V1001A} and plated on FN for two hours. Vinculin^{I997A} and vinculin^{V1001A} exhibit the same localization as vinculin^{WT}. (D,E,F) Box and whisker plots of FA area (D), FA number (E) and cell area (F). Areas were calculated using Matlab (Methods) (n=25. Cells expressing vinculin^{I997A} and vinculin^{V1001A} had fewer and larger FAs, *p-value≤0.05. Cells expressing vinculin^{I997A} were significantly smaller, but those expressing vinculin^{V1001A} were not. Scale bar is 25 μm.

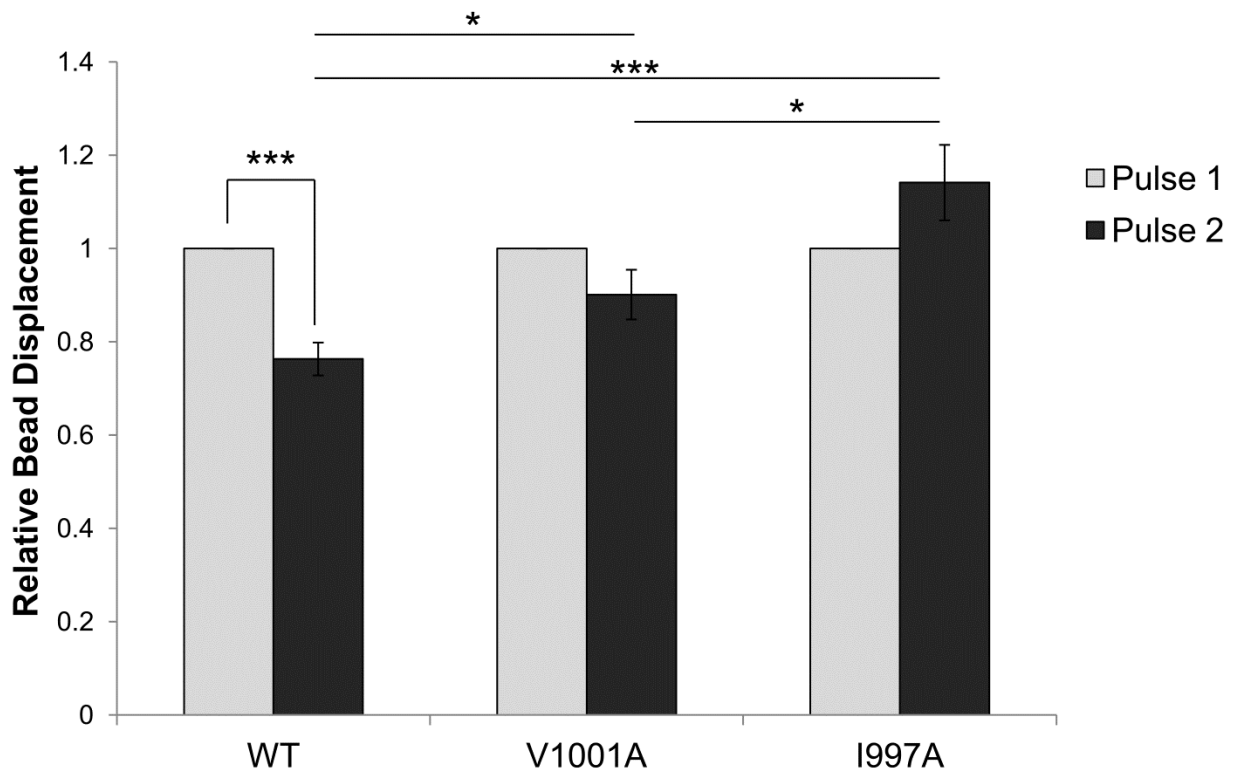

Figure 3.3. Actin binding to vinculin is necessary for the mechanical response to force on integrins. Upon applying pulses of a constant force, a decrease in the relative bead displacement of Vin-/- MEFs transfected with vinculin^{WT} is observed, in contrast to the increase observed for Vin-/- MEFs transfected with vinculin^{I997A}. For the relative bead displacement measurements, two force pulses were applied to FN-coated beads bound to Vin-/- MEFs transfected with either vinculin^{WT} (n=20), vinculin^{V1001A} (n=19) or vinculin^{I997A} (n = 26). * indicates a p-value<0.05. *** indicates a p-value<0.001. Error bars are standard error of the mean. These results indicate that actin binding to vinculin plays a role in vinculin's ability to respond to force.

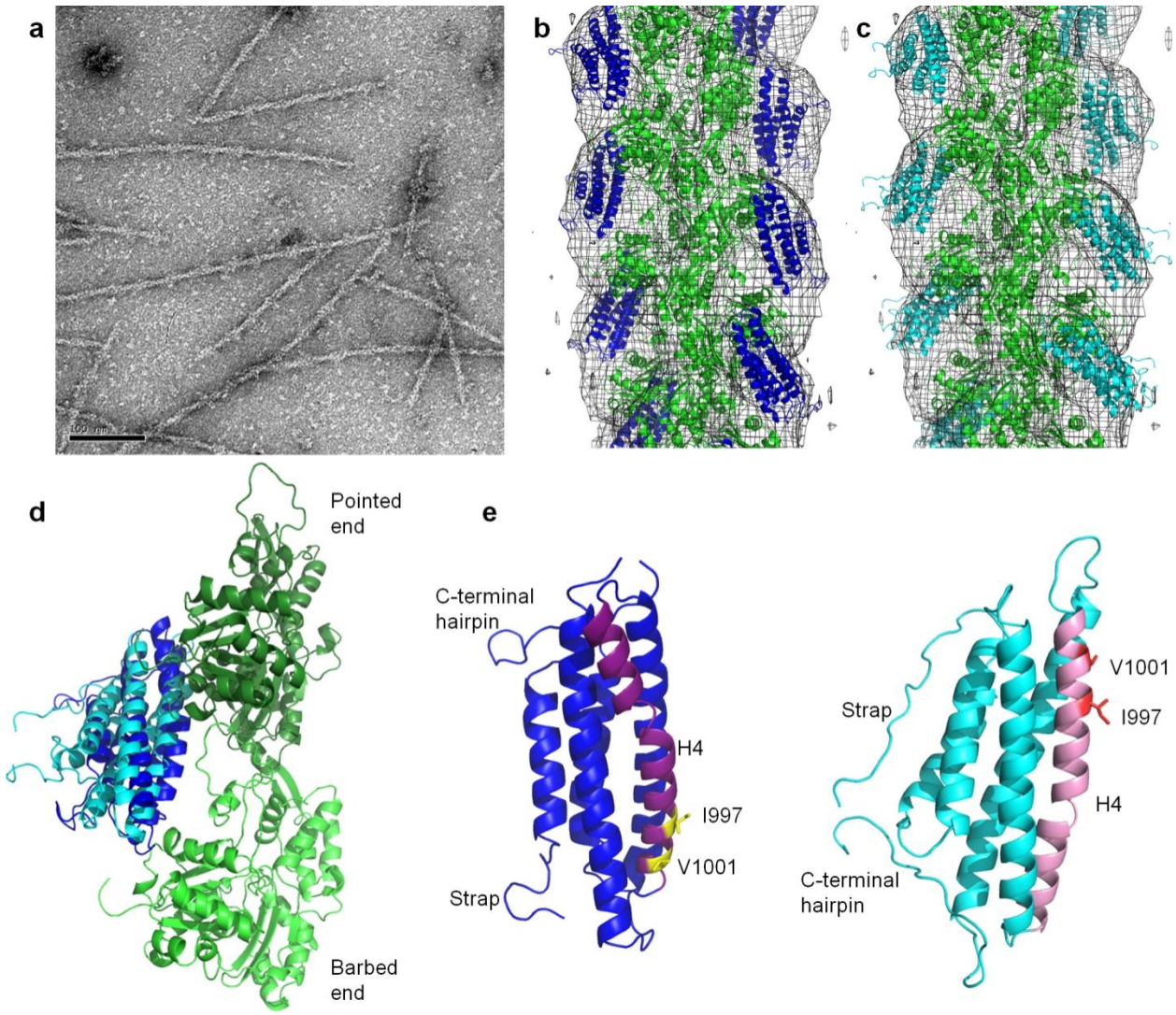

Figure 3.4. The proposed actin binding surface on Vt is consistent with EM reconstruction. (A) Negative stain EM image of F-actin decorated with Vt^{WT}. Scale bar is 100 nm. (B) Manual fit model of Vt bound to F-actin. Crystal structure of the Vt domain (blue ribbon, PDB 1QKR) and the atomic model of F-actin (green ribbon, PDB 1ST6 residues 879-1065) are manually docked into the 3D-reconstruction (gray mesh). (C) DMD model of Vt bound to F-actin. F-actin is in green, Vt in cyan. (D) Comparison of Vt domain orientation from b and c with respect to the two adjacent actin protomers (long-pitch helix F-actin dimer). The color scheme is maintained.

(E, F) Comparison of Vt H4 orientation in the manual fit and DMD models from Band C, respectively. The respective orientation and color scheme of the models has been maintained from D. Note that the manual fit and DMD models are related to each other by an approximately 180° rotation, with H4 at the F-actin interface. H4 is in purple and pink in the manual fit and DMD model, respectively. Residues I997 and V1001 are labeled and shown as sticks, colored in yellow and red in the respective models.

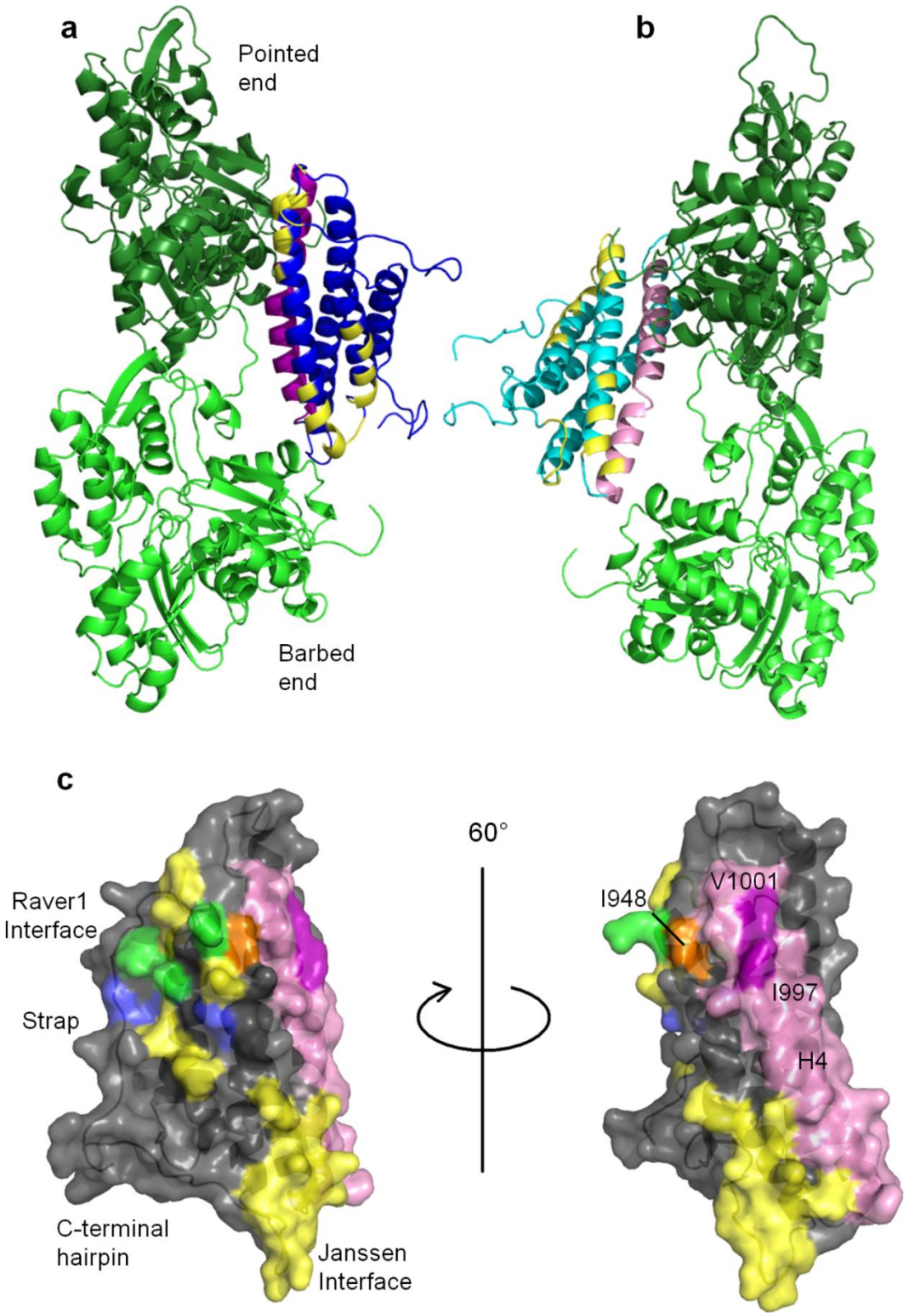
a
Pointed
end
Barbed
end
b
c
Raver1
Interface
Strap
C-terminal
hairpin
Janssen
Interface
60°
I948
V1001
I997
H4

Figure 3.5.The proposed binding surface is not accounted for in the J-model. (A) Manual fit model of the Vt:F-actin complex with the J-model surface mapped on Vt. The actin protomers are in green, with the pointed end on top. Vt is in blue, with H4 in purple. Residues in yellow were identified in the J-model as mediating the Vt:F-actin interaction(*91*). (B) Vt:F-actin complex from DMD model with the J-model surface mapped on Vt. The actin protomers are in green, with the pointed end on top. Vt is in cyan, with H4 in pink. Residues in yellow were identified in the J-model as part of the Vt:F-actin interaction surface(*91*) (C) The J-model surface, raver1 interface, and H4 on Vt. Vt is shown with a semi-transparent surface in gray. Residues in the J-model interface are in yellow. Residues in the raver1 interface are blue(*137*). Those shared between the J-model interface and the raver1 interface are in green. H4 is in pink. I997 and V1001 are in purple and labeled, while I948 is in orange. Two views are shown, rotated 60° from each other. Note that I997 and V1001 are distal from the J-model actin binding interface.

F-actin binding properties of Vt variants and their agreement with the DMD model

Vt Variant	% Vt pelleted at 30 µM F-actin	$\Delta\Delta G_{bind}$ from co-sedimenation	$\Delta\Delta G_{bind}$ from calculation
Vt^{WT} (879-1066)	66 ± 1.3	N/A	N/A
Vt^{I997A}	35 ± 2.6	0.38	1.50
Vt^{V1001A}	48 ± 3.9	0.19	0.48
Vt^{Q1018K}	57 ± 0.6	0.09	1.25
Vt^{D882A}	67 ± 0.5	-0.01	0.02
Vt^{I948A}	63 ± 2.0	0.03	1.18
$Vt^{\Delta C5}$ (879-1061)	62 ± 0.3	N/A	N/A
Vt^{F885A}	76 ± 2.2	-0.09	0.08
Vt^{H906A}	94 ± 1.1	-0.21	0.35
Vt^{L928D}	75 ± 0.3	-0.08	-0.08
$Vt^{\Delta N}$ (893-1066)	78 ± 0.3	N/A	N/A

Table 1. Summary of F-actin binding by Vt variants. Several Vt variants were generated and evaluated for their ability to bind F-actin. The percent of Vt that pellets with F-actin at 30 µM F-actin is reported as a measure of F-actin binding. All variants have been evaluated by NMR analyses (1H-15N 2D HSQC) and appear to fold properly (Figure3.3, data not shown). The Vt variants are grouped into three categories based on their ability to bind F-actin. The mutation sites are mapped on the structure of Vt in Supplemental Figure 3.4B.

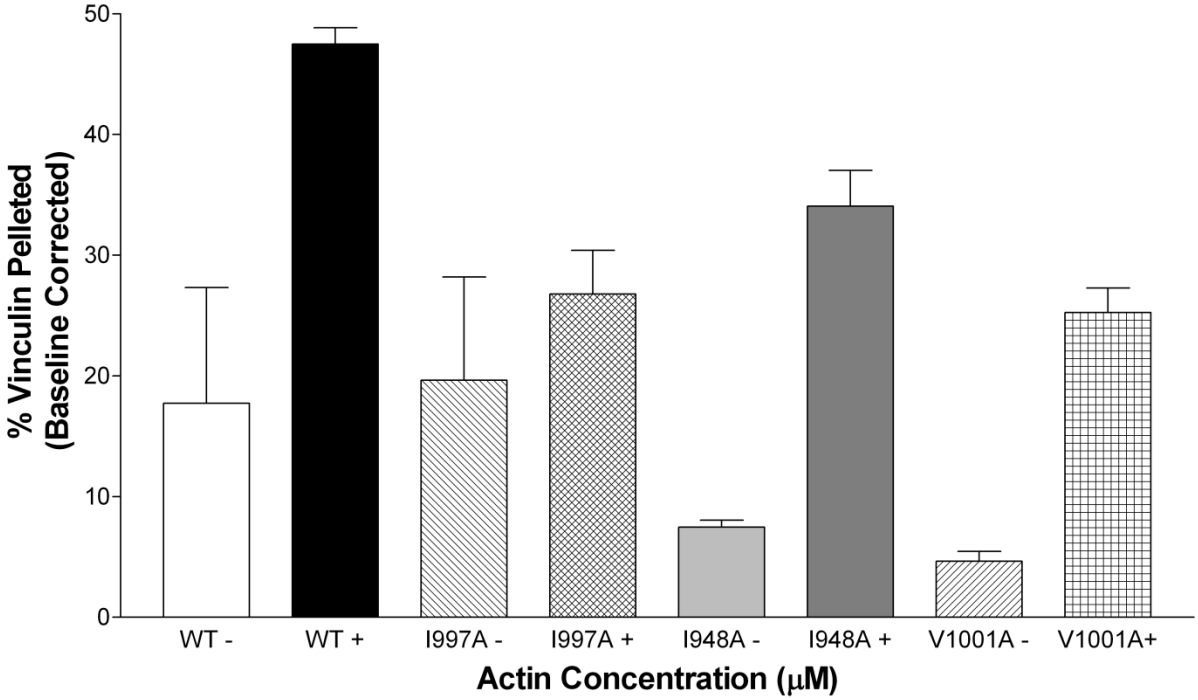

Supplemental Figure 3.1.Binding of F-actin by full-length vinculin^{WT}, vinculin^{I997A}, and vinculin^{I948A}. The percentage of vinculin bound to F-actin (30 μM) is shown, with (+) and without (-) IpaA peptide. Addition of IpaA peptide disrupts autoinhibitory Vh:Vt interactions, exposing the actin-binding site on Vt and allowing it to bind with higher affinity to F-actin. Vinculin^{I997A} and vinculin^{V1001A} show significantly reduced F-actin association compared to vinculin^{WT} in the presence of the activating peptide. Vinculin^{I948A} binds to F-actin similarly to vinculin^{WT}. In the absence of the IpaA peptide, vinculin and its variants bind very little F-actin. Error bars are standard error.

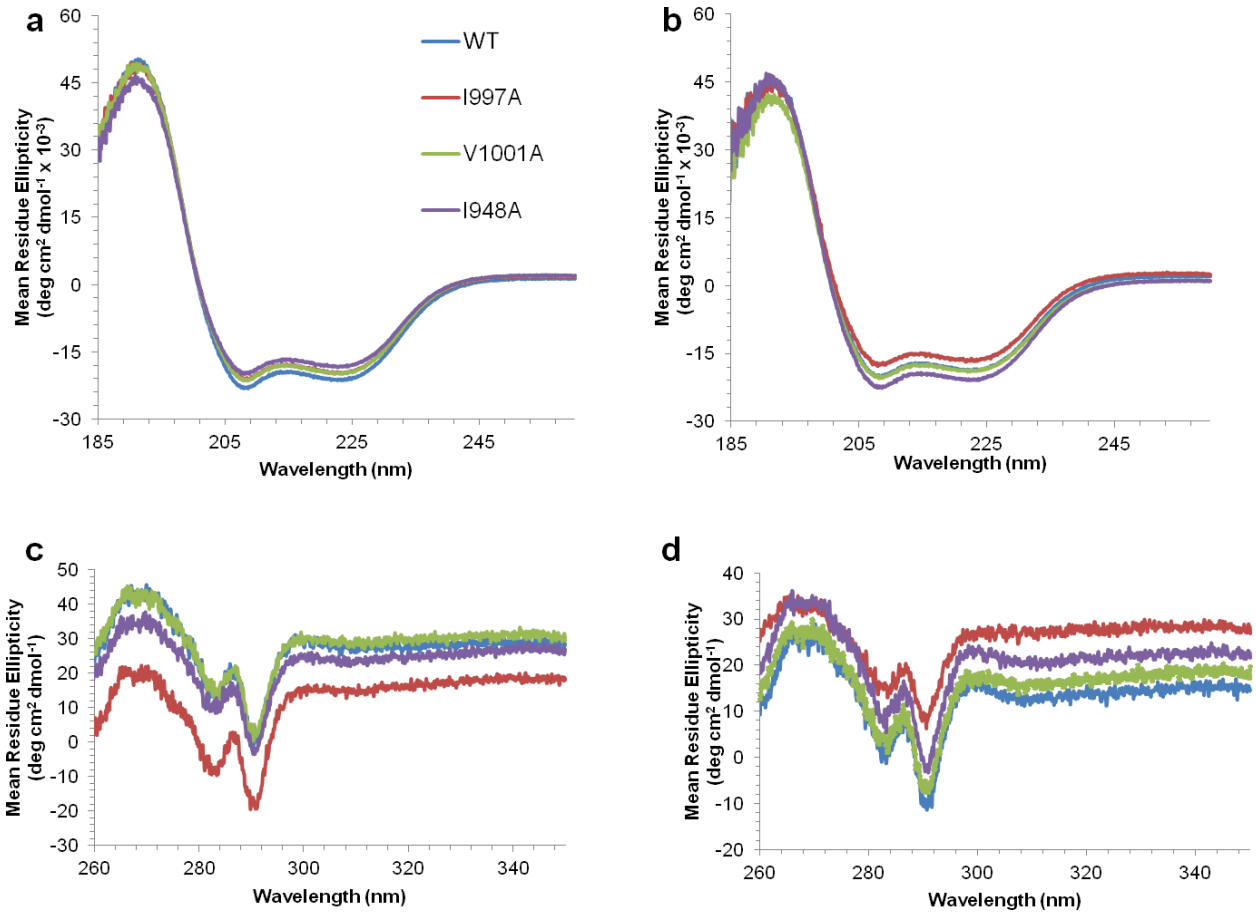

Supplemental Figure 3.2.CD analyses of Vt variants. (A, B) Far-UV spectra of Vt^{WT} and variants Vt^{I997A}, Vt^{V1001A}, and Vt^{I948A} at pH 5.5 (A) and 7.5 (B). All three variants show similar α-helical content to VtWT. (C, D) Near-UV spectra of VtWT and Vt variants at pH 5.5 (C) and 7.5 (D) All Vt proteins exhibit similar spectra showing a distinct pattern between 260 and 300 nm, indicative of tryptophan packing interactions, suggesting that packing interactions between the N-terminal strap and C-terminal arm are retained.

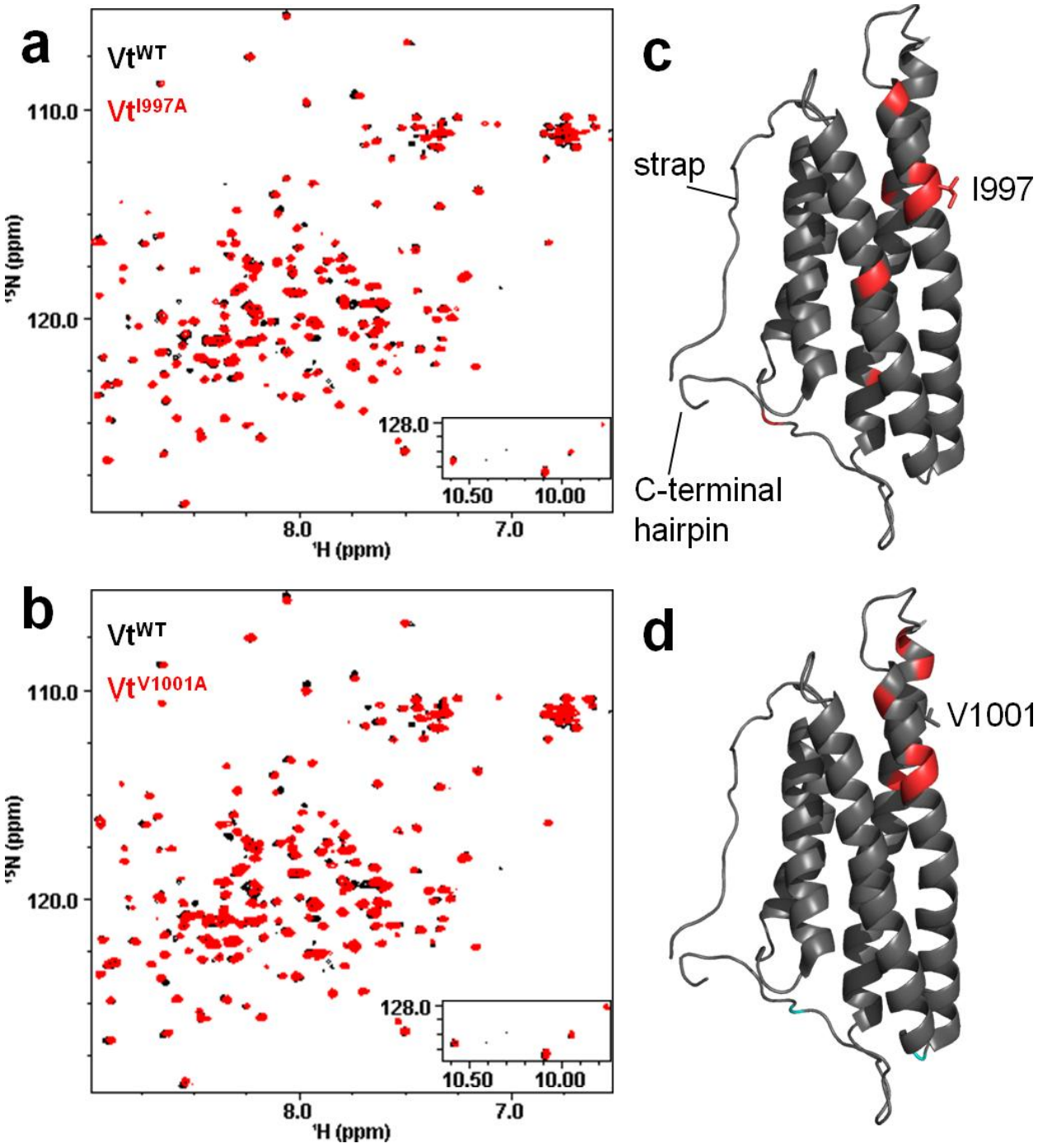

Supplemental Figure 3.3.2D NMR 1H-15N HSQC spectral overlay of Vt^{WT} and Vt variants.1H-15N HSQC of (A) Vt^{I997A} and (B) Vt^{V1001A}. The similarity of the overlaid spectra suggests that the chemical environment of the backbone amides remains largely unchanged. Downfield-shifted peaks are shown in the inset. (C, D) Peaks with significant changes in Vt^{I997A}

and Vt^{V1001A}, respectively, are mapped onto the Vt^{WT} structure. Peaks with significant change in chemical shift (δ ppm > line width) are mapped on the structure in red, while those that exhibit significant broadening (line width > 2*line width WT) are mapped in cyan. Residues that significantly shift in Vt^{I997A} are K956, K996, I997, L998, T1004, V1024, E1040, and V1059. Residues that significantly shift in Vt^{V1001A} are K996, I997, L998, A1003, D1013, E1015, and H1025. The side chain associated with the mutation site is shown in sticks. Residues that shift significantly are close to the site of mutation, suggesting that the perturbations are localized.

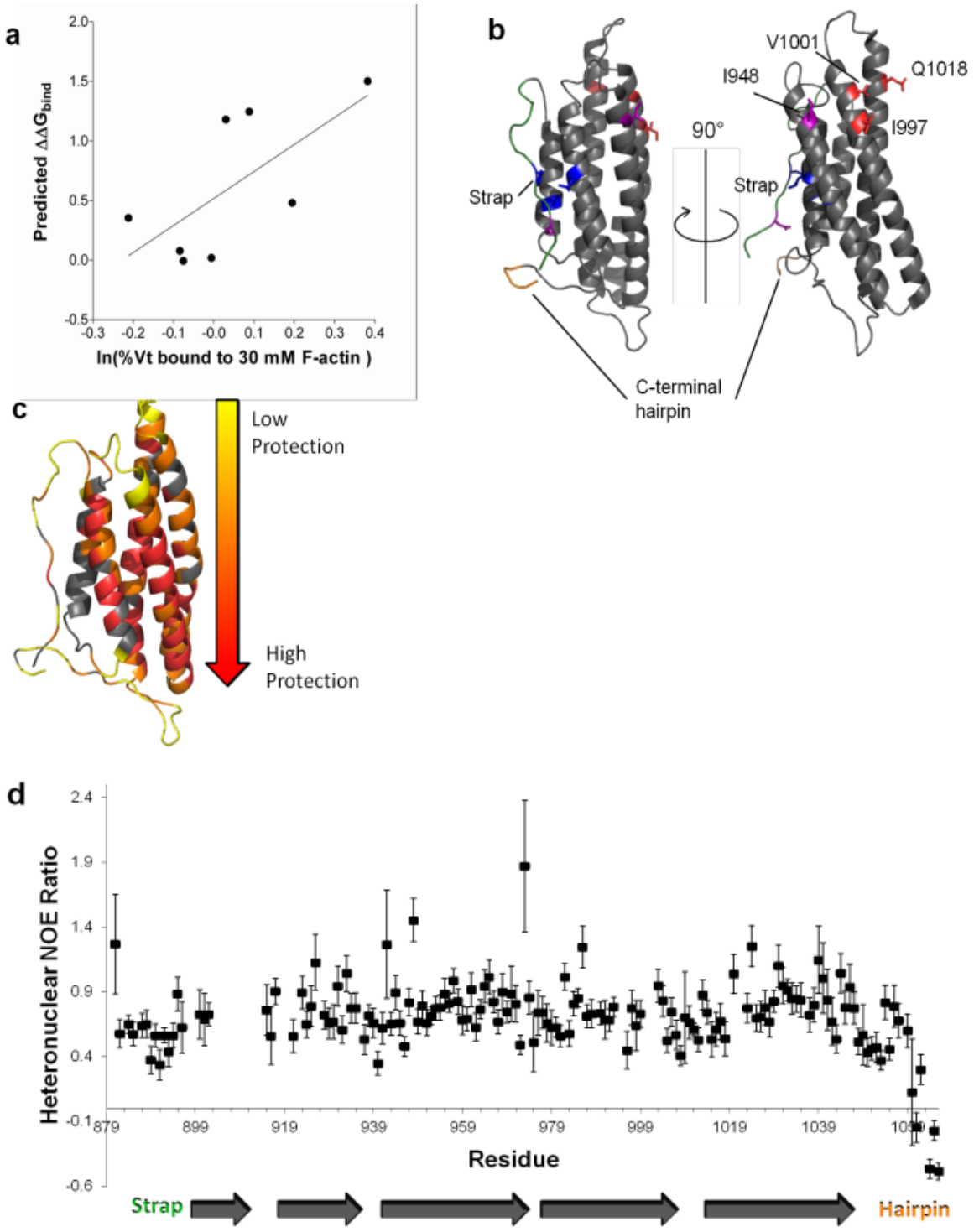

Supplemental Figure 3.4.Evaluation of the DMD model. (A) Evaluation of the Vt-actin DMD model. The natural log of % Vt bound at 30 μM F-actin for different Vt variants is compared

with the MedusaDock1-3 predicted change in free energy of binding for the Vt variants (Table 1) and F-actin. The DMD model shows a reasonable fit to the data (R2 = 0.467). (B) The Vt variants from Table 1 are mapped onto the Vt structure (PDB 1ST6). Residues in red, when mutated, decrease the affinity for F-actin. Residues in purple have no significant effect on actin binding to Vt, and residues in blue, when mutated, increase the affinity for F-actin. The N-terminal strap is in green and the C-terminal hairpin in orange. (C) Protection factors from hydrogen exchange NMR experiments. Residues are colored based upon their protection factors. Residues in red exhibited the greatest protection, with residues in yellow the least. Residues in orange fall in the middle of the spectrum. Residues in gray are not assigned. (D) Heteronuclear NOE NMR spectroscopy data. The graph displays the 15N heteronuclear NOE ratio at 60.78 MHz for Vt^{Q1018K}. Values near 0.8 are indicative of greater rigidity, while lower values indicate greater motion on the ps-ns timescale for the backbone amides. Error bars reflect experimental error. The arrows represent Vt helices, with the N-terminal strap and C-terminal hairpin labeled. These data reveal that in Vt^{Q1018K}, and likely Vt^{WT}, the N-terminal strap and especially the C-terminal hairpin are conformationally mobile.

IV: Phosphorylation at Y1065 in VinculinMediates Actin-Induced Vinculin Dimer Formation, Cell Spreading, and Mechanical Responses to Force

A.Overview

Vinculin is an essential structural adaptor protein that localizes to sites of adhesion and is involved in a number of cell processes including adhering to substrates, spreading, motility, force transduction, and cell survival. The C-terminal vinculin tail (Vt) domain contains the necessary structural components to bind and crosslink actin filaments. Actin binding to Vt causes a conformational change that promotes dimerization necessary for actin filament crosslinking. We have shown that the C-terminal hairpin of Vt is critical for actin-induced Vt dimerization and subsequent actin bundling .Here we show that Y1065 within the C-terminal hairpin, a known Src substrate, regulates Vt-mediated actin bundling. Furthermore, we show that phosphorylation at Y1065 plays a role in the cellular response to mechanical forces upon applying tension to integrins.

B. Introduction

The ability of cells to respond to external stimuli, such as during cell spreading events or in response to pulses of force, requires signaling to be transduced via transmembrane receptors to the actin cytoskeleton. These signals initiate a signaling cascade as the cells mediate their

response to the appropriate stimuli. Integrins constitute a family of transmembrane receptors that typically mediate cell-extracellular matrix interactions (*166*), and can activate a number of signaling pathways and cellular processes, including cytoskeletal rearrangements and assembly of focal adhesions (FAs) (*167, 168*). It has been previously shown that force-mediated activation of integrins by fibronectin (FN) promotes cellular stiffening. One example is integrin-mediated activation of RhoA that leads to an increase in actomyosin contractility and adhesion maturation (*158, 169-171*). Vinculin has also been shown to be recruited to FAs and reinforce the adhesion under tension, although this mechanism is poorly understood (*172*). Consistent with these observations, variants of vinculin that are impaired in actin bundling significantly impair cell stiffening in response to pulses of external force(*39, 173*).

Vinculin is a highly conserved and large (1066 amino acids) structural adaptor protein that localizes to both FAs and adherens junctions (*109, 135*).Vinculin plays an essential role in embryonic development as demonstrated in knockout mice which show defects in heart and neural tube formation and do not survive past day E10.5 (*2*). Fibroblasts isolated from knockout mice exhibit a number of defects, including a rounded morphology, increased motility (*2*), and resistance to apoptosis and anoikis (*9*). Vinculin has been implicated in the regulation of FA turnover (*79*), FA dynamics at the leading edge of migrating cells (*42*), and force transduction (*128*). However, the mechanism by which vinculin regulates these various functions remains to be fully characterized.

Vinculin contains three main domains: a large helical head domain (Vh), a proline-rich linker region, and a tail domain (Vt). Each of these respective regions binds to a number of proteins. While talin, α/β-catenin, α-actinin, MAPK, and IpaA from *Shigella flexneri* bind to Vh (*52-57*), VASP, Cbl-associated protein (CAP)/ponsin, vinexin α/β, nArgBP2, p130CAS, and the

Arp2/3 complex associate with the proline-rich linker (*58-63*). A number of ligands also bind Vt including PKCα, paxillin, Hic-5, raver1, α-synemin, PIP_2, and F-actin (*21, 64-70*). In the autoinhibited conformation, vinculin's scaffold function is impaired by intramolecular interactions between Vt and Vh. Vinculin is considered in its active state upon the release of the Vt and Vh through combinatorial binding of ligands to each domain that lead to recruitment of binding partners to maturing adhesion complexes (*98, 113*). In focal adhesions (FAs), vinculin transduces mechanical cues since it helps link integrins with the cytoskeleton through its association with talin and F-actin.

In recent years, a number of models for how Vt binds to and bundles F-actin have been proposed. Upon binding to F-actin, Vt undergoes a conformational change that allows the exposure of a cryptic dimerization site that enables F-actin bundling (*66, 98*). Janssen *et al*. proposed a structural model of the Vt/F-actin complex using computational docking, negative-stain electron microscopy, in which Vt binds to F-actin through two sites: site one binds via helices 2 and 3 and site two binds through helices 3, 4, and the C-terminus (*91*). In the proposed model, deletion of the N-terminal strap impairs actin bundling while deletion of the C-terminus enhanced actin bundling (*91*). However, contrasting data have arisen that support a distinct hydrophobic Vt interface critical for the association with actin on helix 4(*42, 92,173*). Furthermore, the C-terminal hairpin of Vt is essential for Vt self-association and subsequent F-actin crosslinking (*32, 39*).

Within the C-terminal hairpin, there is a known phosphorylation site and Src substrate, Y1065. Vinculin was one of the first substrates identified to be phosphorylated by the transforming oncogene of Rous sarcoma virus, v-Src (*100*). Previous studies have shown that phosphorylation of Y1065 alters a number of cellular processes including traction forces,

exchange from adhesions, and cell spreading (*102, 103*). Phosphorylation at Y1065 has also been shown to mediate intramolecular interactions with Vh and binding to the Arp2/3 complex (*102, 105*). Within vinculin, Y1065 forms contacts with a number of residues including P878 within Arp2/3 complex binding site (*62*), D882 in the N-terminal strap, and K915 within the loop between helix 1 and 2 (Fig. 1). However, the effects of phosphorylation or mutation to this site on vinculin function have not been explored.

In this study, we provide evidence that Src-mediated phosphorylation of Vt modulates F-actin bundling and disrupts binding to Vh, but retains binding to PIP_2 and actin. Additionally, we show that a common mutation of Y1065 (Y1065F) exhibits an aberrant F-actin bundling capacity and also disrupts binding to Vh, but retains binding to other ligands. These results are consistent with our findings that the C-terminal hairpin of Vt, containing Y1065, is critical for actin induced Vt-dimerization and F-actin bundling. We have structurally characterized alternate Vt variants that either mimic or prevent phosphorylation at this site to study the impact of phosphorylation at Y1065 on cell spreading and cellular stiffening in response to force. Through this combined evidence, we propose a computational docking model that provides the first evidence for what the Vt dimer may look like in order to bundle F-actin and implications for vinculin-mediated F-actin bundling in transducing external forces.

C. Materials and Methods

1. Expression and purification of proteins

Expression of chicken Vt was performed as previously described (*88*). Briefly, cultures were grown at 37°C and were induced with isopropyl β-D-1-thiogalactopyranoside (IPTG; 0.25 mM) prior to dropping the temperature to 18°C for 12-16 hours. Following centrifugation and

resuspension in lysis buffer, cells were lysed by sonication and the lysate cleared by centrifugation. Vt was purified using Ni-NTA-agarose beads (Qiagen; Germantown, MD), the His-tag was removed by Thrombin (Sigma) and loaded onto a cation-exchange chromatography. Vt and full-length vinculin variants were generated by QuikChange site-directed mutagenesis (Stratagene; La Jolla, CA) and sequences verified by DNA sequencing (Genewiz; Research Triangle Park, NC).

Full-length vinculin transformed into *E. coli* strain BL21-DE3 RIPL cells and purified as previously described (*42*, *173*) with minor modifications. Briefly, cells were grown at 37°C prior to induction with IPTG (0.5 mM) for approximately three hours. Pellets were resuspended in lysis buffer (20 mMTris, 150 mMNaCl, 5 mM imidazole, 2 mM β-mercaptoethanol, pH 7.5). Cells were lysed by sonication, and then cleared by centrifugation. The supernatant was loaded onto a Ni-NTA column was washed twice with nickel wash buffer (20 mMTris, 150 mMNaCl, 40 mM imidazole, 5 mM β-mercaptoethanol, pH 7.5) and vinculin was eluted with nickel elution buffer (20 mMTris, 150 mMNaCl, 500 mM imidazole, 5 mM β-mercaptoethanol, pH 7.5). Following removal of the his-tag, vinculin was further purified by anion-exchange (Hiprep Q XL 16/10) column chromatography using a gradient of 0.05 to 1 M NaCl. The final product was evaluated by SDS-PAGE for purity prior to use for biochemical assays.

The kinase domain of c-Src(residues 251-533) kindly provided by J. Kuriyan's lab at the University of California (Berkeley, CA) and was purified as previously described (*174*). The purified protein was stored in 50% glycerol aliquots at -20°C until use.

Expression of GST and GST-VH (residues 1-811) were performed as previously described (*62, 116*) with minor modifications. Briefly, GST-VH was transformed into the *E. coli* strain JM109. 500 mL cultures were grown at 37°C until induced with 0.1 mM IPTG and

cultures were then grown at room temperature 12-16 hours. Cells were lysed in 1X PBS, 1% Triton X-100 in the presence of 1mM phenylmethylsulfonyl fluoride and 10 µg/mL of aprotinin and leupeptin. The proteins were purified by incubation with glutathione-sepharose 4B beads (GE Healthcare) at 4°C for 3 hours and then washed with 1X PBS.

2. Generation of phosphorylated Vt

Following initial purification, WT Vt was dialyzed into phosphorylation reaction buffer (50 mM HEPES, 1 mM $MgCl_2$, 1 mM $MnCl_2$, 1 mM DTT, pH 7.5) prior to incubation with ~1 µM Src and 2 mM ATP at 37°C overnight. To separate phosphorylated Vt, the sample was loaded onto a weak cation-exchange column with buffer A (20 mM Tris, 20 mM NaCl, 2.5 mM EDTA, 1 mM DTT, pH 7.5) subjected to a gradient from 20 mM to 380 mM NaCl. Fractions were collected and verified for phosphorylation by western blot using a phosphotyrosine antibody (Santa Cruz). To calculate the purity of the phosphorylated sample collected through this method, samples were dialyzed in 10 µM ammonium bicarbonate prior to submission for analysis by fourier transform ion cyclotron resonance mass spectrometry.

3. Circular Dichroism (CD)

Spectra were collected from 350-250 nm (near-UV) and 260-190 nm (far-UV) at protein concentrations of 450 and 5 µM, respectively. Data were collected on a Jasco J-815 CD Spectrometer (Jasco; Easton, MD) and on an Applied Photophysics Pistar-180 Spectrometer at 25°C in CD buffer (10 mM potassium phosphate and 50 mM Na_2SO_4, pH 7.5)

4. Thermal stability of Vt

The fast quantitative cysteine reactivity (fQCR) method was used to measure changes in protein stability as previously described (*175*). 1 µM Vt was incubated with 1 mM 4-fluoro-7-aminosulfonylbenzofurzan (ABD-F, Anaspec) in fQCR buffer (25 mM KPO4, 100 mM KCl, pH 7.5) for 1 min at the desired temperature before quenched with 0.1 N HCl. The fluorescence intensity was measured on a PHERAstar plate reader (BMG Labtech). The data were normalized and fit to determine the temperature at which the protein was unfolded, representing the Tm. The slope as Vt transitioned from folded to unfolded was used as an indicator of the cooperativity of the unfolding protein. Data represents the mean ± S.E.M. Data sets were analyzed using the two-tailed Student's *t* test for p-values.

5. NMR Spectroscopy

Vt samples for NMR were prepared from cells grown in M9 media with $^{15}NH_4Cl$ as the sole nitrogen source. The ^{15}N-Vt samples were exchanged into NMR buffer (10 mM KH_2PO_4, 50 mM NaCl, 0.1% NaN_3, 2 mM DTT, and 10% D_2O, pH 5.5) and concentrated to 50µM for WT Vt, Vt Y1065F, Vt Y1065A, and Vt Y1065E and 35 µM for pY-Vt. All heteronuclear single quantum coherence (HSQC) spectra were collected on a Varian INOVA 700 MHz spectrometer at 37 °C5. Processing was done with NMRPipe (*121*) and spectral analysis with NMRViewJ (*149*).

6. Lipid co-sedimentation assays

Vt binding to phosphatidylinositol 4,5-bisphosphate (PIP_2) was evaluated by lipid co-sedimentation assays using small, unilamellar vesicles as previously described(*88, 173*). Relative protein amounts were quantified using ImageJ (*138*).

7. Actin co-sedimentation assays

Actin binding and bundling by Vt and full-length vinculin were measured with a co-sedimentation assay as previously described(*39, 42,173*). Briefly, purified G-actin from rabbit muscle acetone powder (Pel-Freez Biologicals) was polymerized with 2X actin polymerization buffer (20 mM Tris, 200 mM KCL, 5 mM MgCl2, 4 mM DTT, pH 7.5) at room temperature for approximately 30 minutes. To examine the affinity for Vt and full-length vinculin variants for F-actin, a range of F-actin concentrations (0 to 30 µM) was added to 10 µM Vt or full-length vinculin. For co-sedimentations with the full-length vinculin, 100 µM IpaA peptide (Ac-NNIYKAAKDVTTSLSKVLKNIN-NH2) was added. Samples were allowed to incubate at room temperature for 1 hour prior to being subjected to a high-speed spin to assess actin binding (184,200 x g) in a TLA 100 rotor (Beckman Coulter) for 30 minutes. For bundling assays, samples were prepared as described for the actin binding experiment except samples were subjected to a low speed spin (5,000 x g). Pellet and soluble fractions were separated by SDS-PAGE, the band intensity was calculated using ImageJ (*138*), and percentages were calculated as previously described(*39*).

8. Fluorescence microscopy of F-actin bundles

F-actin bundles induced by the addition of Vt variants as well as full-length vinculin variants with or without IpaA, were visualized using fluorescence microscopy, as previously described(*39, 42, 119*). Samples were prepared as described for the actin bundling co-sedimentation assay. 20 µM of polymerized actin was incubated alone or with 10 µM Vt or full-length vinculin at room temperature for 1 h. For reactions containing full-length vinculin variants, samples were prepared with or without 100 µM IpaA. The mixture was then diluted 20-fold with 1X actin polymerization buffer (10 mM Tris, 100 mM KCl, 2.5 mM $MgCl_2$, 2 mM DTT, pH 7.5). Alexa Fluoro-488 phalloidin (Invitrogen, Carlsbad, CA) was added to the reaction to a final concentration of 1.5 µM and then incubated for 5 minutes at room temperature. The sample was further diluted to an actin concentration of 50 nM. Small aliquots were placed on a glass slide and covered with a coverslip. Images were acquired on a Zeiss axiovert 200M microscope equipped with a 63 X objective lens and a Hamamatsu ORCA-ERAG digital camera.

9. Vinculin Head-Tail Pulldowns

Pulldown assays were performed as previously described (*102*) with the following modifications. Purified Vt and Vt variants were dialyzed into TEEAN buffer (20 mM Tris, 150 mM NaCl, pH 7.5). Protein concentration was calculated and adjusted to 10 µM per reaction with TEEAN buffer containing 0.5% CHAPS, 1% BSA, 0.5mM β-mercaptoethanol. Approximately 10 µM of GST and GST-VH were used for the pulldown experiments. Incubations (450µl) were nutated at 4°C for two hours. The samples were collected by brief centrifugation and washed four times in TEEAN. Samples were boiled in sample buffer and separated by SDS-PAGE. Vt protein bands were detected using a rabbit anti-chicken Vt antibody

(*39*), a gift from Dr. Susan Craig (John Hopkins University). Phosphorylated-Vt was detected with a mouse anti-phosphotyrosine antibody (Santa Cruz). GST was detected with a polyclonal anti-GST antibody (Molecular Probes).

10. Cell culture

Vinculin knockout murine embryo fibroblasts were obtained from Dr. Eileen Adamson (Burnham Institute; La Jolla, CA) and grown in Dulbecco's modified Eagle's medium (DMEM; Invitrogen) supplemented with 5% fetal bovine serum and antibiotic-antimycotic solution in 10% CO_2 at 37°C.

11. DNA constructs and transfection

DNA constructs were generated for cell culture as previously reported (*39*). Cells were transfected with GFP-tagged vinculin expression constructs using Lipofectamine (Invitrogen) and Plus Reagent (Invitrogen) according to the manufacturer's protocol and examined 24-72 hours following transfection.

12. RTCA and Spreading

Prior to plating, cells were serum-starved in DMEM media supplemented with 0.5% delipidated BSA and antibiotic-antimycotic solution. Cells were then resuspended in the serum-free delipidated BSA media for approximately two hours. For the real-time cell analyzer (RTCA) xCELLigence System (Acea Biosciences), 3500 cells per well were seeded into the E-plate 16 that was coated with 50 µg/mL FN. Attachment and spreading was monitored by impedance,

given as the arbitrary unit, cell index (CI), was recorded with the RTCA apparatus every 15 seconds over a 4 hour time period. For the spreading assay and subsequent adhesion site analysis, cells were prepared as described above prior to seeding onto glass coverslips coated with 50 µg/mL FN. Cells were fixed for 10 min with 3.7% formaldehyde, washed once with 1X PBS, and examined by light microscopy using a Zeiss axiovert 200M microscope equipped with a 20 X objective lens and a Hamamatsu ORCA-ERAG digital camera. For each coverslip, five random fields containing at least 500 cells were scored as either spread or round. Cells were then permeabilized for 10 min with 0.2% Triton X-100 in PBS and stained with phalloidin (Invitrogen, Carlsbad, CA) and examined by Zeiss axiovert 200M microscope equipped with a 63 X objective lens and a Hamamatsu ORCA-ERAG digital camera. FAs were quantified as previously reported(*39*). Experiments were repeated three independent times and data represents the mean ± S.E.M. Data sets were analyzed using the two-tailed Student's *t* test for p-values.

13. Force Microscopy

Three-dimensional force microscopy (3DFM) was used to apply controlled force to integrins in order to track bead displacements as an indicator of cellular reinforcement. Experiments and analysis were performed as previously described(*173*). Tracked bead displacements were analyzed using the two-tailed Student's *t* test for p-values and are reported as mean ± S.E.M.

14. DMD model generation

Parameters for model generation were similar to those previously described (*173*).

D. Results

1. Mutation and Modification to Y1065 Reveals Subtle Structural Alterations

Phosphorylated Vt (pY-Vt) was prepared by incubating purified Vt with the c-Src kinase domain and separated from unmodified Vt by anion exchange chromatography. Modification of Vt Y1065 by phosphorylation was verified by fourier transform ion cyclotron resonance mass spectrometry and determined to be ~84% phosphorylated (Supplemental Figure4.1). We also generated a series of Y1065 mutations, and performed near and far-UV circular dichroism (CD) spectroscopy experiments to examine the overall secondary and tertiary structure of pY-Vt and Vt variants in comparison to WT Vt. As shown in Figure4.1A, far-UV spectra for Vt 1065 variants and pY-Vt were similar to WT Vt, indicating that mutation or modification to Y1065 does not significantly alter the overall α-helical signature of Vt. Next we examined near-UV spectra of Vt Y1065 variants and pY-Vt. This data is sensitive to tertiary interactions between the N-terminus and C-terminus, due to aromatic packing interactions between W912 in the H1-H2 loop at W1058 in the C-terminal extension (Figure4.1C). While the near-UV spectra of WT Vt and Vt Y1065A are similar, we observe a loss of tryptophan packing signature when Y1065 is mutated to either phenylalanine, glutamic acid, or phosphorylated. These results indicate a disruption in the packing of the tryptophans that could lead to loss of contacts between the N-terminus and C-terminus (Figure4.1B). However, Vt has a high propensity for forming higher ordered non-physiological oligomers in the absence of ligands at concentrations high concentrations (~360 μM), the protein concentration used for experiments is crucial in order to avoid forming non-physiological oligomers (*23*).Overall, these data indicate that VtY1065F, a variant previously used as a typical non-phosphorylatable variant for Vt, does not share some structural characteristics with unmodified WT Vt, a criteria that should be met. Rather, Vt

Y1065A most closely resembles WT Vt. Furthermore, pY-Vt and VtY1065E show the same disruption in tryptophan packing suggesting that phosphorylation and presence of a negatively charged residue alter the conformation of Vt.

To evaluate if mutations or phosphorylation alters the stability of Vt, we performed fast quantitative cysteine reactivity (fQCR), a technique that uses a thiol-reactive fluorescent indicator that binds to cysteines as they become exposed while the protein unfolds over a thermal gradient. The fluorescent readout can be then used to determine the Tm of a protein and provides an indication of the cooperativity as a protein unfolds. Since Vt has three buried cysteines with varying solvent accessibility, this technique is applicable to Vt. As shown in Figure4.1D and E, the T_m of the variants are not significantly different; however, there is less cooperative unfolding transition for pY-Vt and Y1065E, there is a slight change in the structure that alters how the proteins unfold. Overall, these data indicate that while mutation or modification to Y1065 does not alter the overall stability of the protein, presence of a negative charge at Y1065 can slightly alter helix bundle packing interactions.

Next, to understand possible structural variations that might occur upon mutation or phosphorylation of Y1065, we collected two-dimensional ^{1}H-^{15}N heteronuclear single quantum coherence (HSQC) NMR spectra of N^{15}-enriched protein. HSQC NMR spectra are used to monitor the correlation between nitrogen and amide proton pairs from backbone residues (except for proline), which yields a peak in the spectra. By monitoring the position of peaks from backbone amides, we can track local or global perturbations within a protein due to changes introduced in a protein, such as mutations or post-translational modifications, by reporting on the local chemical environment. Furthermore, changes in peak intensity and/or line widths are an indicator of possible changes in the dynamics of the protein. If global perturbations in the

chemical shifts and/or intensity of amide peaks are observed, this can indicate that the introduction of a mutation or addition of a modification alters the structural and dynamic properties of the protein. As shown in Figure4.2, phosphorylation or mutation of Y1065 produces spectral dispersions that indicate a well-folded protein. Overall, the amide resonances do not show significant changes in chemical shift, intensity, or line width in comparison to WT Vt. However, a small subset of NH peaks show changes in chemical shift and/or line width for each variant. These changes have been mapped onto the structure of Vt in Figure 4.2E. These NMR data indicate that mutation or phosphorylation of Y1065 does not significantly alter the helix bundle fold. This is not surprising given previous work examining the NMR spectra of the C-terminal hairpin deletion (Vt ΔC5 and VtΔC2) variant and spectra from these variants overlay well with WT Vt although minor perturbations were also noted with these variants. Notably, small shifts in residues near the loop between helix 1 and 2 and residues within helix 5. It is postulated that these small shifts occur due to loss of the Y1065 phenol since this sidechain forms contacts with residues in the same regions and therefore cause a minor change in the local chemical environment.

2. Y1065 Mutants and Phosphorylated Vt Maintain Lipid Interactions

Based on studies using Vt C-terminal deletion variants (residues 1052-1066) and C-terminal peptides derived from Vt, it has been proposed that the Vt C-terminus is critical for association and insertion of Vt into membranes(*72*, *89*). However, these studies were performed with destabilizing Vt variants or the C-terminal peptide alone, and likely do not accurately portray vinculin's interactions with PIP_2. In fact, we showed that loss of the C-terminal hairpin does not affect the association of Vt with PIP_2 (*88*). Therefore, we anticipated that mutation or

phosphorylation of Y1065 within Vt would not affect PIP_2 association. To verify this, we performed lipid co-sedimentation assays to assess their binding to PIP_2. As shown in Figure 4.3, the Y1065 variants do not alter in their association with PIP_2-containing liposomes. These data support our previous findings that the C-terminal hairpin does not play a role in the association between Vt and PIP_2. Furthermore, studies with a C-terminal peptide indicated that phosphorylation at Y1065 regulates membrane association (*89*), but our data do not support this finding. Rather, our studies indicate that Vt C-terminal peptides do not reliably mimic the intact tail domain.

3. Phosphorylation or mutation at Y1065 does not affect actin binding, but alters actin bundling.

Previous studies that have examined vinculin's ability to bind and bundle actin found that removal of the C-terminus (1052-1066) enhances the ability for vinculin to bundle F-actin (*91*). However, the C-terminus forms interactions with the helical core of Vt and the N-terminal strap, and large C-terminal deletions beyond seven amino acids leads to destabilization of the protein (*79, 88*). The destabilizing effects of large C-terminal deletions are further supported through protease digestion studies (*79*). We previously demonstrated that a C-terminal hairpin deletion mutant (Vt ΔC5) retains the structural integrity and actin binding of Vt, but is significantly disrupted in its ability to bundle actin filaments (*39*). Based on these results, we examined the impact of phosphorylation or mutation at Y1065 on the ability of Vt to bind and consequently bundle F-actin. Consistent with our previous observations that removal of the C-terminal hairpin does not alter actin binding, as shown in Figure 4.4A and Table 2, Vt Y1065 variants and pY-Vt showed a similar association with actin compared to WT Vt in actin co-sedimentation assays (*39, 102*). However, significant differences were observed for actin bundling (Figure4.4B and Table

2). While WT Vt and Vt Y1065A showed approximately the same actin bundling efficiency, Vt Y1065F exhibited significantly higher bundling capacity than WT Vt. In contrast to WT Vt, pY-Vt and Vt Y1065E showed a significant reduction in their bundling efficiency.

To visualize the bundles formed in the presence of the Vt variants, we viewed the F-actin bundles by fluorescence microscopy. As shown in Figure 4.4C, in the absence of Vt we observed single actin filaments but no actin bundles. However, in the presence of WT Vt and Vt Y1065A, most of the filaments are packed into thick actin bundles, similar to bundles previously observed (*39*). Upon incubation of Vt Y1065F with F-actin, larger F-actin bundles are observed, which would account for the high bundling efficiency observed in the actin bundling co-sedimentation assays. As a result of this finding, we have termed Vt Y1065F a "super-bundler." However, upon phosphorylation or mutation to Y1065E, there is a deficiency in the ability of the variants to form bundles that resemble WT Vt. While some small bundles do form, they lack the persistence observed with the native protein. Results from the actin bundling co-sedimentation assays and the bundles observed by fluorescence microscopy both indicate that VtY1065A behaves similarly to WT Vt, while Vt Y1065F shows significant alterations in bundling activity in comparison to WT Vt. Furthermore, phosphorylation or mutation to a phosphomimetic (Y1065E) disrupted actin bundle formation, to approximately the same severity. Previous studies have shown that deletion of the C-terminal hairpin disrupts actin bundling due to a disruption in forming the actin-induced dimer(*39*). Since Y1065 is located within the C-terminal hairpin and we observe similar disruptions in actin bundling, we conclude that phosphorylation at Y1065 can regulate Vt dimer formation and consequently, F-actin bundling.

4. Phosphorylation and Mutations at Y1065F Alter Vinculin Head-Tail Interactions

Structures of full-length vinculin were obtained for its auto-inhibited or inactive conformation (*71*). In both structures, numerous intramolecular contacts were observed between D1 of Vh and Vt, D3 of Vh and Vt, and D4 of Vh and Vt. Consistent with these observations, interactions between Vt and both between D1 and D4 mediate head-tail interactions and control the active state of vinculin (*113*). Src-mediated phosphorylation of vinculin at Y1065 has been implicated in disrupting head-tail interactions to activate vinculin (*102*). As this study did not quantify levels of pY-Vt, we performed head-tail pulldowns with GST-tagged VH (residues 1-811) and we evaluated if head-tail interactions are disrupted in our system. When we performed pulldowns at a ratio of 1:1 of the head:tail, we found that WT Vt and Vt Y1065A retained binding to the head domain (Figure4.5). However, Vt Y1065F, pY-Vt, and Vt Y1065E showed reduced binding to GST-VH, indicating a perturbation in head-tail interactions (Figure4.5). The reduction in binding observed for pY-Vt and Vt Y1065E is not surprising given previous findings that pY-Vt may disrupt autoinhibitory interactions between Vh and Vt(*102*). However, as Vt Y1065F has been used previous as a non-phosphorylatable variant, our findings that Vt Y1065F reduces association with Vh could indicate that observations made with Y1065F in cells could also be attributed to promoting vinculin activation.

To determine whether head-tail defects are observed in the context of full length protein, we performed actin co-sedimentation assays with the Y1065 mutants in full-length vinculin either with or without IpaA peptide. IpaA is a peptide derived from virulent factor from *Shigella flexneri*, which has been shown to be sufficient to activate vinculin *(76).* If the Y1065 mutations greatly perturb head-tail interactions, we expect those variants to bind to F-actin in the absence

of IpaA since F-actin alone is not sufficient to release head-tail intramolecular contacts. In the absence of IpaA, none of the variants are able to bind or bundle actin, indicating the mutations are unable to disrupt head-tail interactions in the context of the full-length protein (Figure4.6). Similar to previous observations, Y1065A vinculin can bind and bundle F-actin similar to WT vinculin in presence of the IpaA peptide. In contrast, Y1065E vinculin is unable to bundle actin in the presence of IpaA whileY1065F vinculin displays a higher bundling efficiency (Figure4.6A and B). These results are consistent with a previous observation where phosphorylation of full-length vinculin does not promote its binding to F-actin (*102*). When F-actin is visualized by fluorescence microscopy, we only see bundle formation with WT, Y1065A, and Y1065F vinculin in the presence of the IpaA peptide (Figure4.6C). These data indicate that the defects observed in head-tail interactions detected by the pulldown assay are not enough to overcome the head-tail intramolecular interactions that would allow the variants to bind F-actin in the absence of the IpaA peptide. Furthermore, these results show comparable behavior between Vt and the full-length protein, which is not surprising, given the structural similarities of Vt when it is both in the full-length molecule and isolated (*71, 168*).

5. Mutation at Y1065 Affects Cell Spreading

To further probe the differences between the Y1065 variants, we explored the impact of these mutants in cells, particularly during cell spreading events. When the F-actin bundling deficient mutant (ΔC5-vinculin) is expressed in cells, the cells are found to be significantly smaller with significantly fewer but slightly larger FAs (*39*). However, previous studies have shown that both Y1065F and Y100F mutants are required for a cell spreading defect (*102*). To

examine cell spreading, we expressed our GFP-vinculin variants in vinculin knockout murine embryonic fibroblasts (Vin -/- MEFs) and were monitored using the real-time cell analyzer (RTCA) xCELLigence system. The RTCA system is an impedance based method that monitors electrical resistance as cells attach and spread on the electrode (given in the arbitrary units, cell index (CI)). As previously reported, Vin -/- MEFs have difficulty in adhering to and spreading on FN while cells expressing WT vinculin and Y1065E vinculin are well spread (Figure 4.7A and B) (*3*). Cells expressing Y1065E vinculin exhibited a higher impedance indicating cells are more spread. In contrast, cells expressing Y1065F vinculin displayed lower impedance suggesting a defect in cell spreading (Figure4.7A and B).

We also visualized cells expressing the vinculin mutants by microscopy to see if their cell morphology corresponds to the CI observed by RTCA. As shown in Figure4.7C, cells expressing WT vinculin and the Y1065 mutants retain vinculin localization to FAs, which is not surprising since Vh is sufficient to localize vinculin to FAs (*40*). The cell area was quantified for cells expressing the vinculin variants and Vin -/- MEFs to examine spreading on FN. Cells expressing Y1065E vinculin are significantly larger while Vin -/- MEFs are significantly smaller, a finding that corresponds to our RTCA observations (Figure4.7D). Quantification of FAs in cells expressing Y1065A and Y1065F vinculin revealed significantly fewer FAs while cells expressing Y1065A and Y1065E vinculin have significantly smaller FAs (Figure4.7E). These results, taken together, suggests that the phosphorylation state of Y1065 and vinculin-mediated actin bundling capacity can mediate cell spreading through its influence on FA number and area.

6. The phosphorylation state of Y1065 regulates the mechanical response applied to integrins

Vinculin plays a critical role in transducing the signals that enable cellular reinforcement (*51, 128*). We have recently shown that direct interactions between vinculin and actin are important for cells to stiffen in response to external pulses of force(*39, 173*). Given our findings that phosphorylation at Y1065 impairs F-actin bundling *in vitro*, we employed three dimensional force microscopy (3DFM) to examine cell stiffening in response to external pulses of force. For these measurements, the relative bead displacement for the first and second pulse was measured (*129*). Cells expressing either WT- or Y1065A vinculin showed a significant decrease in bead displacement indicative of a stiffening response (Figure4.8). However, cells expressing Y1065F or Y1065E vinculin exhibited similar bead displacement upon the second pulse, indicating a lack of a stiffening response. This result is surprising given the *in vitro* actin co-sedimentation assay data, but it could indicate the vinculin-mediated F-actin bundles needs to be tightly attuned to the correct efficiency in order to transduce the signals to attain a cellular stiffening response.

7. Identification of an actin-induced Vt dimer interface

We have previously shown that the C-terminal hairpin is essential for actin-mediated Vt dimerization and F-actin bundling(*39*). Consistent with our previous findings, we have identified Y1065 as a critical residue in mediating F-actin bundle formation. As we have identified many vinculin mutants that show varying actin bundling efficiencies, we employed computational refinement approaches to generate a model for the actin-induced Vt dimer interface (Figure4.9). In the model, Y1065 is shown to insert itself into a hydrophobic cleft at the bottom of the loop

between helix 1 and 2. Mutation to Y1065E or phosphorylation disrupts this interaction, as indicated by the lack of F-actin bundling efficiency. However, mutation to Y1065F would enable it insert itself further into this hydrophobic patch creating a tighter association between Vt molecules and would account for the "super" bundling efficiency observed.

E. Discussion and Conclusions

Vinculin is an essential adaptor protein that has been implicated in a number of cellular processes including cell adhesion, spreading, regulating FA dynamics, and mediating external mechanical cues (*33, 70*). The interaction between vinculin and F-actin is critical for vinculin to operate in FAs as indicated by mutations that selectively disrupt the ability of vinculin to bind or bundle F-actin(*39, 42, 173*). Here, we report characterization of phosphorylated Vt and Y1065 mutants. Modification or select mutations at Y1065 vary in their ability to bundle F-actin and mediate head-tail interactions. Furthermore, we show that in order for cells to spread and transduce forces, vinculin needs to be able to regulate F-actin bundle formation and these processes are regulated by the phosphorylation state of Y1065.

Results from our studies have provided additional characterization of Y1065 mutants to determine their role in modulating vinculin function. Surprisingly, while the common variant to prevent phosphorylation of a tyrosine residue is a mutation to phenylalanine, results from our studies indicate that it is not the best variant to mimic non-phosphorylated WT vinculin. Rather, Y1065A seems to serve as a better non-phosphorylatable variant. As indicated by the near-UV CD spectra (Figure4.1B), pulldowns to examine head-tail interactions (Figure4.5), and actin co-sedimentation assays (Figure4.4 and 4.6), Y1065F appears to have significant alterations in comparison to WT Vt. Additionally, our results indicate that phosphorylation and mutation to a

phosphomimetic impacts not only the tertiary structure (Figure4.1B), and the cooperativity of unfolding proteins in response to increasing temperature (Figure4.1C and D), but it also disrupts binding the Vh (Figure4.5), similar to previous observations (*102*). Moreover, results from our study have provided additional support that the C-terminal hairpin does not associate with acidic phospholipids (*88*) and phosphorylation at Y1065 does not regulate its association (Figure4.3).

Previously, studies that investigated the ability of vinculin to bind and bundle actin have used large, destabilizing deletions (*66, 90,154*). For instance, studies that removed the C-terminus (residues 1052-1066) showed an enhanced actin bundling efficiency (*91*), but this deletion altered the structural integrity of Vt(*88*). We have shown previously that deletion of Y1065 and Q1066 from the C-terminal hairpin is sufficient in order to impair actin bundling while actin binding was unaffected (*32, 39*). It is not surprising that actin bundling is altered when Y1065 is mutated or phosphorylated; however, we were surprised by the varying ability of the mutants to bundle F-actin (Figure4.4B and C; 4.6B and C; Table 2). While the results from the head-tail pulldowns found that Vt Y1065F, pY-Vt, and Vt Y1065E were unable to bind to GST-VH with the same efficiency as WT Vt and Vt Y1065A, actin co-sedimentation assays with full-length vinculin showed that, in the presence of the different mutations, they were unable to bind F-actin unless they were also incubated with the activating IpaA peptide (Figure4.6A). These results suggest that the head-tail interaction defects exhibited by Y1065F and Y1065E are not drastic enough to ablate head-tail intramolecular interactions in the context of the full-length protein. However, further studies would be required in order to examine the impact of these mutations on head-tail interactions in modulating vinculin's activation status in cells. Overall, these data indicate that not only does phosphorylation at Y1065 provide a mechanism for

regulating vinculin-mediated F-actin bundles in cells but that the best variants to better study the impact of Src phosphorylation on vinculin at Y1065 should be Y1065A and Y1065E vinculin.

As demonstrated in Figure4.7, cells expressing vinculin variants are affected by the phosphorylation state at Y1065, as indicated by their ability to spread on FN. As shown by the RTCA data and taking into account the cell area of spread cells, cells expressing Y1065F vinculin do not display a significant spreading defect in comparison to those expressing WT vinculin, which is similar to previous observations (*102*), while cells expressing Y1065E vinculin are significantly larger. Taken together with previous studies that examined actin binding and bundling on cell spreading that showed a significant defect in regulating this process(*39, 173*), it is likely that actin bundling does not play a direct role in dictating cell area during spreading events since the actin bundling-deficient variant, Y1065E vinculin, exhibits a significant increase in the cell area. Rather, the phosphorylation state of Y1065 is the main contributing factor that mediates cell spreading events. Whether it is through association of an unknown binding partner that mediates spreading events via the C-terminal hairpin or the actin-induced dimer, the contribution to cell spreading appears to be phosphorylation dependent. While detection of this binding partner is beyond the scope of this work, future efforts will be directed towards the identification of the binding partner and elucidating its interaction interface.

Our findings that the phosphorylation state of Y1065 can impact FA size and number provides further insight on the factors regulating FA assembly and maturation during cell spreading. FA area can be influenced by a number of factors such as rates of FA formation and turnover, mechanical tension, the density and type of matrix that the cells adhere to, and other unknown factors. Recently, the role of tension in FA growth has become controversial since tension has been initially implied as a critical factor for FA assembly while more recent work has

questioned the impact of tension of FA maturation (*158-161*). We find that cells expressing Y1065A and Y1065F vinculin mutants display significantly fewer FAs. We also find that Y1065A and Y1065E vinculin-expressing cells have significantly smaller FAs. These results indicate that the phosphorylation state of Y1065 helps to mediate FA formation and maturation, and it is likely that a dynamic phosphorylation state is needed for these processes.

As shown previously, vinculin is a crucial component for efficiently transducing forces, whether they are external forces being applied or internally generated forces, and these signals are mediated through its interactions with F-actin (*131-133*). Preventing vinculin's binding to actin or actin bundling has been shown to prevent the cellular reinforcement when external pulses of force are applied to integrins (*39, 173*). We observed that when Y1065 is mutated, cells expressing Y1065A vinculin are able to display a decrease in bead displacement with subsequent pulses of force, thereby indicating a stiffening response (Figure4.8). However, cells expressing Y1065F and Y1065E vinculin are unable to stiffen upon applications of force to integrins (Figure4.8). This observation is not surprising for Y1065E given its bundling defect *in vitro*. However, we were surprised with the lack of stiffening response displayed by cells expressing Y1065F, given the "super-bundling" phenotype displayed by this variant *in vitro*. While we would expect cells to utilize Y1065F vinculin in bundling F-actin, it does not mean that cells will utilize Y1065F's super-bundling capacity. Furthermore, these results suggest that the bundling efficiency displayed by vinculin needs to be tightly controlled in order to attain efficient cellular reinforcement as indicated by the stiffening response displayed by cells expressing Y1065A vinculin. Furthermore, the results from this study indicate that the mechanisms that mediate cellular responses as cells adhere to substrates versus mechanical tension applied via substrate ligands are interpreted by the cell differently and require alternate aspects of vinculin function in

order to respond accordingly. Adhesion reinforcement to external stimuli initiates a complex signaling cascade that leads to recruitment of additional FA proteins. Y1065 or the actin-induced dimer could serve as a scaffold for a novel binding partner and mutation to Y1065F or Y1065E prevents its association due to their alterations on Vt's structure as highlighted in this work. It has been established that Src is activated early in response to force to phosphorylate a number of proteins, and therefore could potentially regulate not only the actin-induced vinculin dimer, but also potentially the binding of a novel interaction partner. Further work is necessary to distinguish if there is a novel binding partner to phosphorylated Y1065 or to the actin-induced vinculin dimer.

Previous studies examining the actin-induced vinculin dimer have shown that both Vt and F-actin undergo a conformation change upon association (*37, 90*). While we are not able to crystallize the actin-induced dimer in order to map the dimer interface, results from this study have provided a starting point to generate a model for the actin-induced Vt dimer interface (Figure4.9). This model is in agreement with previous works examining actin binding and bundling (*39, 173*). Using this model, future work will focus on not only verifying this interface but to characterize the effect of vinculin-mediated actin bundling in cells.

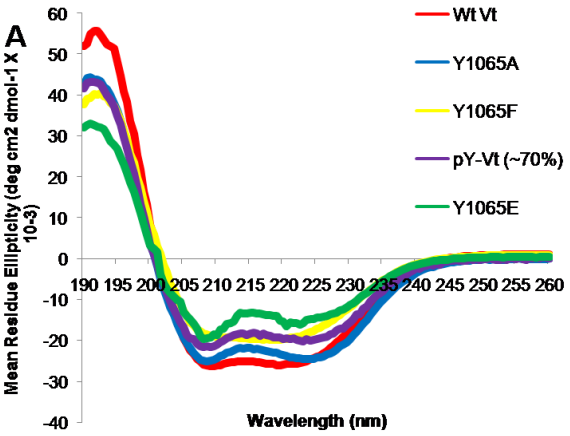

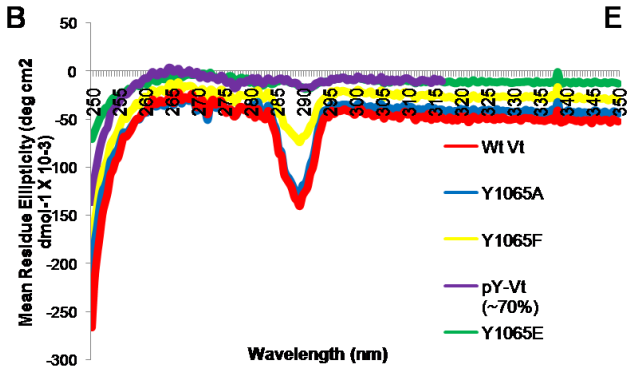

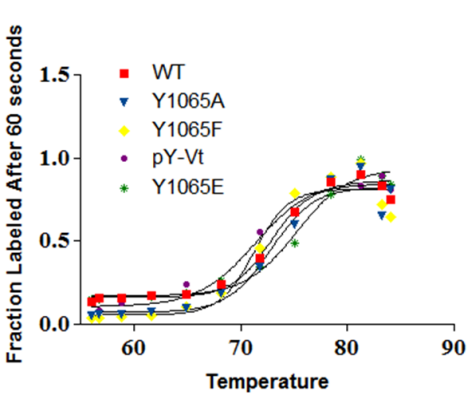

E

Vt Species	Tm (˚C)	Slope
WT	72.85	0.2359
Y1065A	72.82	0.2123
Y1065F	71.26	0.2701
pY-Vt	71.37	0.1636
Y1065E	75.23	0.1808

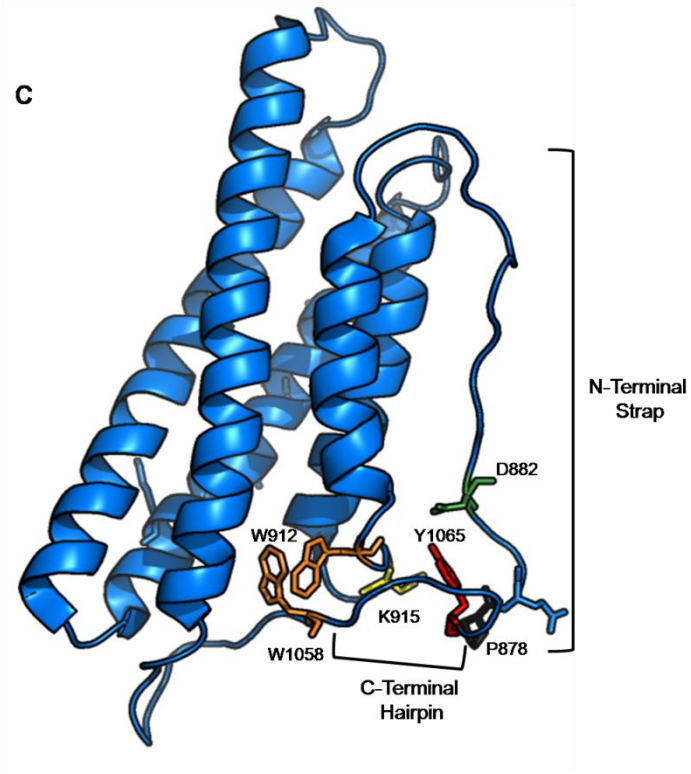

Figure 4.1.CD and fQCR of pY-Vt and Y1065 variants. Comparison of (A) far-UV CD spectra show similar spectral profiles, though significant alterations are observed in the (B) near-UV CD spectra upon phosphorylation and mutation toY1065E. Some alterations in the spectra are also observed upon mutation to Y1065F. Results from these analyses indicate a change in Vt tertiary structure but Vt helical secondary structure is maintained upon mutation to select residues and phosphorylation. (C) The side chain of Y1065 (red) in the C-terminus forms hydrogen bonds with D882 in the strap and K915 in the H1/H2 loop. In full length vinculin, Y1065 also interacts with P878 in the proline rich region. The structure of the C-terminal hairpin is also necessary for proper packing of W912 and W1058. (D) fQCR shows temperature dependence upon exposure of cysteines to 4-(aminosulfonyl)-7-fluoro-2,1,3-benzoxadiazole (ABD). (E) Results indicate no significant changes in stability upon phosphorylation or mutation, but there is a difference in cooperativity of the unfolding protein upon phosphorylation and mutation to Y1065E.

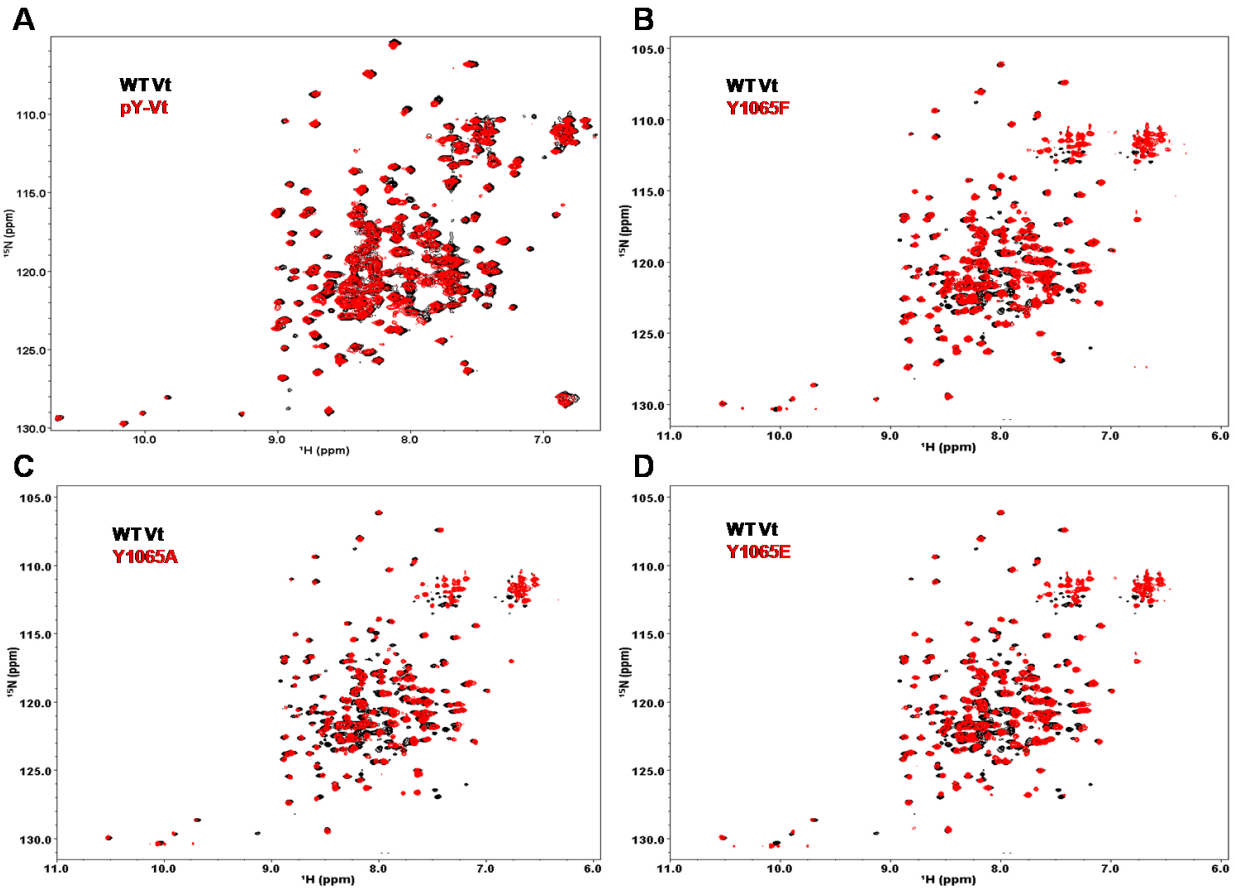
A
WT Vt
pY-Vt
B
WT Vt
Y1065F
C
WT Vt
Y1065A
D
WT Vt
Y1065E
^{15}N (ppm)
^{1}H (ppm)

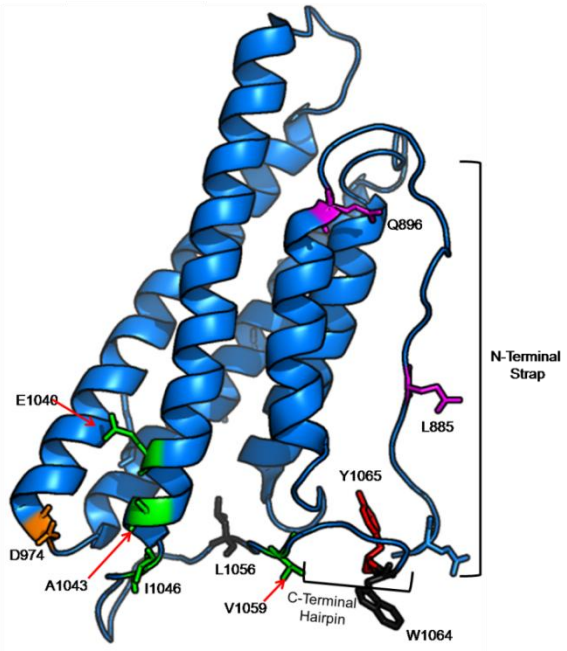
Q896
N-Terminal
Strap
E1046
L885
Y1065
D974
A1043
I1046
L1056
V1059
C-Terminal
Hairpin
W1064

Figure 4.2.2D NMR ^{1}H-^{15}N HSQC spectral overlay of WT Vt and Vt variants. Data were collected on a 700 MHz Varian Inova spectrometer at a protein concentration of 50 µM and phosphorylated protein at 35 µM. WT Vt is in black, with each of the variants in red. All Vt variants appear well-folded. (A) Although pY-Vt overlays well with most of the NH peaks in WT Vt, line broadening is observed for E1040, A1043, I1046, and V1059. (B) Vt Y1065F overlays well WT Vt and displays changes in peaks corresponding to L1056, V1059, and W1064. (B) Vt Y1065E and (C) Vt Y1065A showed greater differences, with shifts in the above peaks, as well as Q896, F885, and Q1066.(E) Changes in the HSQC spectra have been mapped onto the Vt domain with changes caused by Vt Y1065A alone (orange), Vt Y1065A and Vt Y1065E (pink), Vt Y1065A, Vt Y1065E, and Vt Y1065F (black), and pY-Vt (green).

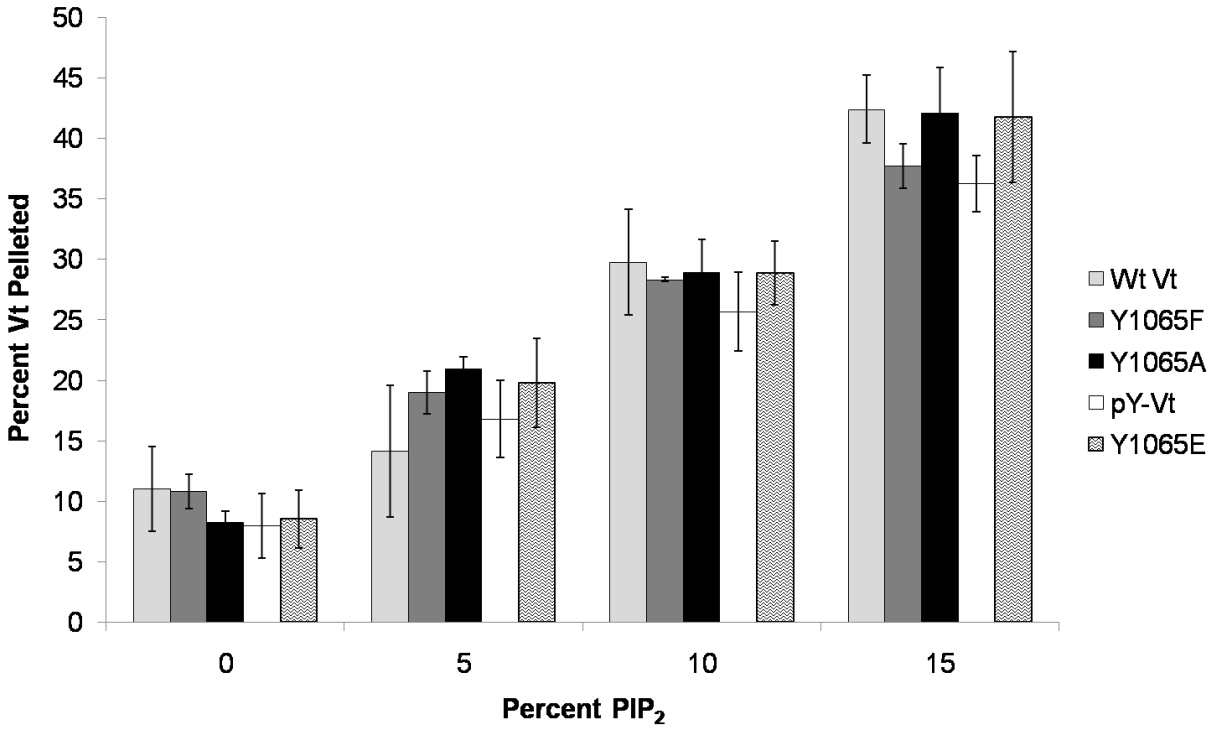

Figure 4.3.Vinculin Y1065 variants and pY-Vt do not affect PIP_2 association. Similar to previous results with a hairpin deletion mutation, VtΔC5 (Palmer *et al*.), both phosphorylation (pY-Vt) and point mutations at Y1065 do not alter binding to liposomes containing PIP_2.

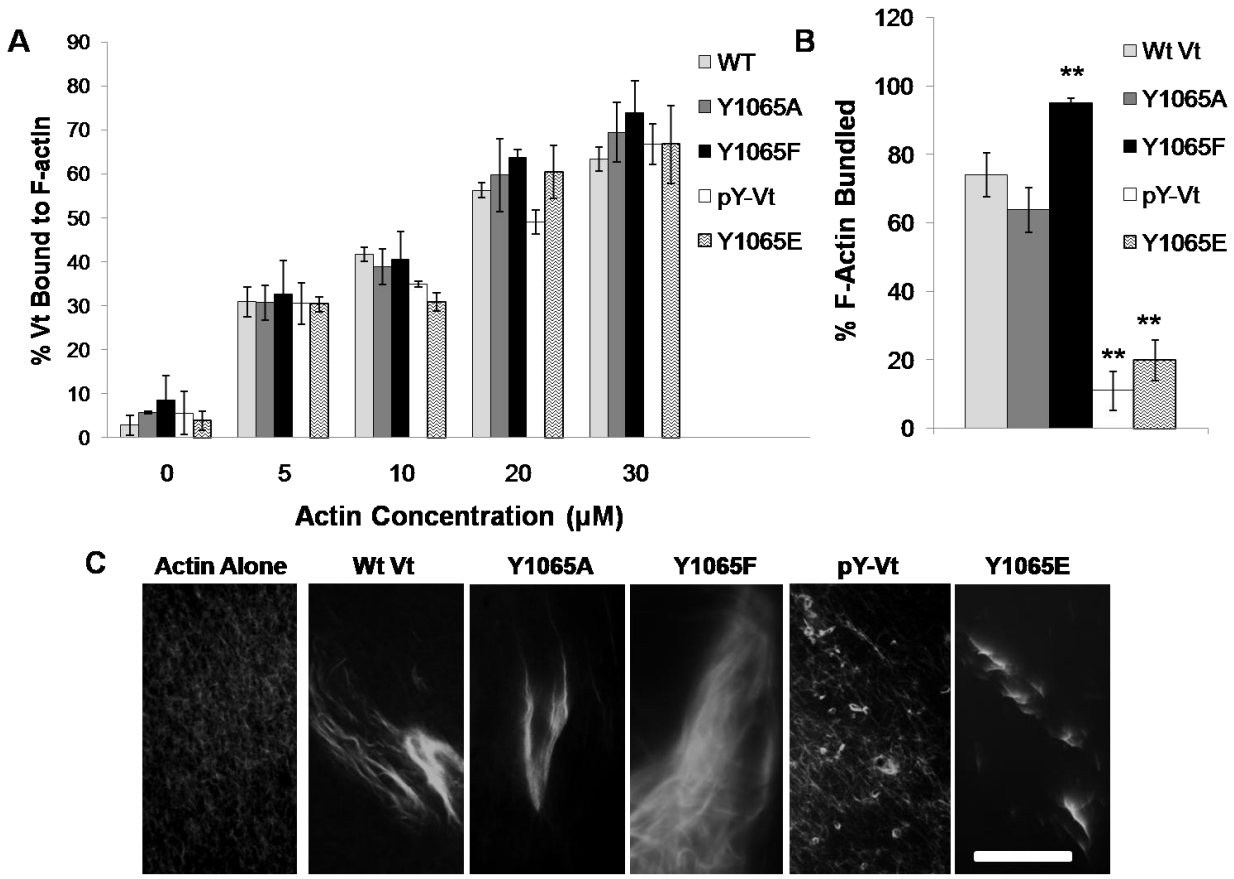

Figure 4.4.Actin binding and bundling with pY-Vt and Vt Y1065 mutants.(A) The different variants of Vt retain actin binding properties but have various actin bundling efficiencies as demonstrated by (B) actin bundling assays and (C) fluorescence microscopy. Vt Y1065E displays a reduced efficiency in actin bundling similar to pY-Vt . In contrast, VtY1065F displays an increase in bundling efficiency over WT Vt while the VtY1065A variant has similar bundling abilities in comparison to WT Vt. **$p \leq 0.001$ comparing Y1065 variants to WT vinculin. Error bars show standard deviation. Scale bar: 25 μm.

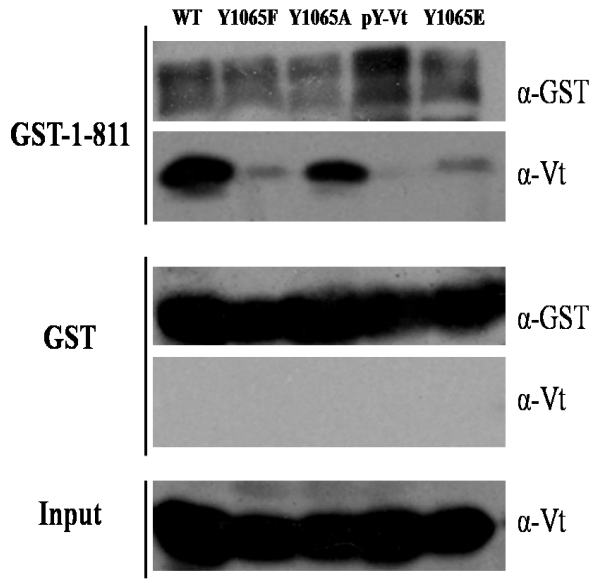

Figure 4.5.Phosphorylation of Y1065 and select Y1065 mutants affect vinculin head-tail interactions. The tail–bead complexes were incubated with either GST alone or the GST-VH domain protein (residues 1-811). Bound proteins were eluted off the beads and probed with the indicated antibodies. WT Vt and Vt Y1065A retain binding to GST-VH. In contrast, Vt Y1065F, Y1065E, and pY-Vt lose binding to GST-VH. Results are representative of three experiments.

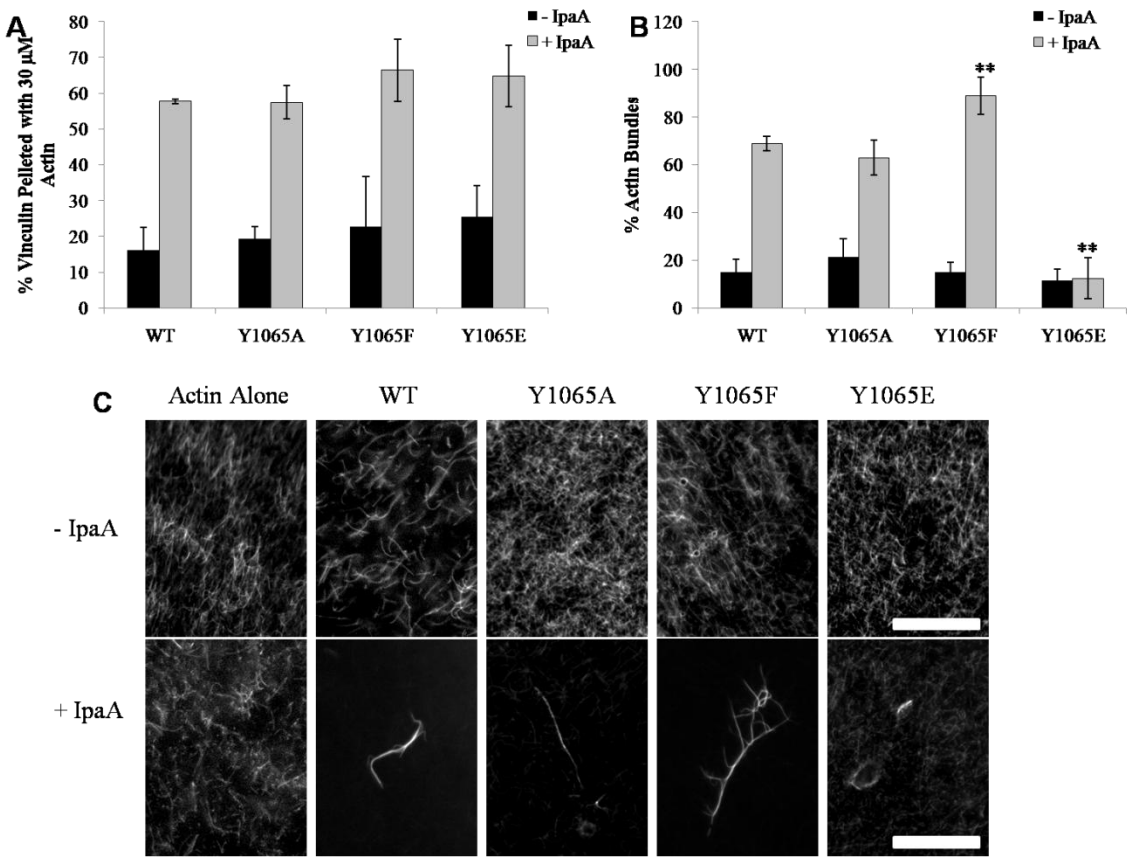

Figure 4.6.Y1065 mutants in full-length vinculin alter actin bundling but not actin binding. (A) The Y1065 mutants retain actin binding properties and are only able to bind in the presence of the activating virulent factor, IpaA. However, similar to their Vt domain counterparts, the Y1065 mutants have various actin bundling efficiencies as demonstrated by (B) actin bundling assays and (C) fluorescence microscopy and they are only able to bundle in presence of IpaA. **p≤ 0.001 comparing Y1065 variants to WT vinculin. Error bars show standard deviation. Scale bar: 25 μm.

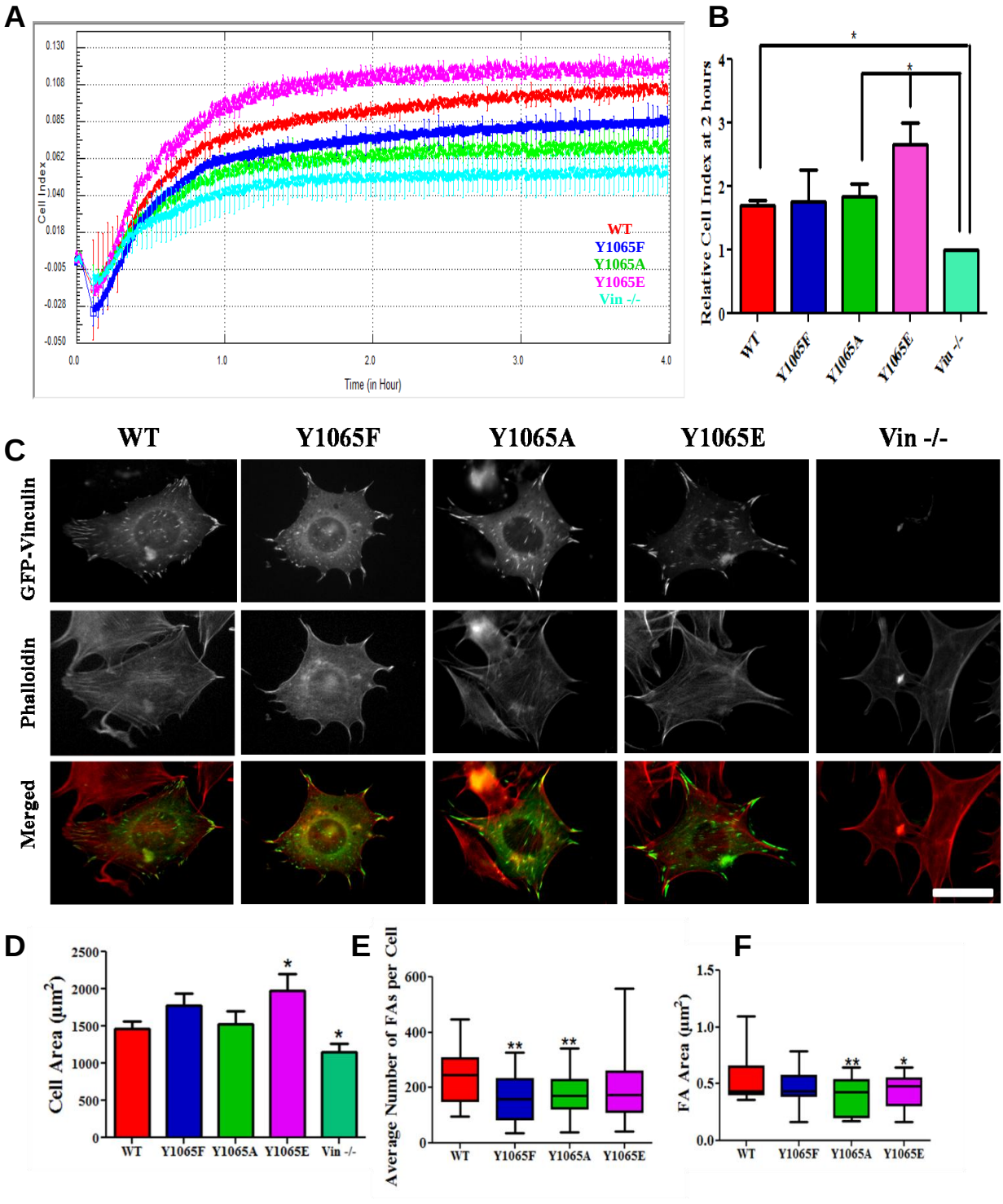

Figure 4.7.Vinculin variants at Y1065 are able to localize to FAs, affect cell spreading and FAs.(A) RTCA using the xCELLigence system shows that Vin-/- cells expressing WT vinculin have higher cell impedance, and hence, more spread, than cells expressing Y1065F- or Vin -/-

MEFs. Cells expressing Y1065A vinculin are more spread than Vin -/- MEFs, while cells expressing Y1065E vinculin are significantly more spread than WT vinculin cells. A representative trace of cell impedance (graphed as cell index (CI)) is taken every 15 seconds for 4 hours; lower impedance indicates less contact with the electrode. Each data point represents an average CI of at least duplicate wells for each condition. (B) A graph showing the relative CI of cells spread on FN two hours following plating, which corresponds to the same time as the pictures shown in (C). Data is the average ± SEM combined from three independent experiments. *p≤ 0.05.(C) Vin-/- MEFs expressing either GFP-tagged WT-, Y1065F-, Y1065A- or Y1065E vinculin or untransfected cells were allowed to adhere and spread on FN for two hours. All variants display localization to FAs (D, E, F). Plots of cell area (D), number of FAs per cell (E) and FA area (F).Cells expressing Y1065F- and Y1065A vinculin had significantly fewer FAs while cells expressing Y1065A- and Y1065E had smaller FAs. Vin -/- MEFs were significantly smaller than cells expressing a vinculin variant, but cells expressing Y1065E vinculin were significantly larger in comparison to WT vinculin cells. Areas were calculated using Matlab (Methods) (WT n=47; Y1065F n=31; Y1065A n=41; Y1065E n=33; Vin -/- n=35).*p-value≤0.05.Error bars are ± S.E.M. Scale bar is 25 μm.

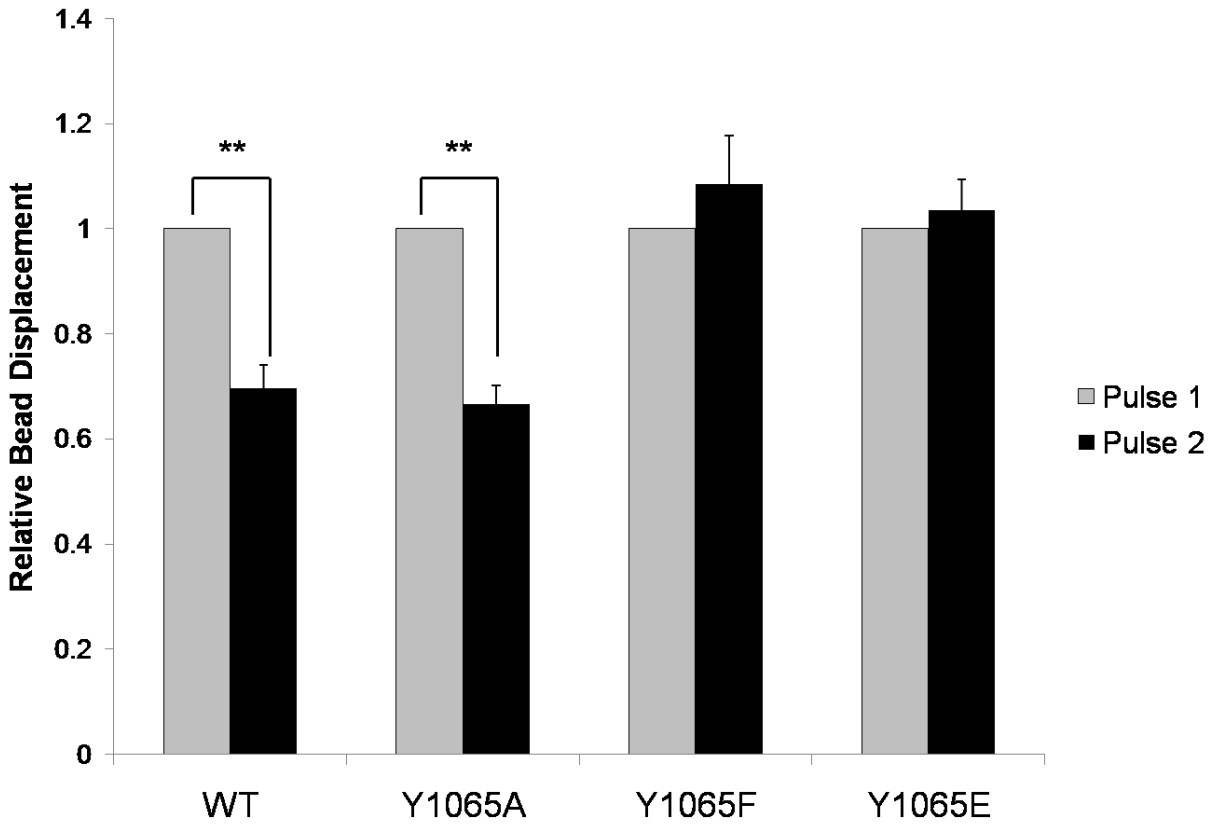

Figure 4.8.The phosphorylation state of Y1065 regulates the mechanical response applied to integrins. Upon applying pulses of a constant force, the relative bead displacement of Vin -/- MEFs transfected with WT vinculin or Y1065A vinculin significantly decreases, whereas the relative bead displacement of Vin -/- MEFs transfected with either Y1065F- or Y1065E vinculin increases significantly. For the relative bead displacement measurements, two pulses of force were applied to FN-coated beads bound to Vin -/- MEFs transfected with either WT vinculin (n=17), Y1065F vinculin (n=15), Y1065A vinculin (n=16), or Y1065E vinculin (n=16). **p≤ 0.001 comparing Y1065 vinculin variants to WT vinculin. Error bars are ± S.E.M.

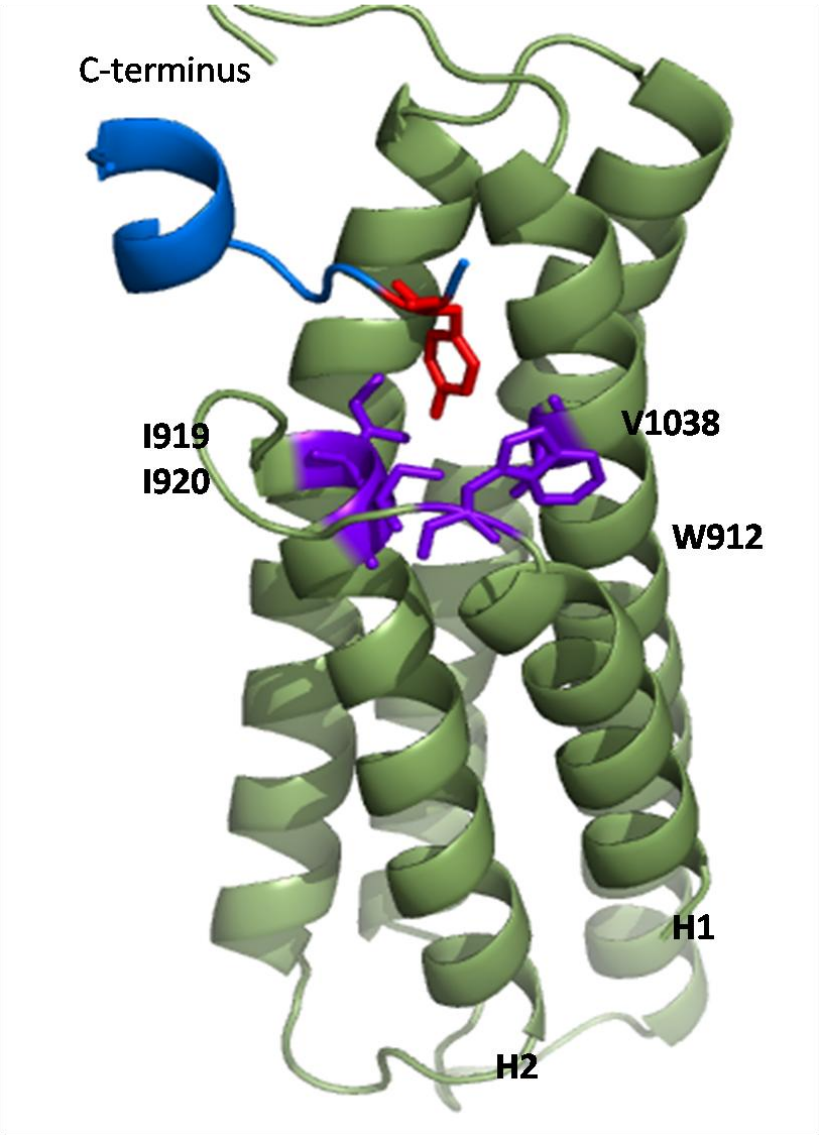

Figure 4.9.Proposed interface of the actin-induced Vt dimer. Using a C-terminal peptide (blue) from one Vt, Y1065 (red) inserts into the hydrophobic cleft (purple) of another Vt monomer (green) at the base of the helical bundle near the loop between helix 1 and 2.

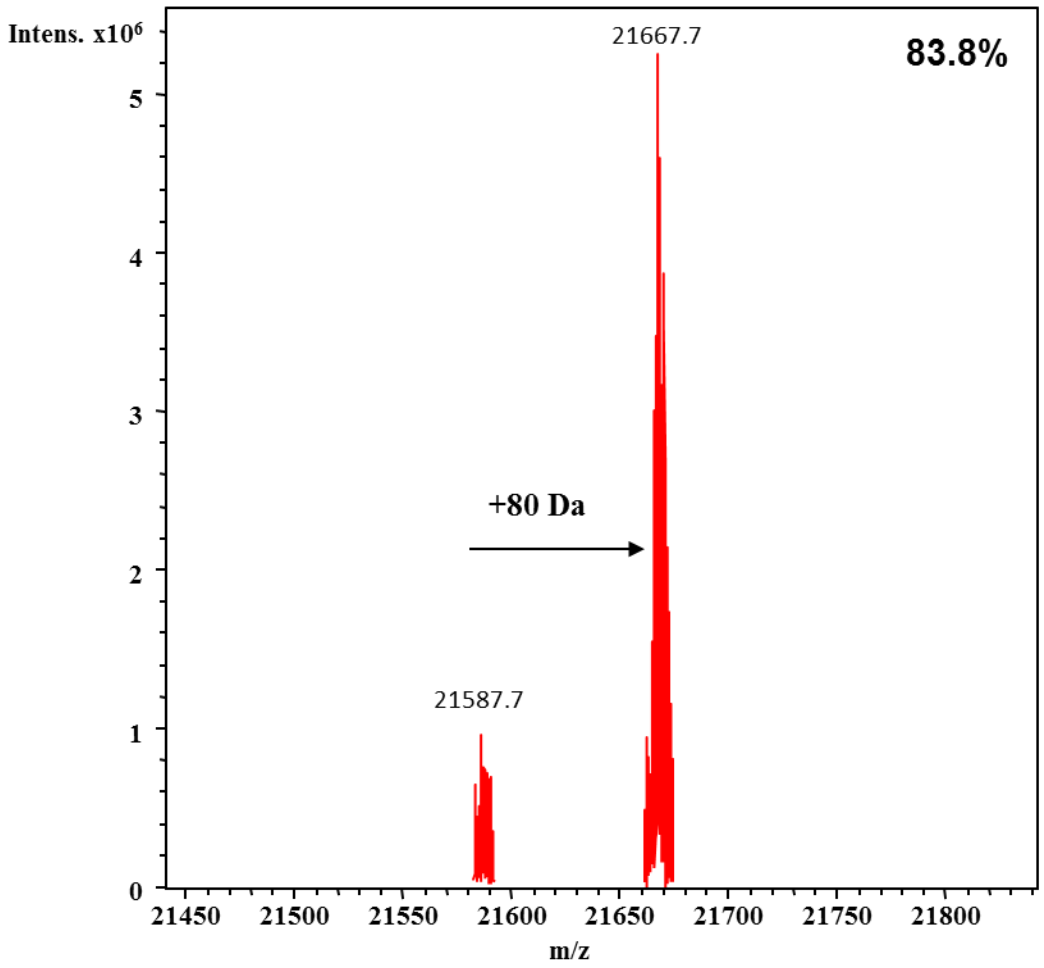

Supplemental Figure 4.1.FTICR-MS verification of Vt 1065 phosphorylation by Src(83.8%).

Vt Variant	Actin Binding (30 µM)	Actin Bundling (20 µM)
WT Vt	65.49 ± 7.79	74.11 ± 6.35
pY-Vt	66.85 ± 4.63	11.04 ± 5.74
Y1065F	73.50 ± 5.28	94.99 ± 1.56
Y1065A	69.50 ± 6.79	63.75 ± 6.53
Y1065N	64.12 ± 7.43	42.17 ± 6.67
Y1065S	70.36 ± 5.27	12.57 ± 5.71
Y1065D	71.01 ± 4.14	51.1 ± 9.38
Y1065E	66.74 ± 8.87	23.82 ± 8.94
Y1065H	57.64 ± 2.32	30.21 ± 2.61

Table 2.Summary of F-actin binding and bundling by Vt Y1065 variants. Several Vt variants were generated and evaluated for their ability to bind and bundle F-actin. The percent of Vt that pellets with F-actin at 30 µM F-actin is reported as a measure of F-actin binding. The percent of F-actin bundled at 20 µM F-actin is reported as a measure of F-actin bundling. Vt concentration for these experiments is 10 µM.

V: Conclusions and Future Directions

A. Overview

Vinculin is an essential cell adhesion protein, found at both FAs and adherens junctions, where it couples transmembrane proteins to the actin cytoskeleton. Through Vt, vinculincan both bind and bundle actin filaments. Binding to actin induces a conformational change in Vt believed to promote the formation of a Vt dimer that crosslinks F-actin. Many studies have examined the role of the vinculin/F-actin interaction and found it has a role in FA formation, FA maturation, mechanotransduction, cell spreading, and migration; however, these studies either delete Vt or introduce destabilizing deletions that are likely to have off target effects and might be responsible for the observed phenotypes. In order to create better tools for studying the role of the vinculin/F-actin interaction, a potential Vt/F-actin binding structural model has been proposed (*91*). In their model, Janssen *et al*. proposed that deletion of the N-terminal strap impairs actin binding while deletion of the C-terminus enhanced the bundling efficiency of Vt(*91*). However, recent data that is presented in this thesis contradicts the model proposed by Janssen *et al*., and suggests that the Vt/F-actin binding model needs to be further refined.

My doctoral dissertation has focused on identifying and using better tools to study vinculin's interactions with F-actin. Through identification of select variants, I have examined the impact of variants that selectively disrupt actin binding or bundling in cells. Furthermore, I

have explored the role of tyrosine phosphorylation in Vt, at Y1065, that impacts Vt-mediated F-actin bundling. Through these studies, I have facilitated in forming a novel model for how Vt not only binds F-actin, but also how Vt self-associates in order to bundle actin filaments. In the sections below, I summarize the findings of this dissertation. Future studies will be aimed at refining the proposed interaction model and further probing the role of the vinculin/F-actin interaction, the actin-induced Vt dimer, and the role of phosphorylation at Y1065 in modulating FA dynamics.

B. The Vinculin C-terminal Hairpin Mediates F-actin Bundle Formation, Focal Adhesion, and Cell Mechanical Properties

Summary of Results

1. In contradiction to previous reports implicating the C-terminal hairpin in mediating Vt's association to F-actin, deletion of the C-terminal hairpin, Vt ΔC5, does not disrupt binding to F-actin. Additionally, deletion of the N-terminal strap does not impact actin binding or bundling.
2. Deletion of the C-terminal hairpin, Vt ΔC5, is crucial for Vt self-association and consequently, F-actin bundling.
3. Vt ΔC5 is structurally similar to WT Vt and retains binding to PIP_2
4. Vt ΔC5 forms a distinct, non-functional dimeric species in comparison to WT Vt.
5. Cells expressing ΔC5-vinculin are significantly smaller with significantly fewer but slightly larger FAs, indicating a defect in cell spreading when allowed to adhere to FN.
6. Cells expressing ΔC5-vinculin are unable to stiffen in response to pulses of force.

C. Identification of a New Actin Binding Surface on Vinculin that Mediates Cellular Mechanical and Focal Adhesion Properties

Summary of Results

1. Identified new variants deficient in actin binding, V1001A and I997A.

2. V1001A and I997A retain a similar structure to WT Vt. While V1001A maintains binding to PIP_2, I997A displays a decreased affinity for PIP_2.

3. Cells expressing V1001A and I997A display a cell spreading defect when allowed to adhere to FN as indicated by RTCA experiments. Cells expressing V1001A have larger and fewer adhesions while cells expressing I997A are significantly smaller and also have larger and fewer FAs.

4. Both mutants display defects in cellular reinforcement.

5. Through EM and DMD, we have identified an alternative actin binding surface.

D. Phosphorylation at Y1065 in Vinculin Mediates Actin-Induced Vinculin Dimer Formation, Cell Spreading, and Mechanical Responses to Force

Summary of Results

1. Phosphorylation or mutation at Y1065 display subtle structural alterations, but overall retain most of the structural characteristics of WT Vt.

2. Y1065 Mutants or pY-Vt maintain interactions with PIP_2.

3. Select Y1065 mutants and pY-Vt disrupts head/tail interactions.

4. Phosphorylation or mutation at Y1065 does not affect actin binding, but alters actin bundling.

5. Mutation at Y1065 affects cell spreading events.

6. The phosphorylation state at Y1065 regulates the mechanical response applied to integrins.

7. Proposed model of the actin-induced Vt dimer interface.

E. Future Directions

Data in this thesis shows select residues that disrupt the F-actin/Vinculin interaction, and the C-terminal hairpin of Vt is essential for actin-induced dimer formation. Furthermore, I have shown that phosphorylation a Y1065 can regulate F-actin bundling and presents a mechanism that allows the regulation of vinculin-mediated F-actin bundling in cells. Future work will include examining the impact of actin-binding deficient mutants in cells. Future efforts should be directed towards determining the other residues involved in the actin-induced Vt dimer interface in order to verify the model proposed in this work. By mutating residues within the proposed dimer interface, future studies can examine the impact of F-actin bundling both *in vitro* and in cells. I have also examined other implications of an actin-bundling deficient mutant present in cells, and I cannot discount the possibility that the dimer interface of the C-terminal hairpin acts as a scaffold for novel binding partners. Finally, I have observed differences in exchange rates from FAs between the different point mutants.

1. Examining actin-binding deficient mutants in cells

Recently, models have been proposed for what the actin/Vt interaction looks like in an effort to understand the conformational dynamics that is required to form the interaction, but to identify select residues to study the role of this interaction in cells. Using one of the variants we identified (I997A), Thievessan *et al*. have shown that vinculin organizes the F-actin network at the leading edge of cells in order to generate traction of the ECM in order to promote FA

formation and turnover (*42*). However, as discussed in Chapter III, the I997A variants have an additional deficiency in binding to PIP_2. Therefore, it would be interesting to characterize the V1001A mutant to a similar extent and compare it to results obtained by the I997A variant to see if the PIP_2 defect contributes to some of the phenotypes observed. We hypothesize that similar phenotypes will be observed for the V1001A variants when FA dynamics are examined based on our observations with the I997A and V1001A variant's impact on cell spreading and response to external pulses of force (Figure 3.3)

2. Identification of other residues involved in the formation of the F-actin-induced Vt dimer

A major question in the vinculin field has been what the actin-induced Vt dimer looks like since it is not possible to crystallize or perform NMR studies on the dimer without F-actin. Since we have identified a possible model through a series of mutations at Y1065, molecular dynamics simulations have identified the hydrophobic patch at the bottom of the loop between helix 1 and 2 as the other interface involved in the formation of the actin-induced vinculin dimer. The next step to verify our proposed model would create mutations within the loop to polar or charged residues in order to disrupt actin-induced dimer formation and perform actin co-sedimentation assays on these variants as a readout. We hypothesize that if this region of Vt is part of the dimer interface then disruption of the hydrophobic properties within this particular site will impact actin bundling but not actin binding.

To probe this interface, we will perform chemical crosslinking to lock the actin-induced dimer into place and send the samples for analysis by mass spectrometry as an additional way to verify our actin-induced Vt dimer interface model. Using a crosslinker (BS3), we have shown that a dimeric species forms in the presence of actin when using C-terminal hairpin deletion mutants (Vt ΔC5 and Vt ΔC2) and it is distinct from the actin-induced dimer formed by WT Vt

(*32*, *39*). Vt ΔC5 was crosslinked in the presence of actin and was analyzed by mass spectrometry. We found three distinct peptides in helices 1, 2, and the C-terminus, which is consistent with observations that mutations or deletions in helix 1 or 2 or the C-terminus significantly impairs actin bundling (*39*). To see if the Y1065 mutants also induced a similar shift in the molecular weight in the presence of actin, we employed similar crosslinking strategies. However, there is no discernable difference between the variants despite their varying bundling efficiencies (data not shown). Since vinculin commonly forms higher order oligomers when Vt is in excess, especially in the presence of a crosslinker, we separated crosslinked bundles in an effort to separate out Vt dimers that form in the presence of actin from non-physiologically relevant dimers. As shown in Table 3, there are subtle differences between the Y1065 mutants with Vt Y1065E displaying a smaller band in the presence of actin. To verify if the lower molecular weight band is consistently observed with actin-bundling deficient mutants, we will perform similar experiments with both Vt ΔC5 and pY-Vt. Furthermore, we will send crosslinked samples for analysis by mass spectrometry.

To decrease the possibility that identical peptides from Vt monomers will be identified, and we lose the idea of orientation, we will use a dead-end linker attached to the peptide by labeling half the Vt with isotope ^{15}N and incubate with unlabeled Vt in a 1:1 ratio. If identical peptides from different monomers are linked together, then by labeling one of the monomers with ^{15}N, the identical peptides should display enough of a difference in weight that would allow them show up in separate populations. By using this method, we will be able to identify other residues involved in the actin-induced Vt dimer and be able to further refine the model.

3. Identify if the residues in the C-terminal hairpin or the F-actin-induced vinculin dimer also serve a scaffolding function in cells.

One question that remains unanswered is how does a vinculin mutation that retains actin binding, but possesses a specific defect in actin-bundling differ from other variants that have been previously used to probe vinculin/F-actin interactions? It has been shown that a vinculin variant cells expressing Y1065F are slightly deficient in its ability to spread on FN (*102*). However, as mentioned earlier, we have recently shown that Vin-/- MEFS re-expressing ΔC5-vinculin are smaller in cell area and have significantly fewer adhesions when cells are allowed to spread on FN (*39*). When C-terminal hairpin deletions are expressed in cells, the phenotype between cells expressing ΔC5-vinculin and ΔC2-vinculin were striking with cells expressing ΔC5-vinculin a significantly higher number and larger of protrusions as cells adhere and spread on FN for two hours (*32*). These data suggest differential roles for the last five amino acids in the C-terminalhairpin of vinculin. Although both deletions lack Y1065, the behavior of the cells as they adhere and spread on FN are very different, indicating that this region of vinculin could serve as a scaffold for a novel binding partner.Furthermore, as described in Chapter IV, Y1065 mutants that are deficient in actin bundling are expressed in cells (Y1065E), the phenotype observed is the exact opposite of what has been observed for the actin binding (I997A & V1001A) and actin bundling (ΔC5) mutants. Where actin binding and bundling mutants display a reduction in cell spreading, as indicated by the cell area after cells have adhered and spread on FN for two hours, as well as have fewer but larger FAs. Cells expressing Y1065E-vinculin show an enhancement in spreading but have significantly smaller FAs. This begs the question: Is the phenotype we observe due to a deficiency in actin bundling or is it due to a binding partner where its association with vinculin is dependent on the phosphorylation state of Y1065?

There are many techniques available in order to identify novel binding partners such as yeast-two hybrids or simply performing co-immunoprecipitations and submit samples to mass spectrometry. However, some of vinculin's interactions can be transient and only detectable in the presence of a crosslinker, such as vinculin's association with VASP (*94*). Furthermore, these techniques do not reveal at which time the interaction occurs during a particular cellular processes, such as during cell spreading or during cellular reinforcement. To determine a potential binding partner, we will utilize the APEX construct and subclone vinculin into the construct and then introduce various point mutations we wish to examine. The APEX enzyme is a peroxidase that upon exposure to biotin-phenol, creates biotin-phenoxyl radicals, a highly reactive molecule that will react to nearby proteins by adding a biotin modification(*176*). After lysing the cells, biotin-tagged proteins are extracted and then can be identified by mass spectrometry. This system will allow us to form an interaction map of vinculin and its binding partners not only in the presence of different vinculin variants, but also when cells are subjected to a number of conditions; such as during adhesion and spreading, whether it is on different ligands or substrates of different stiffnesses, or upon application of external forces through magnetic beads coated with FN. Once a binding partner is identified, the interaction can be verified through co-immunoprecipitations, pulldowns, and immunofluorescence.

4. Investigate FA dynamics in the presence of Y1065 mutants

Within FAs, most proteins recruit to these structures through specific interactions and often exchange between bound and unbound states. FA maturation is impacted when the exchange rates of FA proteins are altered. It is has been suggested that, under certain conditions, a reduction in the exchange rates of FA proteins can lead to a loss of the cellular reinforcement(*134*). A number of parameters can impact the exchange rates of FA proteins such

as location of the FA within the cell, if FAs are initially forming or maturing, or by increasing integrin-ligand interactions through varying ligand concentrations. For instance, varying the concentration of collagen increased the rate of exchange for focal adhesion kinase (FAK) but decreased the rate of exchange for paxillin (*177*).

In the case of vinculin, it will readily exchange from adhesions, but it needs to undergo changes in conformation that impact its activation status since "active" vinculin mutants (T12) lose the ability to exchange from adhesions (*75*). Additionally, it has been shown that, in the presence of Y1065F, vinculin will less readily exchange from FAs while Y1065E-vinculin displays an increased exchange in FAs as shown by the percent of mobile protein(*103*).Furthermore, it has been shown that Y1065F can decrease the rate of exchange of vinculin in nascent FAs if adhesions at the leading edge of migrating keratocytes are analyzed (*104*). Fluorescence recovery after photobleaching (FRAP) is an imaging technique that can measure the rate of exchange and the mobile fraction of a protein in cells. To further probe the Y1065 variants, we examined the exchange rates of variants from FAs using FRAP when cells are plated on two different concentrations of FN. When we calculate the half-life and percent mobile fraction of the vinculin variants, we observe that there is not a significant difference in their exchange rates, but there are differences in the amount of mobile vinculin when cells are plated on a higher density of FN (Table 4). The differences in the amount of mobile protein display a similar trend to observations made by Küpper *et al*(*103*). Interestingly, these differences do not appear when cells are adhered to a lower FN concentration. These results suggest that the density of the ligand can additionally influence the behavior or proteins within FAs.

The amount of tension exerted on adhesions can alter the exchange rates of many FA proteins, including vinculin. When intracellular tension is lost, FA proteins will typically display an increase in their exchange rates(*178*). To test the effects of intracellular tension on the exchange of the vinculin variants, we treated cells with either the Rho-kinase inhibitor (Y - 27632)**,** a myosin-light chain kinase inhibitor (MLCK Inhibitor peptide 18), or both. When cells are treated with the inhibitors, the vinculin variants will rapidly exchange, and there is not a significant difference between the variants, except for Y1065E-vinculin when both inhibitors are added (Table 5). When external tension is applied to FAs, the exchange rates of vinculin will slow in response to higher amounts of force as shown by experiments that can increase stiffness of the substrates (*162*).

In addition to responding to intracellular contractility, cells will exert different amounts of tension on their FAs depending on the type of stress fiber anchored to the adhesion and its location in the cell. FAs at the cell periphery are under higher amounts of tension as shown by stress fiber severing experiments; when stress fibers that are attached to a FA located at the cell periphery are severed, the cell will contract(*179, 180*). However, if stress fibers that are anchored to central FAs are severed, nothing will happen, presumably because central FAs are under less tension. Recent reports have highlighted that the exchange rate of FAK can vary between peripheral versus central FAs (*177*). To test if the exchange rates and percent of mobile protein differ in the presence of the vinculin variants when different amounts of tension are applied, we examined the vinculin variants located in FAs either in the cell center or the periphery. As expected, WT-vinculin more readily exchanges from central adhesions than adhesions located at the cell periphery since central FAs are under less tension (Table 5). Cells expressing Y1065F- and Y1065E-vinculin follow the same patterns as WT-vinculin; however, Y1065A-vinculin fails

to make a distinction between peripheral and central FAs although different amounts of force should be exerted on them (Table 6). Even though the variants display differences in their exchange rates, there is not a significant difference in the percent of protein that will exchange from FAs (Table 6). These data suggests that Y1065A-vinculin displays defects in its exchange. However, these defects in exchange are only observed with the more suitable non-phosphorylatable mutant that we have characterized in Chapter IV. Overall, these results suggest that the phosphorylation state of Y1065 is an important regulator in exchange dynamics and can be influenced by a number of factors such as by the density of ligand plated on substrates and intracellular contractility (Table 4 and 5). In order to understand the role of Y1065 in adhesion dynamics, we would like to investigate if the phosphorylation state of Y1065 can influence other parameters of adhesion dynamics such as adhesion formation and disassembly. To do this, we will track adhesion dynamics through total internal reflection fluorescence (TIRF) microscopy. Based on our observations, there appears to be a difference in how FAs expressing the different vinculin mutants respond to intracellular tension versus external applications of force (Table 5; Figure 4.8). Previous studies have shown that cells expressing Y1065F-vinculn shows a significant reduction in their ability to exert traction forces; however, no other Y1065 mutants were examined (*103*). We would like to examine if FAs containing the Y1065 vinculin mutants also display a difference in exerting forces on their substrate as measured through traction force microscopy. By examining these additional parameters in FA dynamics, we will gain a more comprehensive understanding of how phosphorylation at Y1065 can influence vinculin behavior.

F.Conclusions

Although the role of vinculin in FAs has been studied since its discovery, there are a number of questions that remain about its interactions with its binding partners and how this

protein is regulated. While vinculin has been shown to mediate a number of cellular processes, the types of tools used to study this protein are often not structurally characterized, and many of them cause the protein to be destabilized. As a result, it is likely that current tools used to study vinculin in cells lead to a number of unforeseen cellular consequences. In this dissertation, I provide evidence for select mutations that impact Vt's actin binding and bundling properties and examine these variants in cells.

While it appears that Vt's actin binding and bundling function can mediate a number of cellular processes, the exact reason behind this remains to be discovered since we cannot distinguish if the phenotypes we observe are attributed to vinculin-mediated F-actin bundle formation or phosphorylation of Y1065. Currently there are a few possibilities for observed phenotypes. One possibility is that, within FAs, the actin-induced dimer and F-actin bundling is present and without phosphorylation at Y1065, vinculin gets locked into this conformation and displays difficulty in exchanging from FAs. This would explain why we see a decrease in the exchange rate of Y1065A-vinculin and why Y1065F-vinculin is less mobile, although there is not a difference in its exchange rate, and why Y1065E-vinculin is highly mobile (Table 4). Another possibility is that phosphorylation at Y1065 helps activate vinculin in order for it be efficiently recruited and regulated in FAs. This would explain why there is a low percentage of phosphorylated vinculin present in cells and why there are multiple populations of vinculin present within FAs (*74, 100,102*). Finally, Y1065 or the actin-induced dimer itself is the binding site for an unknown binding partner (Figure 5.1). In order to differentiate between the possibilities, future efforts will mutate residues that help mediate the actin-induced dimer that were identified in Chapter IV. By disrupting the other interface responsible for the actin-induced dimer, we can begin to differentiate between the different possibilities presented above and

determine if effects on FA dynamics and mechanotransduction are caused solely by phosphorylation at Y1065 or if the actin-induced dimer plays a role as well.

Vt	Bundling Efficiency	Other Species	Dimer	Additional Trimer Species	Higher Order Oligomer
WT	~75%		42	70	85
Y1065F	~95%		46	60	
Y1065E	~23%	35	46	55	
Y1065A	~65%		42	70	

Table 3. Summary of crosslinking studies with Y1065 mutants. Crosslinking experiments were conducted at room temperature for 40 min. Final Vt concentration was 2.5 μm; BS3 concentration was 25 μm; Western blots of WT Vt and Vt Y1065 mutants in the presence of increasing concentrations of actin probed against Vt (data not shown). At a ratio of 2:1, crosslinked bundles were pelleted and separated from the supernatant the contains non-physiological crosslinked Vt oligomer species. By pelleting the crosslinked bundles, we would be able to see the Vt species responsible for actin bundling and if there was a difference between the Y1065 mutants. Experiments were performed twice. A summary of the bands that were detected in the crosslinked bundle sample in the duplicate experiment are reported above.

Variant	Half-life (seconds)	% Mobile Fraction	Half-life (seconds)	% Mobile Fraction	% Mobile Fraction (Küpper *et al.*)
FN Concentration	50 µg/mL		10 µg/mL		
WT	56.58 ± 4.75	84.08 ± 1.21	61.09 ± 8.75	77.43 ±2.54	63
Y1065A	53.86 ± 6.357	74.31 ± 4.52	62.07 ± 11.12	79.21 ± 4.95	
Y1065F	53.79 ± 4.20	53.79 ± 4.97	52.97 ± 9.11	68.90 ± 3.50	59
Y1065E	55.82 ± 2.36	96.54 ± 5.11	60.76 ± 7.31	76.26 ± 2.01	76

Table 4. Results of FRAP experiments when cells are plated on two FN concentrations. Cells were either resuspended in 0.5% delipidated BSA media with antibiotic-antimycotic for 2 hours prior to plating onto 10 µg/mL FN for 3 hours or cells were seeded onto 50 µg/mL for 24 hours in FBS (fetal bovine serum) supplemented DMEM. The exchange rates and percent mobile fraction of GFP-vinculin was calculated by fitting a two phase exponential association curve. Errors are standard of the mean (S.E.M.). For 50 µg/mL, WT n=12, Y1065A n=14, Y1065F n=13, Y1065E n=9. For 10 µg/mL, WT n=10, Y1065A n=9, Y1065F n=9, Y1065E n=12.

Variant	**T ½**		
Treatment	Y -27632	MLCK Inhibitor Peptide 18	Both
WT	14.79 ± 0.68	40.53 ± 2.74	21.40 ± 1.13
Y1065A	14.50 ± 0.84	39.32 ± 1.47	12.94 ± 1.27
Y1065F	7.932 ± 0.92	29.95 ± 1.74	14.25 ± 1.64
Y1065E	24.46 ± 1.35	50.20 ± 1.84	5.54 ± 1.56

Table 5. Loss of intracellular tension increases the exchange for all the Y1065 mutants. Cells were pretreated with either Y-27532 (5 µM) for 30 minutes prior to imaging or MLCK inhibitor peptide 18 (10 µM) for 2 hours, or both. The exchange rates of GFP-vinculin and its variants was calculated by fitting a two phase exponential association curve. Errors are standard of the mean (S.E.M.).

Variant	Location	Half-life (seconds)	% Mobile Fraction
WT	Peripheral	62.45 ± 7.75	84.55 ± 1.40
	Central	43.24 ± 2.93	93.03 ± 6.04
Y1065A	Peripheral	57.96 ± 10.39	77.23 ± 7.34
	Central	56.36 ± 7.98	71.90 ± 4.97
Y1065F	Peripheral	74.20 ± 6.19	81.52 ± 11.52
	Central	43.27 ± 6.03	81.90 ± 2.65
Y1065E	Peripheral	67.10 ± 2.21	105.8 ± 8.47
	Central	37.79 ± 4.47	92.42 ± 4.30

Table 6. Exchange rates of Y1065 mutants vary depending on FA location. Cells were seeded onto 50 µg/mL FN for 24 hours in DMEM supplemented with FBS. The exchange rates and percent mobile fraction for GFP-vinculin and its variants was calculated by fitting a two phase exponential association curve. Errors are standard of the mean (S.E.M.).

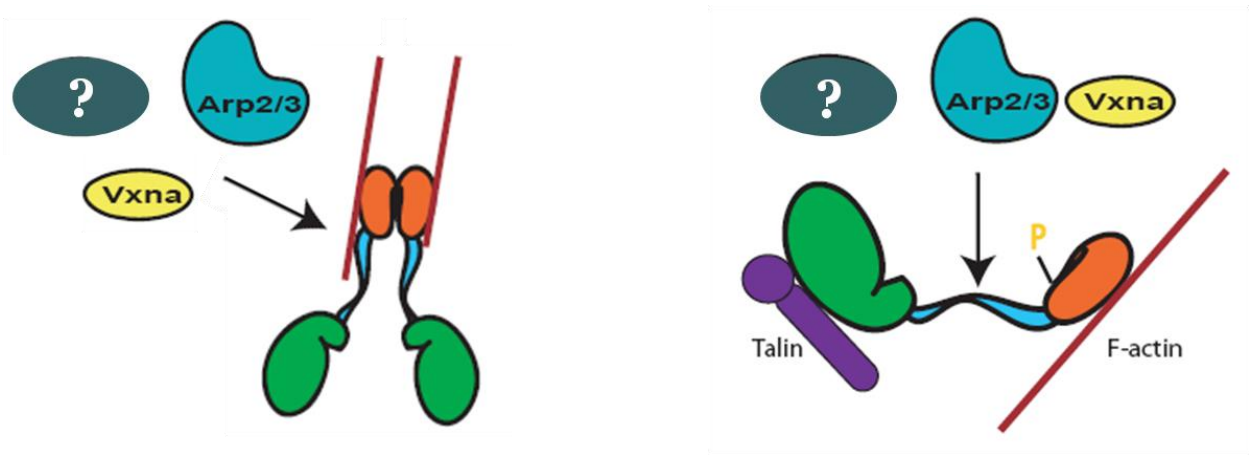

Figure 5.1Possible scaffolding interfaces for potential binding partners. Binding partners could utilize the actin-induced dimer (left) as part of their scaffolding interface when recruited to vinculin (Vh (green); proline rich linker (blue); Vt (orange)). Alternatively, binding partners could be regulated by the phosphorylated state of Y1065 (yellow).

WORKS CITED

1. Rodriguez Fernandez, J.L., et al., Suppression of vinculin expression by antisense transfection confers changes in cell morphology, motility, and anchorage-dependent growth of 3T3 cells. J Cell Biol, 1993. **122**(6): p. 1285-94.

2. Xu, W., H. Baribault, and E.D. Adamson, Vinculin knockout results in heart and brain defects during embryonic development. Development, 1998. **125**(2): p. 327-37.

3. Xu, W., J.L. Coll, and E.D. Adamson, Rescue of the mutant phenotype by reexpression of full-length vinculin in null F9 cells; effects on cell locomotion by domain deleted vinculin. J Cell Sci, 1998. **111 (Pt 11)**: p. 1535-44.

4. Coll, J.L., et al., Targeted disruption of vinculin genes in F9 and embryonic stem cells changes cell morphology, adhesion, and locomotion. Proc Natl Acad Sci U S A, 1995. **92**(20): p. 9161-5.

5. Vasile, V.C., et al., Obstructive hypertrophic cardiomyopathy is associated with reduced expression of vinculin in the intercalated disc. Biochem Biophys Res Commun, 2006. **349**(2): p. 709-15.

6. Zemljic-Harpf, A.E., et al., Heterozygous inactivation of the vinculin gene predisposes to stress-induced cardiomyopathy. Am J Pathol, 2004. **165**(3): p. 1033-44.

7. Vogel, B., et al., In-vivo characterization of human dilated cardiomyopathy genes in zebrafish. Biochem Biophys Res Commun, 2009. **390**(3): p. 516-22.

8. Barstead, R.J. and R.H. Waterston, Vinculin is essential for muscle function in the nematode. J Cell Biol, 1991. **114**(4): p. 715-24.

9. Subauste, M.C., et al., Vinculin modulation of paxillin-FAK interactions regulates ERK to control survival and motility. J Cell Biol, 2004. **165**(3): p. 371-81.

10. Nelson, E.S., et al., Vinculin activators target integrins from within the cell to increase melanoma sensitivity to chemotherapy. Mol Cancer Res, 2011. **9**(6): p. 712-23.

11. Rodriguez Fernandez, J.L., et al., Suppression of tumorigenicity in transformed cells after transfection with vinculin cDNA. J Cell Biol, 1992. **119**(2): p. 427-38.

12. Kawahara, E., R. Tokuda, and I. Nakanishi, Migratory phenotypes of HSC-3 squamous carcinoma cell line induced by EGF and PMA: relevance to migration of loosening of adhesion and vinculin-associated focal contacts with prominent filopodia. Cell Biol Int, 1999. **23**(3): p. 163-74.

13. Lifschitz-Mercer, B., et al., Expression of the adherens junction protein vinculin in human basal and squamous cell tumors: relationship to invasiveness and metastatic potential. Hum Pathol, 1997. **28**(11): p. 1230-6.

14. Meyer, T. and U. Brinck, Immunohistochemical detection of vinculin in human rhabdomyosarcomas. Gen Diagn Pathol, 1997. **142**(3-4): p. 191-8.

15. Sadano, H., M. Inoue, and S. Taniguchi, Differential expression of vinculin between weakly and highly metastatic B16-melanoma cell lines. Jpn J Cancer Res, 1992. **83**(6): p. 625-30.

16. Somiari, R.I., et al., High-throughput proteomic analysis of human infiltrating ductal carcinoma of the breast. Proteomics, 2003. **3**(10): p. 1863-73.

17. Belkin, A.M., et al., Diversity of vinculin/meta-vinculin in human tissues and cultivated cells. Expression of muscle specific variants of vinculin in human aorta smooth muscle cells. J Biol Chem, 1988. **263**(14): p. 6631-5.

18. Rudiger, M., et al., Differential actin organization by vinculin isoforms: implications for cell type-specific microfilament anchorage. FEBS Lett, 1998. **431**(1): p. 49-54.

19. Glukhova, M.A., et al., Meta-vinculin distribution in adult human tissues and cultured cells. FEBS Lett, 1986. **207**(1): p. 139-41.

20. Thoss, F., et al., Metavinculin: New insights into functional properties of a muscle adhesion protein. Biochem Biophys Res Commun, 2013. **430**(1): p. 7-13.

21. Huttelmaier, S., et al., Raver1, a dual compartment protein, is a ligand for PTB/hnRNPI and microfilament attachment proteins. J Cell Biol, 2001. **155**(5): p. 775-86.

22. Witt, S., et al., Comparative biochemical analysis suggests that vinculin and metavinculin cooperate in muscular adhesion sites. J Biol Chem, 2004. **279**(30): p. 31533-43.

23. Thompson, P.M., C.E. Tolbert, and S.L. Campbell, Vinculin and metavinculin: oligomerization and interactions with F-actin. FEBS Lett, 2013. **587**(8): p. 1220-9.

24. Koteliansky, V.E., et al., Developmental changes in expression of adhesion-mediating proteins in human aortic smooth muscle. Biochem Soc Trans, 1991. **19**(4): p. 1072-6.

25. Belkin, A.M., et al., Immunolocalization of meta-vinculin in human smooth and cardiac muscles. J Cell Biol, 1988. **107**(2): p. 545-53.

26. Gimona, M., et al., Smooth muscle specific expression of calponin. FEBS Lett, 1990. **274**(1-2): p. 159-62.

27. Olson, T.M., et al., Metavinculin mutations alter actin interaction in dilated cardiomyopathy. Circulation, 2002. **105**(4): p. 431-7.

28. Vasile, V.C., et al., Identification of a metavinculin missense mutation, R975W, associated with both hypertrophic and dilated cardiomyopathy. Mol Genet Metab, 2006. **87**(2): p. 169-74.

29. Rangarajan, E.S., et al., A helix replacement mechanism directs metavinculin functions. PLoS One, 2010. **5**(5): p. e10679.

30. Vasile, V.C., et al., A missense mutation in a ubiquitously expressed protein, vinculin, confers susceptibility to hypertrophic cardiomyopathy. Biochem Biophys Res Commun, 2006. **345**(3): p. 998-1003.

31. Wells, Q.S., et al., Familial dilated cardiomyopathy associated with congenital defects in the setting of a novel VCL mutation (Lys815Arg) in conjunction with a known MYPBC3 variant. Cardiogenetics, 2011. **1**(1).

32. Tolbert, C.E., K. Burridge, and S.L. Campbell, Vinculin regulation of F-actin bundle formation: What does it mean for the cell? Cell Adh Migr, 2013. **7**(2).

33. Peng, X., et al., New insights into vinculin function and regulation. Int Rev Cell Mol Biol, 2011. **287**: p. 191-231.

34. Gardel, M.L., et al., Mechanical integration of actin and adhesion dynamics in cell migration. Annu Rev Cell Dev Biol, 2010. **26**: p. 315-33.

35. Wolfenson, H., et al., The heel and toe of the cell's foot: a multifaceted approach for understanding the structure and dynamics of focal adhesions. Cell Motil Cytoskeleton, 2009. **66**(11): p. 1017-29.

36. Ezzell, R.M., et al., Vinculin promotes cell spreading by mechanically coupling integrins to the cytoskeleton. Exp Cell Res, 1997. **231**(1): p. 14-26.

37. Wen, K.K., P.A. Rubenstein, and K.A. DeMali, Vinculin nucleates actin polymerization and modifies actin filament structure. J Biol Chem, 2009. **284**(44): p. 30463-73.

38. Le Clainche, C., et al., Vinculin is a dually regulated actin filament barbed end-capping and side-binding protein. J Biol Chem, 2010. **285**(30): p. 23420-32.

39. Shen, K., et al., The vinculin C-terminal hairpin mediates F-actin bundle formation, focal adhesion, and cell mechanical properties. J Biol Chem, 2011. **286**(52): p. 45103-15.

40. Humphries, J.D., et al., Vinculin controls focal adhesion formation by direct interactions with talin and actin. J Cell Biol, 2007. **179**(5): p. 1043-57.

41. Marg, S., et al., The vinculin-DeltaIn20/21 mouse: characteristics of a constitutive, actin-binding deficient splice variant of vinculin. PLoS One, 2010. **5**(7): p. e11530.

42. Thievessen, I., et al., Vinculin-actin interaction couples actin retrograde flow to focal adhesions, but is dispensable for focal adhesion growth. J Cell Biol, 2013. **202**(1): p. 163-77.

43. Janmey, P.A. and D.A. Weitz, Dealing with mechanics: mechanisms of force transduction in cells. Trends Biochem Sci, 2004. **29**(7): p. 364-70.

44. Lo, C.M., et al., Cell movement is guided by the rigidity of the substrate. Biophys J, 2000. **79**(1): p. 144-52.

45. Mierke, C.T., et al., Mechano-coupling and regulation of contractility by the vinculin tail domain. Biophys J, 2008. **94**(2): p. 661-70.

46. Boccafoschi, F., et al., The role of mechanical stretching in the activation and localization of adhesion proteins and related intracellular molecules. J Cell Biochem, 2011. **112**(5): p. 1403-9.

47. Coyer, S.R., et al., Nanopatterning Reveals an ECM Area Threshold for Focal Adhesion Assembly and Force Transmission that is regulated by Integrin Activation and Cytoskeleton Tension. J Cell Sci, 2012.

48. Balaban, N.Q., et al., Force and focal adhesion assembly: a close relationship studied using elastic micropatterned substrates. Nat Cell Biol, 2001. **3**(5): p. 466-72.

49. Grashoff, C., et al., Measuring mechanical tension across vinculin reveals regulation of focal adhesion dynamics. Nature. **466**(7303): p. 263-6.

50. Humphries, J.D., et al., Vinculin controls focal adhesion formation by direct interactions with talin and actin. J Cell Biol, 2007. **179**(5): p. 1043-57.

51. Ji, L., J. Lim, and G. Danuser, Fluctuations of intracellular forces during cell protrusion. Nat Cell Biol, 2008. **10**(12): p. 1393-400.

52. Hazan, R.B., et al., Vinculin is associated with the E-cadherin adhesion complex. J Biol Chem, 1997. **272**(51): p. 32448-53.

53. Watabe-Uchida, M., et al., alpha-Catenin-vinculin interaction functions to organize the apical junctional complex in epithelial cells. J Cell Biol, 1998. **142**(3): p. 847-57.

54. Wachsstock, D.H., J.A. Wilkins, and S. Lin, Specific interaction of vinculin with alpha-actinin. Biochem Biophys Res Commun, 1987. **146**(2): p. 554-60.

55. Gingras, A.R., et al., Mapping and consensus sequence identification for multiple vinculin binding sites within the talin rod. J Biol Chem, 2005. **280**(44): p. 37217-24.

56. Tran Van Nhieu, G., A. Ben-Ze'ev, and P.J. Sansonetti, Modulation of bacterial entry into epithelial cells by association between vinculin and the Shigella IpaA invasin. Embo J, 1997. **16**(10): p. 2717-29.

57. Holle, A.W., et al., In situ mechanotransduction via vinculin regulates stem cell differentiation. Stem Cells, 2013.

58. Mandai, K., et al., Ponsin/SH3P12: an l-afadin- and vinculin-binding protein localized at cell-cell and cell-matrix adherens junctions. J Cell Biol, 1999. **144**(5): p. 1001-17.

59. Kioka, N., et al., Vinexin: a novel vinculin-binding protein with multiple SH3 domains enhances actin cytoskeletal organization. J Cell Biol, 1999. **144**(1): p. 59-69.

60. Kawabe, H., et al., nArgBP2, a novel neural member of ponsin/ArgBP2/vinexin family that interacts with synapse-associated protein 90/postsynaptic density-95-associated protein (SAPAP). J Biol Chem, 1999. **274**(43): p. 30914-8.

61. Brindle, N.P., et al., The focal-adhesion vasodilator-stimulated phosphoprotein (VASP) binds to the proline-rich domain in vinculin. Biochem J, 1996. **318 (Pt 3)**: p. 753-7.

62. DeMali, K.A., C.A. Barlow, and K. Burridge, Recruitment of the Arp2/3 complex to vinculin: coupling membrane protrusion to matrix adhesion. J Cell Biol, 2002. **159**(5): p. 881-91.

63. Janostiak, R., et al., CAS directly interacts with vinculin to control mechanosensing and focal adhesion dynamics. Cell Mol Life Sci, 2013.

64. Wood, C.K., et al., Characterisation of the paxillin-binding site and the C-terminal focal adhesion targeting sequence in vinculin. J Cell Sci, 1994. **107 (Pt 2)**: p. 709-17.

65. Ziegler, W.H., et al., A lipid-regulated docking site on vinculin for protein kinase C. J Biol Chem, 2002. **277**(9): p. 7396-404.

66. Huttelmaier, S., et al., Characterization of two F-actin-binding and oligomerization sites in the cell-contact protein vinculin. Eur J Biochem, 1997. **247**(3): p. 1136-42.

67. Johnson, R.P., et al., A conserved motif in the tail domain of vinculin mediates association with and insertion into acidic phospholipid bilayers. Biochemistry, 1998. **37**(28): p. 10211-22.

68. Bellin, R.M., et al., Synemin may function to directly link muscle cell intermediate filaments to both myofibrillar Z-lines and costameres. J Biol Chem, 2001. **276**(34): p. 32330-7.

69. Ziegler, W.H., R.C. Liddington, and D.R. Critchley, The structure and regulation of vinculin. Trends Cell Biol, 2006. **16**(9): p. 453-60.

70. Carisey, A. and C. Ballestrem, Vinculin, an adapter protein in control of cell adhesion signalling. Eur J Cell Biol, 2011. **90**(2-3): p. 157-63.

71. Bakolitsa, C., et al., Structural basis for vinculin activation at sites of cell adhesion. Nature, 2004. **430**(6999): p. 583-6.

72. Bakolitsa, C., et al., Crystal structure of the vinculin tail suggests a pathway for activation. Cell, 1999. **99**(6): p. 603-13.

73. Cohen, D.M., et al., Two distinct head-tail interfaces cooperate to suppress activation of vinculin by talin. J Biol Chem, 2005. **280**(17): p. 17109-17.

74. Chen, H., et al., Spatial distribution and functional significance of activated vinculin in living cells. J Cell Biol, 2005. **169**(3): p. 459-70.

75. Cohen, D.M., et al., A conformational switch in vinculin drives formation and dynamics of a talin-vinculin complex at focal adhesions. J Biol Chem, 2006. **281**(23): p. 16006-15.

76. Chen, H., D.M. Choudhury, and S.W. Craig, Coincidence of actin filaments and talin is required to activate vinculin. J Biol Chem, 2006. **281**(52): p. 40389-98.

77. Izard, T., G. Tran Van Nhieu, and P.R. Bois, Shigella applies molecular mimicry to subvert vinculin and invade host cells. J Cell Biol, 2006. **175**(3): p. 465-75.

78. Kanchanawong, P., et al., Nanoscale architecture of integrin-based cell adhesions. Nature, 2010. **468**(7323): p. 580-4.

79. Saunders, R.M., et al., Role of vinculin in regulating focal adhesion turnover. Eur J Cell Biol, 2006. **85**(6): p. 487-500.

80. Johnson, R.P. and S.W. Craig, The carboxy-terminal tail domain of vinculin contains a cryptic binding site for acidic phospholipids. Biochem Biophys Res Commun, 1995. **210**(1): p. 159-64.

81. Chandrasekar, I., et al., Vinculin acts as a sensor in lipid regulation of adhesion-site turnover. J Cell Sci, 2005. **118**(Pt 7): p. 1461-72.

82. Fukami, K., et al., alpha-Actinin and vinculin are PIP2-binding proteins involved in signaling by tyrosine kinase. J Biol Chem, 1994. **269**(2): p. 1518-22.

83. Gilmore, A.P. and K. Burridge, Regulation of vinculin binding to talin and actin by phosphatidyl-inositol-4-5-bisphosphate. Nature, 1996. **381**(6582): p. 531-5.

84. Sechi, A.S. and J. Wehland, The actin cytoskeleton and plasma membrane connection: PtdIns(4,5)P(2) influences cytoskeletal protein activity at the plasma membrane. J Cell Sci, 2000. **113 Pt 21**: p. 3685-95.

85. Zamir, E. and B. Geiger, Molecular complexity and dynamics of cell-matrix adhesions. J Cell Sci, 2001. **114**(Pt 20): p. 3583-90.

86. Steimle, P.A., et al., Polyphosphoinositides inhibit the interaction of vinculin with actin filaments. J Biol Chem, 1999. **274**(26): p. 18414-20.

87. Diez, G., et al., Anchorage of vinculin to lipid membranes influences cell mechanical properties. Biophys J, 2009. **97**(12): p. 3105-12.

88. Palmer, S.M., et al., Lipid binding to the tail domain of vinculin: specificity and the role of the N and C termini. J Biol Chem, 2009. **284**(11): p. 7223-31.

89. Wirth, V.F., et al., Vinculin's C-terminal region facilitates phospholipid membrane insertion. Biochem Biophys Res Commun, 2010. **398**(3): p. 433-7.

90. Johnson, R.P. and S.W. Craig, Actin activates a cryptic dimerization potential of the vinculin tail domain. J Biol Chem, 2000. **275**(1): p. 95-105.

91. Janssen, M.E., et al., Three-dimensional structure of vinculin bound to actin filaments. Mol Cell, 2006. **21**(2): p. 271-81.

92. Golji, J. and M.R. Mofrad, The interaction of vinculin with actin. PLoS Comput Biol, 2013. **9**(4): p. e1002995.

93. Palmer, S.M., M.D. Schaller, and S.L. Campbell, Vinculin tail conformation and self-association is independent of pH and H906 protonation. Biochemistry, 2008. **47**(47): p. 12467-75.

94. Huttelmaier, S., et al., The interaction of the cell-contact proteins VASP and vinculin is regulated by phosphatidylinositol-4,5-bisphosphate. Curr Biol, 1998. **8**(9): p. 479-88.

95. Molony, L. and K. Burridge, Molecular shape and self-association of vinculin and metavinculin. J Cell Biochem, 1985. **29**(1): p. 31-6.

96. Abe, C., et al., Monomeric and dimeric conformation of the vinculin tail five-helix bundle in solution studied by EPR spectroscopy. Biophys J, 2011. **101**(7): p. 1772-80.

97. Jockusch, B.M. and G. Isenberg, Interaction of Alpha-Actinin and Vinculin with Actin - Opposite Effects on Filament Network Formation. P Natl Acad Sci-Biol, 1981. **78**(5): p. 3005-3009.

98. Johnson, R.P. and S.W. Craig, F-actin binding site masked by the intramolecular association of vinculin head and tail domains. Nature, 1995. **373**(6511): p. 261-4.

99. Janssen, M.E., et al., The C-terminal tail domain of metavinculin, vinculin's splice variant, severs actin filaments. J Cell Biol, 2012. **197**(5): p. 585-93.

100. Sefton, B.M., et al., Vinculin: a cytoskeletal target of the transforming protein of Rous sarcoma virus. Cell, 1981. **24**(1): p. 165-74.

101. Perez-Moreno, M., et al., Vinculin but not alpha-actinin is a target of PKC phosphorylation during junctional assembly induced by calcium. J Cell Sci, 1998. **111 (Pt 23)**: p. 3563-71.

102. Zhang, Z., et al., The phosphorylation of vinculin on tyrosine residues 100 and 1065, mediated by SRC kinases, affects cell spreading. Mol Biol Cell, 2004. **15**(9): p. 4234-47.

103. Kupper, K., et al., Tyrosine phosphorylation of vinculin at position 1065 modifies focal adhesion dynamics and cell tractions. Biochem Biophys Res Commun, 2010. **399**(4): p. 560-4.

104. Mohl, C., et al., Becoming stable and strong: the interplay between vinculin exchange dynamics and adhesion strength during adhesion site maturation. Cell Motil Cytoskeleton, 2009. **66**(6): p. 350-64.

105. Moese, S., et al., The Helicobacter pylori CagA protein disrupts matrix adhesion of gastric epithelial cells by dephosphorylation of vinculin. Cell Microbiol, 2007. **9**(5): p. 1148-61.

106. Golji, J. and M.R. Mofrad, A molecular dynamics investigation of vinculin activation. Biophys J, 2010. **99**(4): p. 1073-81.

107. Janmey, P.A. and C.A. McCulloch, Cell mechanics: integrating cell responses to mechanical stimuli. Annu Rev Biomed Eng, 2007. **9**: p. 1-34.

108. Parsons, J.T., A.R. Horwitz, and M.A. Schwartz, Cell adhesion: integrating cytoskeletal dynamics and cellular tension. Nat Rev Mol Cell Biol, 2010. **11**(9): p. 633-43.

109. Geiger, B., J.P. Spatz, and A.D. Bershadsky, Environmental sensing through focal adhesions. Nat Rev Mol Cell Biol, 2009. **10**(1): p. 21-33.

110. Geiger, B. and A. Bershadsky, Assembly and mechanosensory function of focal contacts. Curr Opin Cell Biol, 2001. **13**(5): p. 584-92.

111. Byrne, B.J., et al., Chicken vinculin and meta-vinculin are derived from a single gene by alternative splicing of a 207-base pair exon unique to meta-vinculin. J Biol Chem, 1992. **267**(18): p. 12845-50.

112. Maeda, M., et al., Dilated cardiomyopathy associated with deficiency of the cytoskeletal protein metavinculin. Circulation, 1997. **95**(1): p. 17-20.

113. Johnson, R.P. and S.W. Craig, An intramolecular association between the head and tail domains of vinculin modulates talin binding. J Biol Chem, 1994. **269**(17): p. 12611-9.

114. Kroemker, M., et al., Intramolecular interactions in vinculin control alpha-actinin binding to the vinculin head. FEBS Lett, 1994. **355**(3): p. 259-62.

115. Weiss, E.E., et al., Vinculin is part of the cadherin-catenin junctional complex: complex formation between alpha-catenin and vinculin. J Cell Biol, 1998. **141**(3): p. 755-64.

116. Weekes, J., S.T. Barry, and D.R. Critchley, Acidic phospholipids inhibit the intramolecular association between the N- and C-terminal regions of vinculin, exposing actin-binding and protein kinase C phosphorylation sites. Biochem J, 1996. **314 (Pt 3)**: p. 827-32.

117. Borgon, R.A., et al., Crystal structure of human vinculin. Structure, 2004. **12**(7): p. 1189-97.

118. Fisher, J.K., et al., Thin-foil magnetic force system for high-numerical-aperture microscopy. Rev Sci Instrum, 2006. **77**(2): p. nihms8302.

119. Dixon, R.D., et al., Palladin is an actin cross-linking protein that uses immunoglobulin-like domains to bind filamentous actin. J Biol Chem, 2008. **283**(10): p. 6222-31.

120. Palmer, S.M. and S.L. Campbell, Backbone 1H, 13C, and 15N NMR assignments of the tail domain of vinculin. Biomol NMR Assign, 2008. **2**(1): p. 69-71.

121. Francis, S.E., et al., Central roles of alpha5beta1 integrin and fibronectin in vascular development in mouse embryos and embryoid bodies. Arterioscler Thromb Vasc Biol, 2002. **22**(6): p. 927-33.

122. Johnson, B.A. and R.A. Blevins, NMR View: A computer program for the visualization and analysis of NMR data. J Biomol NMR, 1994. **4**(5): p. 603-14.

123. Elfenbein, A., et al., Suppression of RhoG activity is mediated by a syndecan 4-synectin-RhoGDI1 complex and is reversed by PKCalpha in a Rac1 activation pathway. J Cell Biol, 2009. **186**(1): p. 75-83.

124. Berginski, M.E., et al., High-resolution quantification of focal adhesion spatiotemporal dynamics in living cells. PLoS One, 2011. **6**(7): p. e22025.

125. Bausch, A.R., W. Moller, and E. Sackmann, Measurement of local viscoelasticity and forces in living cells by magnetic tweezers. Biophys J, 1999. **76**(1 Pt 1): p. 573-9.

126. Dzamba, B.J., et al., Cadherin adhesion, tissue tension, and noncanonical Wnt signaling regulate fibronectin matrix organization. Dev Cell, 2009. **16**(3): p. 421-32.

127. Beil, M., et al., Sphingosylphosphorylcholine regulates keratin network architecture and visco-elastic properties of human cancer cells. Nat Cell Biol, 2003. **5**(9): p. 803-11.

128. Grashoff, C., et al., Measuring mechanical tension across vinculin reveals regulation of focal adhesion dynamics. Nature, 2010. **466**(7303): p. 263-6.

129. O'Brien, E.T., et al., Magnetic Manipulation for Force Measurements in Cell Biology. Method Cell Biol, 2008. **89**: p. 433-+.

130. Goldmann, W.H., et al., Differences in elasticity of vinculin-deficient F9 cells measured by magnetometry and atomic force microscopy. Exp Cell Res, 1998. **239**(2): p. 235-42.

131. Pasapera, A.M., et al., Myosin II activity regulates vinculin recruitment to focal adhesions through FAK-mediated paxillin phosphorylation. J Cell Biol, 2010. **188**(6): p. 877-90.

132. Galbraith, C.G., K.M. Yamada, and M.P. Sheetz, The relationship between force and focal complex development. J Cell Biol, 2002. **159**(4): p. 695-705.

133. Ulrich, T.A., et al., Probing cellular mechanobiology in three-dimensional culture with collagen-agarose matrices. Biomaterials, 2010. **31**(7): p. 1875-84.

134. von Wichert, G., et al., Force-dependent integrin-cytoskeleton linkage formation requires downregulation of focal complex dynamics by Shp2. Embo J, 2003. **22**(19): p. 5023-35.

135. Mao, Y.S. and H.L. Yin, Regulation of the actin cytoskeleton by phosphatidylinositol 4-phosphate 5 kinases. Pflugers Arch, 2007. **455**(1): p. 5-18.

136. Ji, L., J. Lim, and G. Danuser, Fluctuations of intracellular forces during cell protrusion. Nat Cell Biol, 2008. **10**(12): p. 1393-400.

137. Lee, J.H., et al., Raver1 interactions with vinculin and RNA suggest a feed-forward pathway in directing mRNA to focal adhesions. Structure, 2009. **17**(6): p. 833-42.

138. Abramoff, M.D., P.J. Magalhaes, and S.J. Ram, Image Processing with ImageJ. Biophotonics International, 2004. **11**(7): p. 36-42.

139. Strzelecka-Golaszewska, H., et al., Chicken-gizzard actin: polymerization and stability. Eur J Biochem, 1980. **104**(1): p. 41-52.

140. Heymann, J.B. and D.M. Belnap, Bsoft: image processing and molecular modeling for electron microscopy. J Struct Biol, 2007. **157**(1): p. 3-18.

141. Frank, J., et al., SPIDER and WEB: processing and visualization of images in 3D electron microscopy and related fields. J Struct Biol, 1996. **116**(1): p. 190-9.

142. Egelman, E.H., A robust algorithm for the reconstruction of helical filaments using single-particle methods. Ultramicroscopy, 2000. **85**(4): p. 225-34.

143. Fujii, T., et al., Direct visualization of secondary structures of F-actin by electron cryomicroscopy. Nature, 2010. **467**(7316): p. 724-8.

144. Pettersen, E.F., et al., UCSF Chimera--a visualization system for exploratory research and analysis. J Comput Chem, 2004. **25**(13): p. 1605-12.

145. Wriggers, W., Using Situs for the integration of multi-resolution structures. Biophys Rev, 2010. **2**(1): p. 21-27.

146. Ramachandran, S., et al., Automated minimization of steric clashes in protein structures. Proteins, 2011. **79**(1): p. 261-70.

147. Ding, F., et al., Ab initio folding of proteins with all-atom discrete molecular dynamics. Structure, 2008. **16**(7): p. 1010-8.

148. Dokholyan, N.V., et al., Discrete molecular dynamics studies of the folding of a protein-like model. Fold Des, 1998. **3**(6): p. 577-87.

149. Johnson, B.A. and R.A. Blevins, Nmr View - a Computer-Program for the Visualization and Analysis of Nmr Data. J Biomol NMR, 1994. **4**(5): p. 603-614.

150. Hwang, T.L., et al., Application of phase-modulated CLEAN chemical EXchange spectroscopy (CLEANEX-PM) to detect water-protein proton exchange and intermolecular NOEs. Journal of the American Chemical Society, 1997. **119**(26): p. 6203-6204.

151. Hwang, T.L., P.C. van Zijl, and S. Mori, Accurate quantitation of water-amide proton exchange rates using the phase-modulated CLEAN chemical EXchange (CLEANEX-PM) approach with a Fast-HSQC (FHSQC) detection scheme. J Biomol NMR, 1998. **11**(2): p. 221-6.

152. Farrow, N.A., et al., Backbone dynamics of a free and phosphopeptide-complexed Src homology 2 domain studied by 15N NMR relaxation. Biochemistry, 1994. **33**(19): p. 5984-6003.

153. Yin, S.Y., F. Ding, and N.V. Dokholyan, Eris: an automated estimator of protein stability. Nat Methods, 2007. **4**(6): p. 466-467.

154. Menkel, A.R., et al., Characterization of an F-actin-binding domain in the cytoskeletal protein vinculin. J Cell Biol, 1994. **126**(5): p. 1231-40.

155. Hamiaux, C., et al., Structural mimicry for vinculin activation by IpaA, a virulence factor of Shigella flexneri. EMBO Rep, 2006. **7**(8): p. 794-9.

156. Atienza, J.M., et al., Dynamic monitoring of cell adhesion and spreading on microelectronic sensor arrays. J Biomol Screen, 2005. **10**(8): p. 795-805.

157. Carisey, A., et al., Vinculin regulates the recruitment and release of core focal adhesion proteins in a force-dependent manner. Curr Biol, 2013. **23**(4): p. 271-81.

158. Lessey, E.C., C. Guilluy, and K. Burridge, From Mechanical Force to RhoA Activation. Biochemistry, 2012. **51**(38): p. 7420-32.

159. Chrzanowska-Wodnicka, M. and K. Burridge, Rho-stimulated contractility drives the formation of stress fibers and focal adhesions. Journal of Cell Biology, 1996. **133**(6): p. 1403-1415.

160. Riveline, D., et al., Focal contacts as mechanosensors: externally applied local mechanical force induces growth of focal contacts by an mDia1-dependent and ROCK-independent mechanism. Journal of Cell Biology, 2001. **153**(6): p. 1175-1186.

161. Oakes, P.W., et al., Tension is required but not sufficient for focal adhesion maturation without a stress fiber template. J Cell Biol, 2012. **196**(3): p. 363-74.

162. Dumbauld, D.W., et al., How vinculin regulates force transmission. Proc Natl Acad Sci U S A, 2013. **110**(24): p. 9788-93.

163. Dominguez, R., Actin-binding proteins--a unifying hypothesis. Trends Biochem Sci, 2004. **29**(11): p. 572-8.

164. Dominguez, R., Actin filament nucleation and elongation factors--structure-function relationships. Crit Rev Biochem Mol Biol, 2009. **44**(6): p. 351-66.

165. Thompson, P.M., C.E. Tolbert, and S.L. Campbell, Vinculin and metavinculin: Oligomerization and interactions with F-actin. FEBS Lett, 2013.

166. Hynes, R.O., Integrins: bidirectional, allosteric signaling machines. Cell, 2002. **110**(6): p. 673-87.

167. Critchley, D.R., Focal adhesions - the cytoskeletal connection. Curr Opin Cell Biol, 2000. **12**(1): p. 133-9.

168. Ridley, A.J., et al., Cell migration: integrating signals from front to back. Science, 2003. **302**(5651): p. 1704-9.

169. Wang, N., J.P. Butler, and D.E. Ingber, Mechanotransduction across the cell surface and through the cytoskeleton. Science, 1993. **260**(5111): p. 1124-7.

170. Matthews, B.D., et al., Cellular adaptation to mechanical stress: role of integrins, Rho, cytoskeletal tension and mechanosensitive ion channels. Journal of cell science, 2006. **119**(Pt 3): p. 508-18.

171. Guilluy, C., et al., The Rho GEFs LARG and GEF-H1 regulate the mechanical response to force on integrins. Nat Cell Biol, 2011. **13**(6): p. 722-7.

172. Balaban, N.Q., et al., Force and focal adhesion assembly: a close relationship studied using elastic micropatterned substrates. Nat Cell Biol, 2001. **3**(5): p. 466-72.

173. Thompson, P.M.,et al., Identification of a new actin binding surface on vinculin that mediates mechanical cell and focal adhesion properties. Structure, 2013.

174. Cable, J., et al., In vitro phosphorylation of the focal adhesion targeting domain of focal adhesion kinase by Src kinase. Biochemistry, 2012. **51**(11): p. 2213-23.

175. Isom, D.G., et al., A miniaturized technique for assessing protein thermodynamics and function using fast determination of quantitative cysteine reactivity. Proteins, 2011. **79**(4): p. 1034-47.

176. Rhee, H.W., et al., Proteomic mapping of mitochondria in living cells via spatially restricted enzymatic tagging. Science, 2013. **339**(6125): p. 1328-31.

177. Le Devedec, S.E., et al., The residence time of focal adhesion kinase (FAK) and paxillin at focal adhesions in renal epithelial cells is determined by adhesion size, strength and life cycle status. J Cell Sci, 2012. **125**(Pt 19): p. 4498-506.

178. Wolfenson, H., et al., Actomyosin-generated tension controls the molecular kinetics of focal adhesions. J Cell Sci, 2011. **124**(Pt 9): p. 1425-32.

179. Tanner, K., et al., Dissecting regional variations in stress fiber mechanics in living cells with laser nanosurgery. Biophys J, 2010. **99**(9): p. 2775-83.

180. Chang, C.W. and S. Kumar, Vinculin tension distributions of individual stress fibers within cell-matrix adhesions. J Cell Sci, 2013. **126**(Pt 14): p. 3021-30.